KAUNAS UNIVERSITY OF TECHNOLOGY

RAMIN PASHAZADEH

SYNTHESIS AND STUDIES OF MULTIFUNCTIONAL MATERIALS BASED ON QUINOXALINE OR PYRIDOPYRAZINE AS ACCEPTOR MOIETIES

2019, Kaunas

KAUNO TECHNOLOGIJOS UNIVERSITETAS

RAMIN PASHAZADEH

DAUGIAFUNKCINIŲ MEDŽIAGŲ, TURINČIŲ AKCEPTORINIUS CHINOKSALINO ARBA PIRIDOPIRAZINO FRAGMENTUS, SINTEZĖ IR TYRIMAS

Daktaro disertacija
Technologiniai mokslai, medžiagų inžinerija (T 008)

2019, Kaunas

List of Abbreviations

ΔE_{ST}	singlet-triplet energy gap
η_{ext}	external quantum efficiency
η_{int}	internal quantum efficiency
τ	emission lifetime
^{o}C	degrees Celsius
k_r	rate constant of radiative decay
λ	reorganization energy
λ_{ab}	wavelength of absorption band
λ_{ex}	excitation wavelength
λ_{fl}	maximum fluorescence wavelength
-i	initial
-g	ground
-f	fumed
-h	heated
-m	molten
-d	drop casted
-dh	drop casted after heating
CzQx	2,3-di(9*H*-carbazol-9-yl)quinoxaline
tCzQx	2,3-bis(3,6-di-tert-butyl-9*H*-carbazol-9-yl)quinoxaline
MeOQx	2,3-bis(3-methoxy-9*H*-carbazol-9-yl)quinoxaline
MeO2Qx	2,3-bis(3,6-dimethoxy-9*H*-carbazol-9-yl)quinoxaline
AzQx	2,3-bis(10,11-dihydro-5H-dibenzo[b,f]azepin-5-yl)quinoxaline
IDBQx	2,3-bis(4-(10,11-dihydro-5H-dibenzo[b,f]azepin-5-yl)phenyl)quinoxaline
OIDBQx	2,3-bis(4-(2,8-dimethoxy-10,11-dihydro-5*H*-dibenzo[*b,f*]azepin-5-yl)phenyl)quinoxaline
ISBQx	2,3-bis(4-(5H-dibenzo[*b,f*]azepin-5-yl)phenyl)quinoxaline
TOCQx	2,3-bis(3-(*tert*-butyl)-6-methoxy-9*H*-carbazol-9-yl)quinoxaline
TOCPP	9,9'-(pyrido[2,3-*b*]pyrazine-2,3-diyl)bis(3-(*tert*-butyl)-6-methoxy-9*H*-carbazole)
tCzPP	9,9'-(pyrido[2,3-*b*]pyrazine-2,3-diyl)bis(3,6-di-*tert*-butyl-9*H*-carbazole)
MeO2PP	9,9'-(pyrido[2,3-b]pyrazine-2,3-diyl)bis(3,6-dimethoxy-9H-carbazole)
$Pd_2(dba)_3$	tris(dibenzylideneacetone)dipalladium(0)
AIE	aggregation induced emission
Am	amorphous
XPhos	2-dicyclohexylphosphino-2′,4′,6′-triisopropylbiphenyl
^{13}C NMR	carbon nuclear magnetic resonance
CT	charge transfer

CV	cyclic voltammetry
Cz	carbazole
d	doublet
dba	dibenzylideneacetone
DCM	dicholoro methane
dd	double doublet
DF	delayed fluorescence
DMAC	9,9-dimethyl-9,10-dihydroacridine
DMF	dimethylformamide
DMSO	dimethylsulfoxide
DSC	differential scanning calorimetry
dt	doublet of triplet
$E_{1/2}$	half-wave potential of a reversible redox process
EA	electron affinity
E_g^{opt}	optical band gap
EBL	electron blocking layer
EIL	electron injection layer
EL	electroluminescence
E_T	triplet energy
ETL	electron transporting layer
EtOAc	ethyl acetate
Fc	ferrocene
FWHM	full width at half maxima
J	coupling constant
h	hours
HBL	hole blocking layer
HIL	hole injection layer
Hex	hexane
^{1}H NMR	proton nuclear magnetic resonance
HOMO	highest occupied molecular orbital
HTL	hole transporting layer
HTM	hole transporting material
Hz	hertz
ICT	intramolecular charge transfer
IDB	iminodibenzyl
IP	ionization potential
ISB	iminostilbene
ISC	intersystem crossing
ITO	indium tin oxide
LUMO	lowest unoccupied molecular orbital
LE	locally excited
m	multiplet
MCL	mechanochromic luminescence
MeOH	methanol
mmol	millimol

m.p.	melting point
MS	mass spectrometry
m-MTDATA	4,4′,4″-tris[phenyl(*m*-tolyl)amino]triphenylamine
m/z	mass-to-charge ratio
Na	sodium
NBS	N-bromosuccinimid
NPB	*N*,*N*′-di(1-naphthyl)-*N*,*N*′-diphenyl-(1,1′-biphenyl)-4,4′-diamine
PBD	polybutadiene
PF	prompt fluorescence
PHOLED	phosphorescent organic light-emitting diode
PL	photoluminescence
PVK	poly(9-vinylcarbazole)
PXRD	powder X-ray diffraction
PXZ	phenoxazine
Qx	quinoxaline
RT	room temperature
RTP	room temperature phosphorescence
s	singlet
Sol.	solvent
SOC	spin-orbit coupling
t	triplet
t-Bu	*tert*-butyl
TADF	thermally activated delayed fluorescence
TAPC	4,4′-cyclohexylidenebis[*N*,*N*-bis(4-methylphenyl)benzenamine]
TCTA	tris(4-carbazoyl-9-ylphenyl)amine
T_d	decomposition temperature (5% weight loss)
T_g	glass transition temperature
THF	tetrahydrofuran
TGA	thermogravimetric analysis
Tol.	Toluene
TOC	3-(*tert*-butyl)-6-methoxy-9*H*-carbazole
TPBi	2,2′,2″-(1,3,5-benzinetriyl)-tris(1-phenyl-1-H-benzimidazole)
UV	ultraviolet
vis	visible
V_{on}	turn-on voltage

Table of Contents

1. INTRODUCTION

Given the prominent role of colors in daily life, their influence on mood, feelings, emotions and signal action, enormous efforts have been devoted to generate artificial, cheap and accessible chromophores. Dye molecules with conjugated multiple bonds absorb light. In conjugated molecules, electrons in p-orbitals can be shared over molecules, and, as the extent of conjugation increases, electrons delocalize easily across the adjacent aligned p-orbitals, and the energy difference between the highest occupied molecular orbital and the lowest unoccupied molecular orbitals decreases.

Replacement of carbon atoms of the aromatic ring(s) with nitrogen atoms disturbs electron delocalization over molecules and withdraw electron density toward nitrogen atom, consequently, enhances electron withdrawing capacity of molecules. For example, quinoxaline, which consists of two aromatic rings, benzene and pyrazine, is one of the strong electron withdrawing synthons which has been used for the construction of luminogens with various applications [1–3].

In chemistry, incorporation of electron donating and electron withdrawing units into conjugated molecules, giving rise to shift the spectrum to longer wavelengths. In the case of dyes that are assembled by strong electron accepting and electron donating units, electron density from the donor towards the acceptor increases and leads to a stronger dipole moment [4]. These concepts reflect the fact that a variety of small chromophores in the range of the visible spectrum can be prepared for application in different fields, such as organic photovoltaic devices, organic light emitting diodes, stimuli-responsive (smart) materials, and organic field-effect transistors [5–8]. Consequently, the push-pull system plays an eminent role in chromophore architecture.

Since the 1990s, smart materials and organic light emitting diodes (OLEDs) are arena of material research which have attracted a great deal of interest from academia to industrial researchers. Smart materials which are capable to tune the color in the presence of external stresses are applicable for indicator, sensor and reflect environment variations. Mechanochromic materials (MCL) which are also named as smart materials undergo alterations of their mechanical and/or optical properties in response to environmental changes and external stimulation, such as pressure, temperature, moisture, pH, smashing, ultra sound, electric/magnetic fields etc [9]. These processes are reversible and occur due to variations in morphology, conformations or chemical structures. Tribochromic and piezochromic behavior refer to application of mechanical and pressing forces, respectively, which lead to color changes, and thermochromic materials are capable of tuning their color in response to temperature changes [10]. Despite big efforts, the design of mechanoresponsive materials still remains a challenge, and synthesis of multicolor pure organic compounds is still rare [9].

Nowadays, organic light emitting diodes (OLEDs) are widely spread around the world. They are used in smart phones and large screen displays including TV screens. The first report of organic electroluminescent (EL) materials was delivered in 1953 by Bernanose group [11]. The huge impact on the development of OLEDs was made

by Tang and Van Slyke who fabricated a device with 1% EQE under a practical operating electric field of 10 V [12]. Since then, rapid progress in the design and synthesis of EL materials has been done. Phosphorescent OLEDs represent the second generation of OLEDs which emit light from the triplet state. In these devices, precious noble metal complexes facilitate intersystem crossing from the excited singlet state to the triplet state [13]. The next generation of OLEDs represents devices based on thermally activated delayed fluorescence (TADF) [14]. TADF materials are fully organic compounds containing no noble metals. They harvest both singlet and triplet excitons to emit photons from the singlet state. One of the great privileges of fully organic materials is their wide variety, which makes TADF-based OLEDs very promising.

Generally, vacuum thermal deposition is the dominant method for the manufacturing of OLEDs. However, thermally evaporated OLEDs are expensive and need special conditions to hold high vacuum in spacious evaporation chambers [15]. In contrast, solution-processed devices have attracted great interest due to the low cost of manufacturing and possibility of large area deposition. However, solution processing of OLEDs has not proven its merits yet in terms of device efficiency [16].

The enhanced prevalence of purely organic luminogens and their emergence as semiconductors and mechanochromic materials have become the alternative for expensive noble metals. Fully organic electronically active compounds containing no toxic and expensive noble metals have always been an incentive because of the vast potential range of molecular architectures and a variety of fields of application.

The aim of this work is low-cost and simple synthesis of new purely organic luminogens based on quinoxaline and pyridopyrazine as the acceptors and the investigation of the properties of the synthesized materials.

The tasks set for the achievement of the above stated aim are as follows**:**
- Synthesis of new derivatives of quinoxaline containing carbazole, iminodibenzyl, iminostilbene fragments as electron donor moieties.
- Preparation of compounds containing a strong acceptor, pyridopyrazine.
- Design, synthesis and characterization of new electron donors, 3-(*tert*-butyl)-6-methoxy-9*H*-carbazole and 2,8-dimethoxy-10,11-dihydro-5*H*-dibenzo[*b,f*]azepine.
- Research of the influence of the phenylene linkage between the donor and the acceptor in terms of their photophysical characteristics.
- Investigation of the strength of the donor on the optical, photophysical, mechanochromic and electrochemical properties of the compounds.
- Fabrication and characterization of OLEDs while using the newly synthesized materials

The novelty of the work:

- Four new luminogens containing quinoxaline and carbazole moieties have been generated; they demonstrate mechanochromism and delayed fluorescence at room temperature.

- Through a substitution of quinoxaline with pyrido[2,3-*b*]pyrazine, new mechanochromic luminescent and thermally activated delayed fluorescence materials have been generated.
- Three new donors, i.e., 3-(*tert*-butyl)-6-methoxy-9*H*-carbazole, 3-methoxy-9*H*-carbazole and 2,8-dimethoxy-10,11-dihydro-5*H*-dibenzo[*b,f*]azepine have been designed, synthesized and characterized.
- Three new room temperature phosphorescent materials have been developed, and donor and bridge effects on their properties have been investigated; iminodibenzyl is proposed as a promising moiety to suppress non-radiative decay.

The practical value of the work:

The synthesized products have been applied to fabricate OLEDs. Mechanochromic luminescent materials can be applied as stimuli-responsive materials.

Contribution of authors:

The following table demonstrates contribution of the author and other persons to this work. The obtained results were analyzed by the author, except for photophysical and electrochemical results that were analyzed in collaboration with Piotr Pander. For the compounds described in chapter 4.2, NMR spectroscopy measurements were done by the author.

Contribution	Author	Piotr Pander	Algirdas Lazauskas	Audrius Bučinskas	Laura Pečiulytė	Jurate Simokaitienė	Greta Ragaitė
Design	▨						
Synthesis	▨						
Characterization	▨						
Cyclic voltammetry	▨						
MCL measurements	▨	▨					
Photophysical measurements	▨	▨					
Device fabrication		▨					
NMR	▨						▨
Single crystal XRD				▨			
Powder XRD			▨				
Thermal analysis					▨		

2. LITERATURE REVIEW

2.1. Mechanochromic materials

Organic π-conjugated materials comprising electron donating and electron accepting scaffolds have rendered enormous potential application in material science including stimuli-responsive materials, organic light emitting diodes, solar cells and biotechnology [4–8]. Although significant efforts have been devoted to the construction of luminophores exhibiting mechanically induced luminescence, the principle of their design still remains ambiguous.

Since the first report on pure organic mechanoluminescent (MCL) materials by Araki *et al*. [17] in 2007, this field has been attracting considerable attention. MCL materials are defined as a category of compounds that, upon external stimuli, switch their solid-state luminescent properties. Photoluminescence alteration occurs via different stimulations, such as mechanochromism, thermochromism, vapochromism, piezochromism, etc. [18]. Typically, mechanical stimulation, such as grinding or shearing, induces the amorphous and metastable phase, and heating or fuming restores the initial assembly and its photoluminescence color. MCL materials are useful for application in security inks, data storage, sensors and memory devices [19, 21]. In smart materials, self-recovering is another phenomenon that occurs when the phase transition temperature is lower than room temperature to tune the metastable state [22, 23].

In MCL materials based on the different external stresses, molecular packing, intermolecular interactions and conformation between the donor and the acceptor are disrupted or changed. These alterations result in tuning the PL wavelength, excited state lifetime, and emission quantum yield; consequently, changes in the wavelength and emission intensity of molecules are induced [24, 25]. In many cases, phase transitions from crystalline to amorphous induce MCL behavior, and these transitions are recognized by powder X-ray diffraction analysis [25]. Although for molecules in the crystalline form single crystal XRD analysis yields enough information about molecular orientations, intermolecular interaction and twist angles, in amorphous forms, the molecular packing is unknown.

Understanding the driving mechanism of color tuning during the stimuli-responsive process is still a challenge. Gaining insight into the microstructure and the influence of stimulation on the molecular packing and intramolecular alteration is possible via phase transition, PL spectra, lifetime and excited singlet/triplet energy measurements research [25, 26]. From this point of view, it is worth noting the assay effect of aggregations on the optical properties.

Molecules with planar π-conjugation in their solid forms experience various packing modes, such as J-aggregation, H-aggregation and excimer (Fig. 2.1). Stacking mode or aggregation indicates a pattern of assembly between the adjacent molecules. J-type aggregation manifests interaction between the head-to-tail of chromophore units, and H-type refers to face-to-face interactions. Intermolecular interaction between two identical molecules in their ground state results in the formation of dimers. Excited dimers are called excimers. According to the exciton theory, when

two individual molecules are brought together to make a dimer, the excited state of the aggregated molecule split into two new energy levels (Fig. 2.1): one with a lower energy, and the other with a higher energy than that of the monomer [27–30]. In H-type aggregates, the lower state is stabilized, and the emission is red-shifted; besides, non-radiative decays are predominant, and molecules lose their excitation energy as heat or vibrations to environment. The mechanical force or compression usually causes a shortened distance between the adjacent molecules and the condensed phase (H-type aggregation or excimer formation). Subsequently, leads to a strong intermolecular π-π interaction, which usually results in a longer lifetime, low PL quantum yield, red-shifted PL spectrum as well as broadened and weakened fluorescent emission band. Generally, J-type is characterized by slightly red-shifted and intense fluorescence and a high PL quantum yield [30].
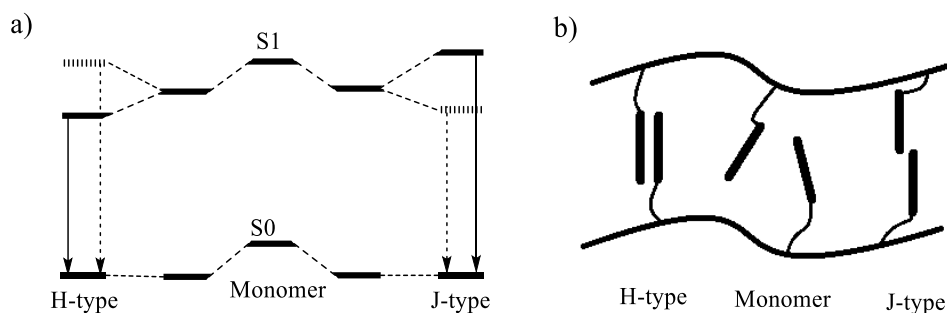
Fig. 2.1 Arrangement effects on (a) photoluminescence, (b) different aggregation modes.

Luminescent mechanochromic materials are divided into different categories based on physical molecular forms and emissions. MCL materials have been developed based on inorganic complexes, polymers and organic compounds [31–35]. *Mechanofluorescent* and *mechanophosphorescent* are the terms to describe materials according to their emission origin and lifetime [24, 36]. Phosphorescent luminescent materials exhibit strong spin orbit coupling, mainly designed upon organo metal complexes, which results in the conversion of singlet to triplet exciton so that to achieve 100% emission from the long-lived triplet state [37, 38].

In piezochromic materials, the effect of the distance between adjacent fluorophores has been approved by color changing through compression, so, typically, after decompression, the original color gets gradually restored [39]. This is ascribed to the fact that molecular packing has not been perturbed, whereas the color shifting arises from distance alteration.

Mechanochromism has been seen to vary across a range of compounds, such as organic, organometallic, polymer and liquid crystalline (LC) compounds. In the following subchapter, the effect of mechanical forces on the luminescent switching of materials has been summarized.

2.2. Two color switching

To date, many compounds with two color tuning have been reported. Color alteration has reported for a single compound, dye(s) blended with polymer or mixture of more than one dye. In this section, some examples of MCL structures design shall be represented.

One of the renowned structures of MCL is the cyano-distyrylbenzene scaffold; new features have been reported through simple alteration of its chemical structure. These compounds by planar and conjugated structures facilitate π-π interactions and excimer formation. In 2002, Weder and Loewe probed PL of oligo (*p*-phenylene vinylenes) as a dopant which was blended with linear low-density polyethylene (LLDPE) as the host [40]. Compounds **1** and **2** in the solid powder state emit in the red and yellow region at 644 nm and 550 nm, respectively. The emission character of the blends altered via tensile deformation and annealing. The luminescence of the compound changed from red to green via annealing at 85 °C or 95 °C, overlapping with the melting point of the host, which was attributed to the mobility of the host materials. The red color of the blend originated from the excimer formation that, through stretching, changed to green, which suggests that monomeric forms dominate (Fig 2.2). In 2008, the Weder group again reported MCL characteristics of liquid crystals; they suggested the same core structure, like in dyes **1** and **2**, just with long alkyl chains (Fig 2.2) and compared their behavior. The increasing length of the aliphatic group results in hypochromism [41].
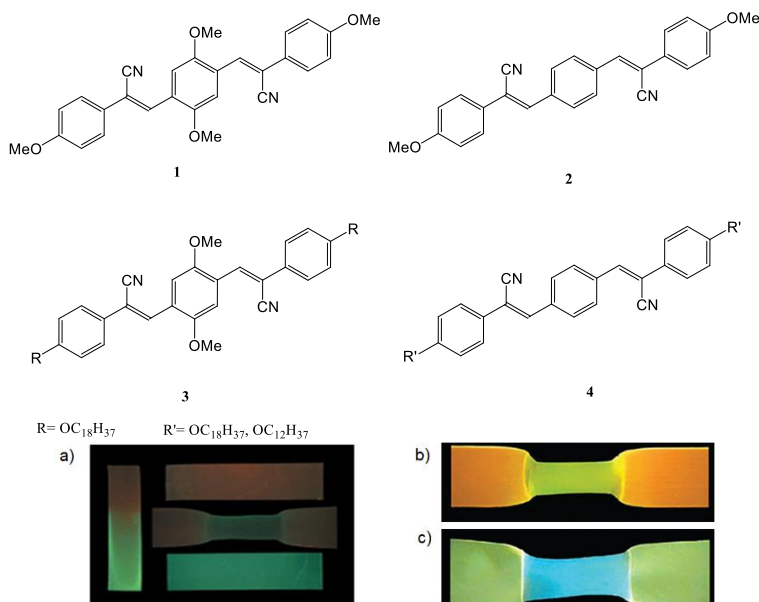
Fig. 2.2 Molecular structure of compounds **1–4** and images of their blend films with LLDPE under UV light. Effect of tension or annealing on blend films of **1** (a), **3** (b) and **4** (c).

The liquid crystal demonstrated blue fluorescence in both solid powder and solution which was ascribed to monomer formation. Upon compressing liquid crystals

3 and **4**, the blue emission changed to yellow accompanied by broadening of spectra, which is characteristic to excimer emission. Upon annealing, compressed liquid crystals recover the initial emission color, and the transition from the nematic phase to the sematic phase is observed. Therefore, the compounds have both thermochromic and piezochromic characteristics regarding responses to temperature and pressure.

In 2011, Park and Yoon reported a similar structure to the above mentioned one (Fig 2.3) which exhibited AIE and MCL behaviors [42]. The compounds presented polymorphic characteristics with two phases. One phase showed a short wavelength with head-to-tail aggregations whereas the other phase featured a long wavelength with dimeric coupling, which was attributed to the π-π overlap.
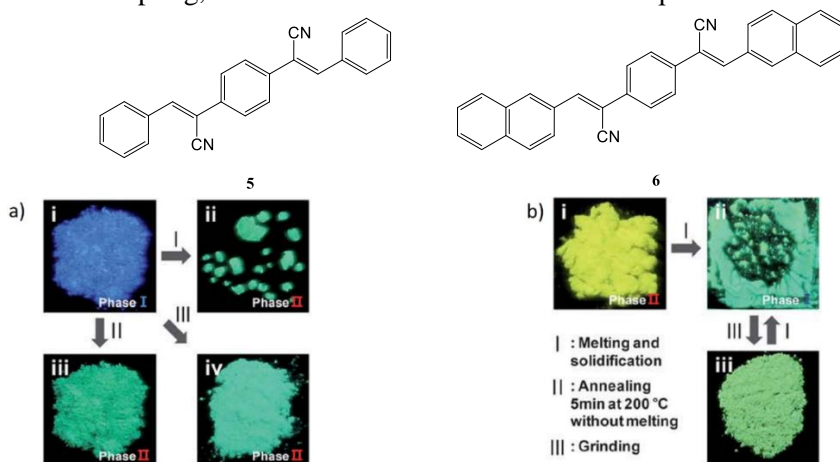
Fig. 2.**3** (a) Chemical structure of compounds **5** and **6**. Photos of compound (a) **5** and (b) **6** powders under 365 nm UV light.

Weder *et al.* in 2017 [43] studied simultaneous exposure of luminophore **7** to mechanical and thermal treatment (Fig. 2.4). Pristine luminophore with yellow fluorescence under mechanical grinding turned to reddish-orange luminescence at ambient temperature. In this process, the crystalline phase changed to the amorphous phase. On the contrary, grinding the pristine form alongside heating at 100 °C resulted in the hypsochromic shift and led to yellow-green emission. Moreover, the XRD analysis of the powder exhibited the crystalline-crystalline phase transition.
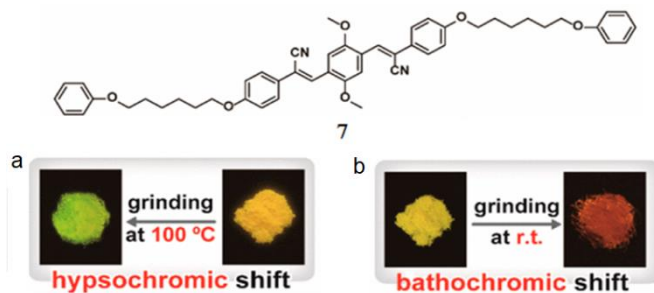
Fig. 2.4 Color variation of compound **7** under mechanical grinding (a) at 100 °C and (b) at ambient temperature.

16

Mechanoresponsive luminescent materials have also been reported as having organo metallic complexes with gold, boron, zinc (II), platinum (II) or copper (I), etc. 9-Anthryl gold (I) isocyanide complexes **8–10** (Fig. 2.5) under mechanical stimulation demonstrated an unprecedented emission bathochromic shift from 448 nm to the IR region (900 nm); this data was published in 2017 by Ito *et al*. [44]. In general, the emission of the pristine state for these complexes arises from the intramolecular charge transfer from the aryl component on the metal to another aryl that is named as the *ligand-to-ligand charge transfer* (LLCT). Moreover, after external stimulation, the yellow emission of the luminophore is attributed to aurophilic interactions, which arises from the *metal-metal-to-ligand charge transfer* (MMLCT). A prominent bathochromic shift after grinding has been observed through the extension of the π-conjugation of the aryl moiety in gold.
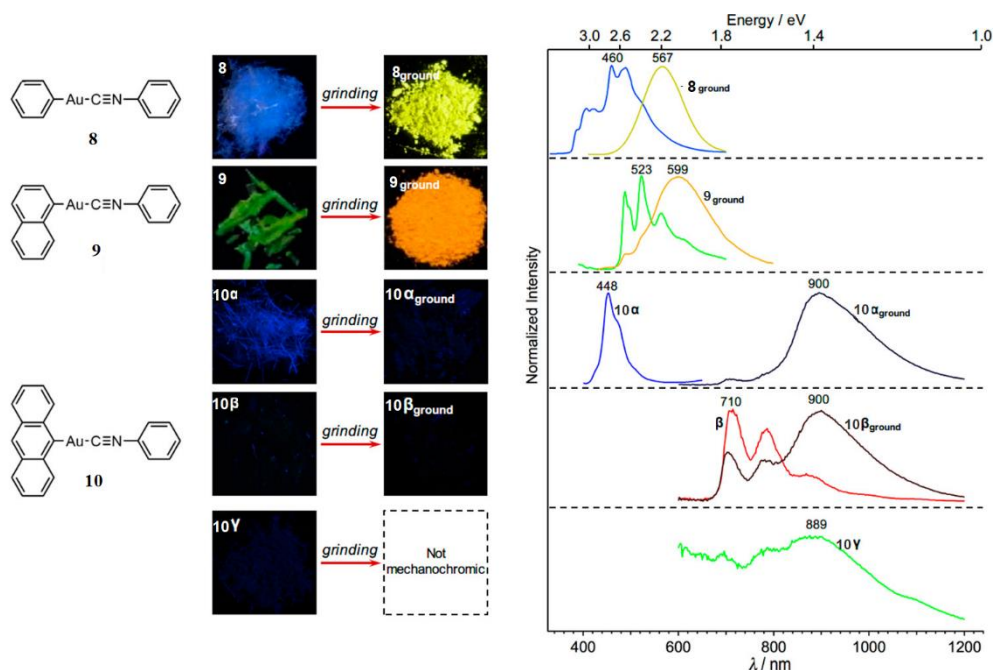
Fig. 2.5 Chemical structure and color variation of compounds **8–10** under grinding.

Ito and coworkers in 2008 presented gold (I) isocyanide complex **11** whose emission shifted from blue to yellow when ground [45]. Upon grinding, a stable crystal phase converted to a stable amorphous phase, thus it neither recovered the initial blue form nor transformed to another form (Fig. 2.6a). The authors suggested that MCL behavior arises from aurophilic (Au-Au) interactions. Subsequently, in 2016, Ito *et al*. reported mechano-stimulation of similar structure **12** (Fig 2.6b), where triethylene glycol (TEG) groups were introduced into the aryl moiety [46]. In this case, the addition of TEG groups resulted in different phase transition features, thus the grinding led to a 'transient' amorphous phase that continuously underwent to another crystalline phase. Therefore, three phases were observed, C1-[A]-C2; besides, every phase demonstrated a different emission color. The original initial phase

17

showed blue luminescence that, under grinding, changed to yellow emission, which, within seconds, vanished and converted to green emission.
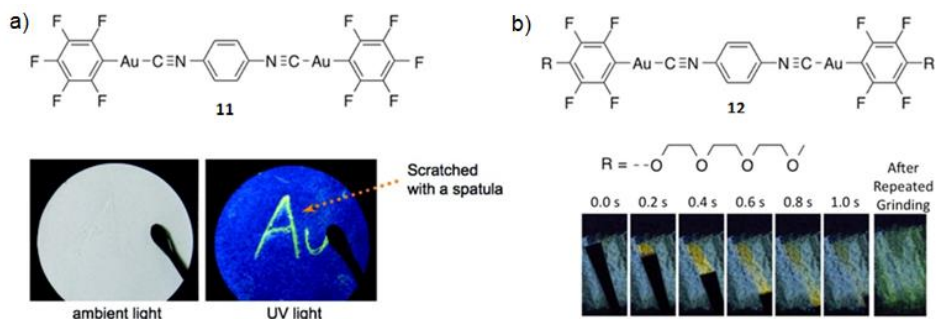
Fig. 2.6 Gold (I) isocyanide complex **11** with two-color variation. Self-recovering complex **12** regarding crystal-amorphous-crystal variation.

The mechanochromic character of chiral compound, binaphthyl gold (I) isocyanide complex **13**, was reported in 2016 by Ito *et al*. [47]. According to Wallach's rule, racemic crystals are denser than these homotopic crystals. In this work, racemic crystals exhibited yellowish-green emission (Fig. 2.7c), whereas homochiral [*S*] crystals exhibited green emission (Fig. 2.7d). The grinding of these crystals changed both crystals to the amorphous phase with similar luminescence.
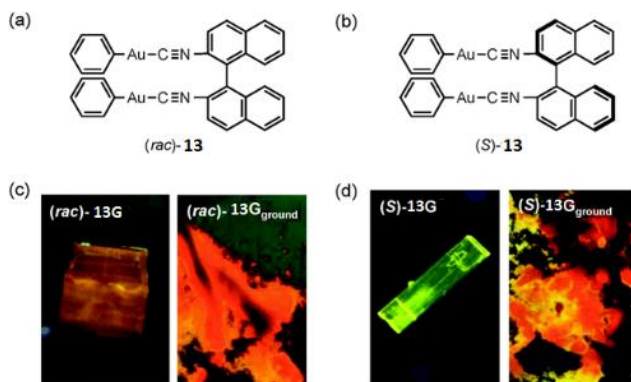
Fig. 2.7 Photograph of gold complexes (rac)-**13** and (S)-**13** in the crystalline form and after grinding.

2.3. Multicolor switching materials

Up to now, a variety of MCL molecules have been reported, and luminogens usually feature phase transition and color tuning between two colors. Despite major efforts, the synthesis of compounds with multicolor switching still remains a challenge. In the subchapter below, some organometallic and organic compounds demonstrating multichromism are discussed.

2.3.1 Multicolor switching in small organic molecules

In 2012, Tian and his team reported multichromism upon applying pressure for a molecule of 9,10-bis((*E*)-2-(pyrid-2-yl)vinyl)anthracene (**14**), and it covered a range of colors from green to red [48]. High-pressure measurements were conducted by using a diamond anvil cell (DAC). As depicted in Fig. 2.8, the molecule emission spectrum exhibited a 124 nm piezochromic shift, which, under atmospheric pressure, peaked at 528 nm. Through enhancing the pressure to 7.92 GPa, showed an emission spectrum peak at 652 nm. To gain insight into intermolecular influences on fluorescence alteration, three polymorph crystals were prepared (C1, C2 and C3). Single crystal analyses disclosed that the crystal with green emission adopted the packing mode of J-aggregation, while the orange crystal with emission at 579 nm demonstrated H-aggregation. In the case of red emission, face-to-face stacking causes dimers and results in high overlapping between adjacent molecules.
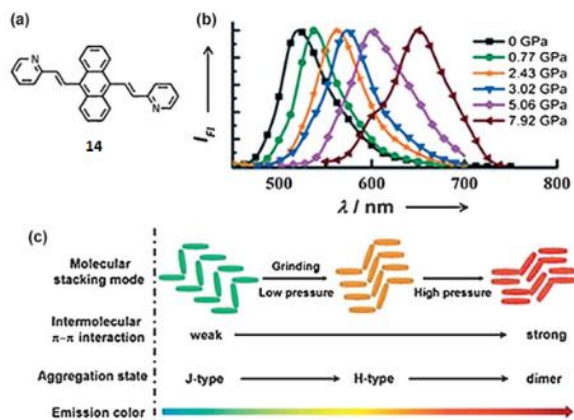
Fig. 2.8 a) Molecular structure of compound **14**. b) PL spectra of compound **14** under external pressure. c) Molecular assembly and corresponding color variation in different aggregations.

(*Z*)-4-(2-cyano-2-(4'-(diphenylamino)-[1,1'-biphenyl]-4-yl)-vinyl)benzonitrile (**15**) was prepared by Zhang's group. It exhibited intramolecular charge transfer features [49]. This fluorophore spectrum indicated 111 nm wavelength shift upon applying mechanical grinding. The initial form was of green color, showed emission at 507 nm, and, upon gently grinding, the fluorescence immediately turned yellow, and then switched to orange which peaked at 608 nm (Fig. 2.9d). After fully grinding the powder, fluorescence changed to the red color at 618 nm. In this molecule, two mechanisms influenced color tuning, either intermolecular interactions or conformational changes, which the latter can be ascribed to tuning the states between the LE and CT states. The molecule responded to the compression process, the wavelength with increasing pressure gradually increased, and the intensity decreased (Fig. 2.9b and 2.9c). As depicted in Figure 2.9e, the green luminophore at 6.09 GPa emitted red color at 608 nm. Besides, the molecule showed to be self-recovering, and, after releasing hydrostatic pressure, it turned back to the original state.
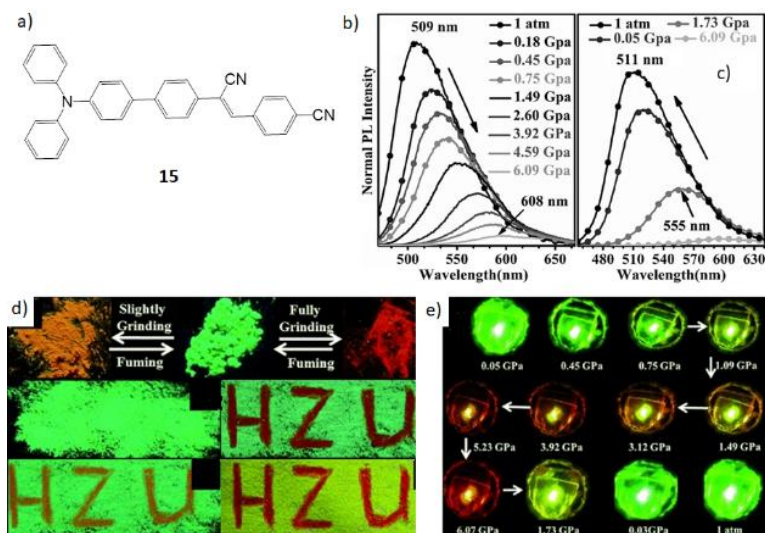
Fig. 2.9 a) Molecular structure of compound **15**. b) PL spectra of compound **15** upon compression and c) after decompression. d) Images of compound **15** under grinding, shearing and e) hydrostatic pressure.

Furthermore, Zhang group, in terms of stock shifts, proposed that the observed green powder fluorescence arose from the local excited state (LE), whereas the yellow emission was ascribed to the coexistence of LE and CT states. On the other hand, the domination of the CT state was attributed to high red-shifted powder emission.

Ma *et al.* reported a four-color switching luminophore containing 6-hydroxylbenzothiazole and tetraphenylethene moieties (Fig. 2.10a) in structure **16** [50]. The molecule with a hydroxyl group had the capability to respond to acid-base stimuli and responded to the protonation-deprotonation process. The pristine form emission was blue at 454 nm, whereas fumigation through concentrated hydrochloric acid vapors resulted in turning the color to yellow with an emission peak at 550 nm. The initial color was recovered through exposure to ammonium hydroxide vapors.
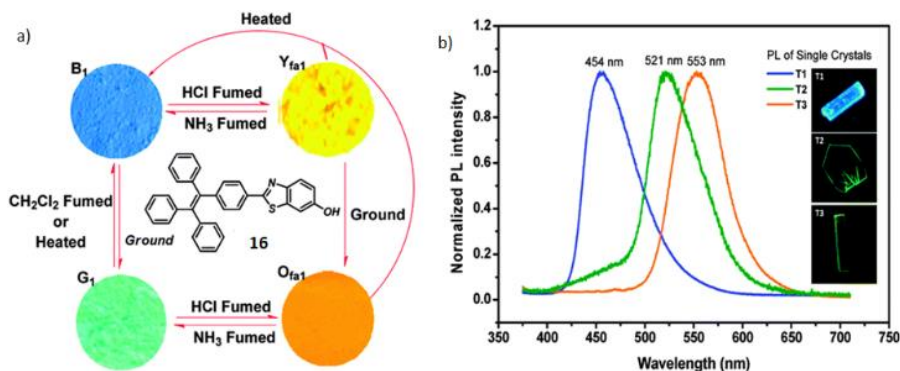
Fig. 2.10 Chemical structure and color variation of compound **16** under external stresses (a). PL spectra of single crystals (b).

Moreover, upon grinding with a pestle or shearing with a spatula, the fluorescence peak of the initial form changed to the blue-green color at 492 nm. Upon fuming and annealing, the initial color was restored. When the ground form was treated with vapour of hydrochloric acid, luminescence turned to orange and peaked at 565 nm. Again, deprotonation with NH_3 blue-green emission (in the ground form). In addition, grinding the protonated form led to the production of an orange powder, which, by heating the ground form, had its initial state restored. This shows that, after heating, the molecule is deprotonated, and HCl gas is released.

Cyano distyrylbenzene **17** containing two carbazole groups indicated piezochromic fluorescence as well as aggregation-enhanced emission (Fig 2.11) which was reported by Lu *et al.* in 2016 [51]. The original emission of fluorophore at 1 atm was green, and gradual compression caused red-shifting; eventually, at 9.21 GPa, red emission was seen. Color reversibility was achieved by releasing the pressure to 1 atm. Additionally, pressurizing affected the emission intensity; thus, at higher pressures, a lower intensity was observed. This evidence reflects the fact that decreasing the intermolecular distance between adjacent molecules leads to a decrease of the radiative transition rate.
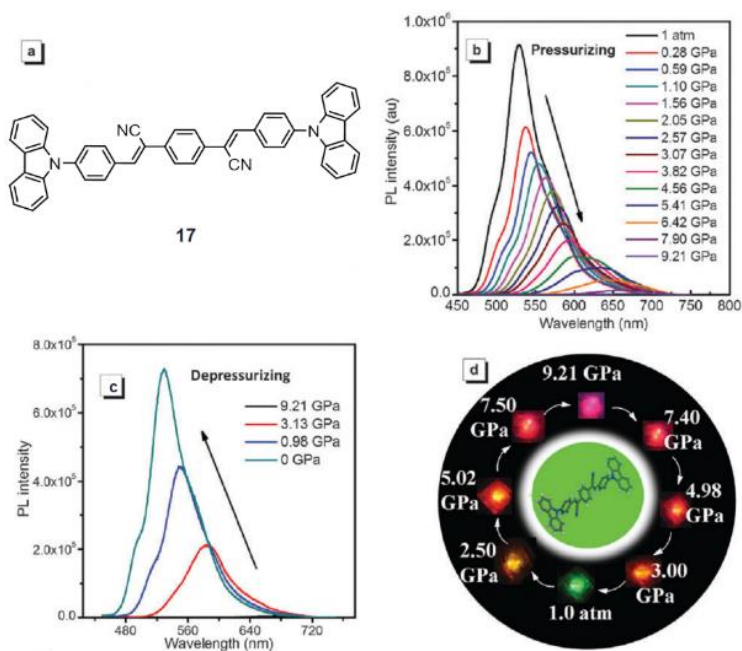
Fig. 2.11 a) Molecular structure of compound **17**. b) PL spectra under compression, c) decompression process and d) color changes by compression.

Tricolor emission was reported by Saito, Yamaguchi and team in 2013 [52]. Organic fluorophore, tetrathiazolylthiophene derivative **18**, demonstrated a response to mechanical grinding and hydrostatic compression (Fig 2.12). The molecule in the polymethyl methacrylate (PMMA) film showed blue emission. The crystal exhibited yellow luminescence with the maximum wavelength of 556 nm. On the contrary, after

mechanical grinding of the crystal, the emission blue-shifted up to 66 nm and showed green color at 490 nm. Therefore, tricolor emissions were obtained by changing the solid environment. Single-crystal analyses illustrated face-to-face interaction between 2,5-dithiazolylthiophene skeletons resulting in excimer performance. Conversely, grinding caused disorder in the molecular structure, which resulted in increasing distance between excimers, and luminescence spectrum peaked at 490 nm. When hydrostatic pressure was conducted on the crystal the fluorescence gradually red-shifted, which accompanied with decreased intensity. Eventually, at 3.2 GPa, orange emission of the fluorophore emerged at 609 nm. It is noteworthy that, under decompression, the emission gradually blue-shifted, and, at ambient pressure, the original yellow color recovered. High-pressure single-crystal XRD analysis indicated that, by increasing pressure, the void space between the adjacent molecules in face-to-face dimers was reduced, which resulted in a bathochromic shift.
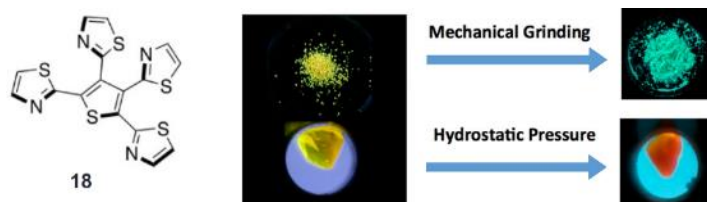
Fig. 2.12 Structure and responses to external forces of tetrathiazolylthiophene **18**.

Dong *et al*. in 2012 reported color alteration among deep blue, sky blue and green emissions [53]. Luminophore **19** consists of alkoxy groups in para position introduced to tetraphenylethylene (TPE). The slow evaporation of solvent yielded a deep blue crystal with an emission peak at 448 nm, and, upon grinding, the luminescence color transferred to green at 491 nm. Besides, after heating compounds to melting, the color changed to green. The annealing of the ground form causes the hypsochromic shift, at 90 °C, the color turned back to the initial deep blue, and at 115 °C it switched to sky blue.
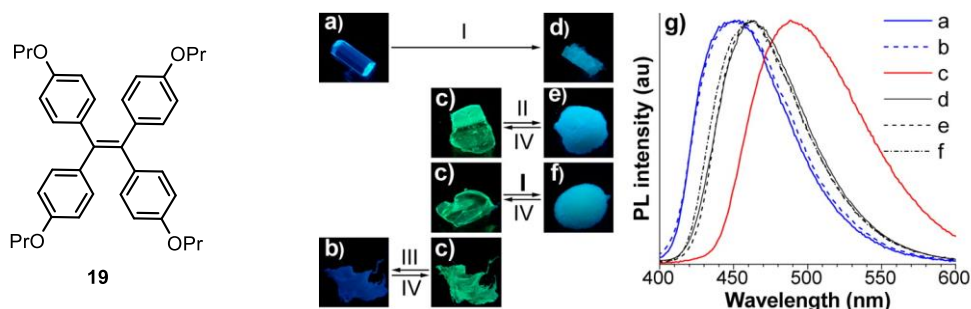
Fig. 2.13 Chemical structure and images of compound **19** under UV illumination: (a) deep blue crystal form, (b) amorphous fumed by acetone, (c) amorphous, (d) sky blue crystalline, and (e, f) amorphous annealed at (e) 90 °C and (f) 115 °C. (g) PL spectra. Conditions: I, 115 °C, 1 min; II, 90 °C, 1 min; III, fuming with acetone vapor, 5 min; iv, heating to melt and quickly cooling.

2.3.2. Multicolor switching in liquid crystals

The first multicolor tuning behavior of liquid crystals in response to external stimuli was reported by Sagara and Kato in 2011 [54]. Luminophore of 9,10-bis(phenylethynyl)anthracene (**20**) demonstrated a cubic, columnar and mesomorphic phase (Fig. 2.14). The cubic phase was formed by heating to 146 °C and emitted reddish-orange color peaking at 630 nm. The longer lifetime component at room temperature implied excimer formation of the luminescent cores. Under applying shearing at 90 °C, the cubic metastable state converted to the stable columnar phase with green emission. Meanwhile, shearing the cubic form at room temperature resulted in transformation to the yellow color, and the mesomorphic form was obtained. Color tuning is reversible, and, upon heating, the mesomorphic phase at 145 °C emission would be returned to the reddish-orange color. A shorter wavelength for a mesomorphic phase and its broader peak with its maxima at 583 nm was attributed to a partial-overlap excimer of the aromatic cores. Typically, for partial-overlap excimers, the lifetime is shorter than normal overlap excimers, and it was observed in highly viscous compounds like Langmuir-Blodgett films and polymers.
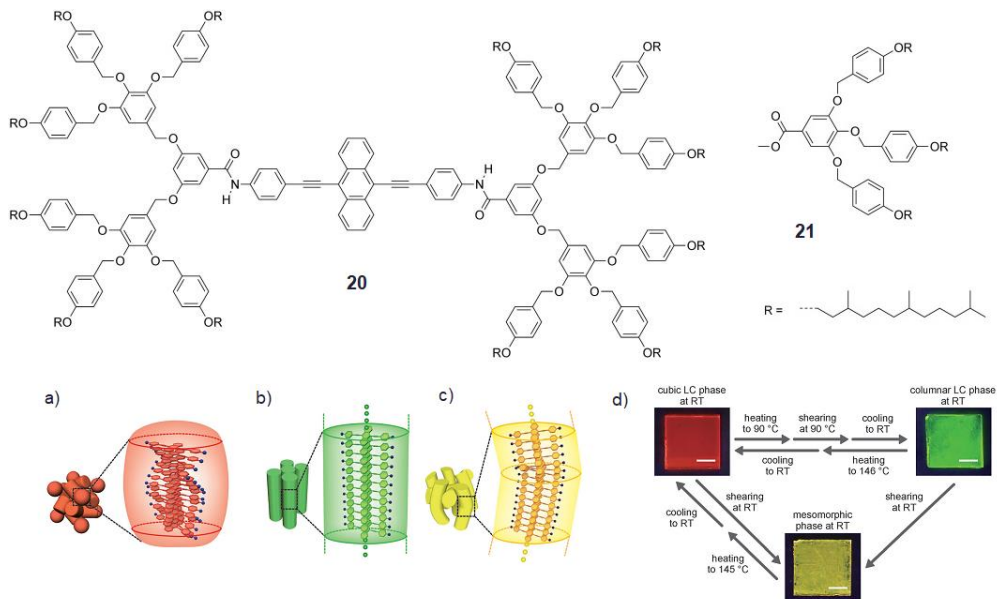
Fig. 2.14 Chemical structure of compounds **20–21**. Molecular assembly: a) cubic b) columnar c) mesomorphic. d) Pictures of compounds illustrating thermo- and mechano-responsive behavior.

Multicolor switching in supramolecular polymers (Fig 2.15) responding to mechano- and thermochromism was described in 2017 by Weder and team [55]. The core scaffold was cyano distyryl benzene **22** to support π-π stacking, and the alkyl chain comprising hydrogen bonds was used to support supramolecular polymerization of the chromophore. The precipitated form of the compound displayed orange emission at 622 nm, and its featureless peak was accompanied with a long lifetime,

25.8 ns, which indicates the formation of an excimer. Heating the material above its melting level altered the emission into the green region with the maxima peak at 520 nm, whereas its lifetime went down to 1.4 ns, which implies a monomer formation. After cooling the green state to the ambient temperature, red emission with 24.9 ns lifetime was observed. Upon grinding both orange and red forms, the color converted to yellow and centered at the 562 nm emission band. However, the yellow color demonstrates a short lifetime with 14.6 ns, since it is longer than lifetime of solution in DMF (1.4 ns); thus the yellow emission may be assigned to the formation of an excimer.
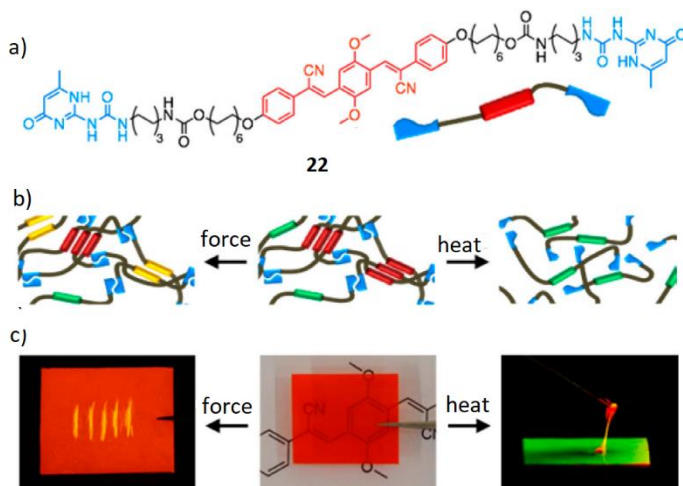
Fig. 2.15 a) Chemical structure, b) schematic assembly and c) color variation of polymer **22** under mecanical force and annealing.

2.3.3. Multicolor switching in organometallic compounds

Tetracolor luminescence switching was reported by Ito in 2015 [56]. Gold (I) isocyanide complex **23** contained tetrafluoro pyridine. The initial form demonstrated a yellow emission band with a peak at 564 nm, and, after treating with acetone, the emission band converted to the blue color at 486 nm (Fig. 2.16). Notably, the complex is barely soluble in acetone, and its acetone solution is not emissive. Under drying of the blue state in air, the luminescence turned to the green color with a spectrum peak at 533 nm. In addition, upon gentle and hard grinding of the green form, the emission transferred to the yellow and orange color range, respectively.
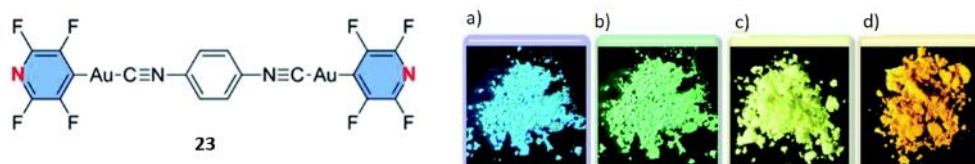
Fig. 2.16 Chemical structure, a) initial color and changes upon b) exposure to acetone, c) gentle grinding and d) hard grinding of compound **23**.

2.4. MCL and TADF treatments

Thermally activated delayed fluorescence material (TADF) **24** in the solid state showed deep-blue light emission responding to mechanical stimulus was reported by Cheng and co-workers in 2015 [57]. After grinding in a mortar with a pestle, its fluorescence turned to green with an emission peak at 510 nm. Upon mechanical force, the crystalline form converted to the amorphous form. The green form converted to the pristine form after exposure to DCM vapor.

Multicolor switching and TADF luminophore **25** introduced by using phenothiazine derivatives was reported by Takeda *et al.* in 2017 [58]. Because of having a large sulfur element in the structure of phenothiazine, this donor exhibited two different conformers: quasi-equatorial and quasi-axial. After the recrystallization of compound **25** in a different solvent, two polymorphs were obtained, yellow and orange. The grinding of the initial forms changed the color to red with an emission peak at 673 nm, and, when trying to restore the initial forms by fuming and annealing, the emission peak blue-shifted to 596 nm and 646 nm, respectively. The initial forms were obtained through the recrystallization of the ground state. Compound **25** containing *tert*-butyl groups in the phenothiazine the same behavior. Green luminophore altered to red via grinding in mortar and pestle; fumigation and annealing led to yellow and red luminophores, respectively. Again, the initial forms were obtained by recrystallization.

Swager and Baldo *et al.* introduced two-color tuning compound **26** (Fig 2.17) when phenothiazine was used as the electron donor [59]. Green powder after grinding provided yellow light emission. Fumigation by DCM vapor or heating over T_g temperature restored the initial color.
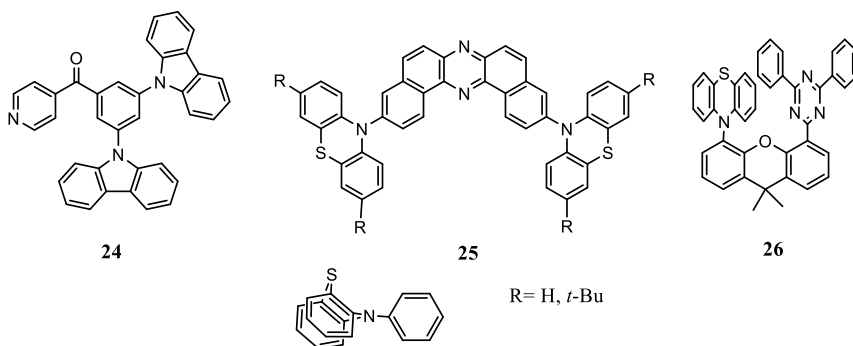
Fig. 2.17 Molecular structure of compounds **24–26** with MCL+TADF characteristics.

## 2.5. Thermally activated delayed fluorescence

Organic light emitting diodes drew significant efforts owning to their low power consumption, flexibility and high external quantum efficiencies. However, many organic molecules were introduced for application in OLEDs, considering the synthesis procedure (fewer steps) and reaction conditions to be synthesized in a large

scale; the material price and their hazardousness are important parameters in the preparation of materials for a field that is relevant to the industry. Moreover, commercialized OLEDs, which were made based on triplet emitters, contain expensive, scarce and toxic noble metals, such as iridium, platinum or osmium, thus they are only seen as a temporary option [61–64].

The major breakthrough in the semiconductor technology was made in 1987, when Tang and Van Slyke reported first promising multilayer OLEDs by using tris(8-quinolinolato)aluminum (III) (Alq₃) and 4,4-cyclohexylidenebis[*N*,*N*-bis(4-methylphenyl)benzenamine] (TAPC) as an emitter and a hole transporting layer (HTL), respectively; then, these thin organic layers were sandwiched between the cathode and the anode [13]. The device showed EQE about 1%, high luminance at 1000 cdm^{-2} and DC voltage at 10 V. Indeed, this report accelerated the research of OLEDs both in the academic circles and in the industry.

Three years later, in 1990, Burroughes and other members of Friend's group fabricated an OLED device with an emitting polymer [65]. The first generation OLED emitted light by a radiative recombination of singlet excitons. In OLEDs, three-fourths of electrically injected holes and electrons form triplets, and one-fourth are singlets. Thus it seems rational to strive to gain the emission from triplet states with 75% of population, but, because of the long life of triplet excitons, nonradiative decay in the form of heat may predominate. The second generation of OLEDs reported in 1998 by Baldo *et al*. was constructed based on organo-metal compounds in order to accomplish 100% of internal electroluminescence quantum efficiency [66]. Literally, noble metals facilitate spin orbit-coupling and, through intersystem crossing (ISC) process accelerates the conversion of excitons from the excited singlet states to the excited triplet states so that to harvest both singlet and triplet excitons to achieve 100% quantum efficiency. Despite substantial effort in phosphorescent OLEDs, the synthesis of blue emitters remains a huge challenge; their lifetimes are several times shorter than those of red and green OLEDs[67–69].

The major fundamental limitation in fluorescence OLED is that 25% of the generated excitons are singlets. In 2009, Adachi's group reported the influence of temperature on the intensity of fluorescence in porphyrine complexes (Fig. 2.18a) [70]. By increasing the temperature, the emission intensity was increased as well. Later on, in 2012, Adachi *et al.* published the first series of OLED compounds (Fig. 2.18b) with an ability to cultivate fluorescence from the excited triples state which were termed as the third generation OLEDs [71].
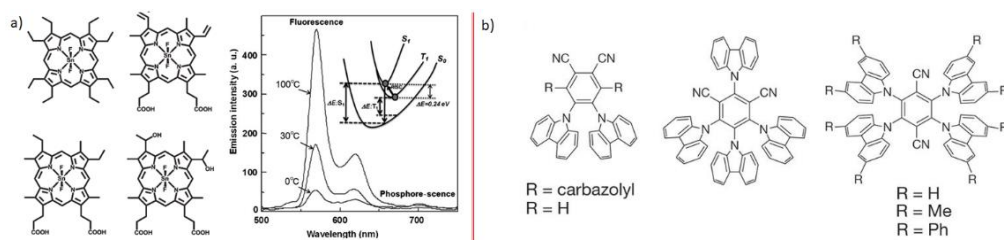
Fig. 2.18 a) Effect of temperature on PL intensity. b) Chemical structure of organic TADF molecules.

Therefore, with this breakthrough, a new way in the design and preparation of OLEDs opened up, which was denoted as TADF-OLED, and it was poised to allow the production of high performance devices. The advances in TADF spurned on efforts to develop metal-free OLEDs, which was followed up by scientists around the world in order to implement commercial application [72]. The driving mechanism in TADF arose from a small splitting energy gap between the excited singlet and triplet states which enabled dark triplet excitons to up-convert into singlet emissive state via reverse intersystem crossing (rISC). The procedure leading to utilize both singlet and triplet excitons and generate bright singlet excitons with 100% internal quantum efficiency [71, 73]. So far, to achieve the low excited S-T gap and TADF compounds, three main routes have been described:

1- Having a high torsion angle between the donor and the acceptor (Fig. 2.19a) so that to minimize the orbital overlapping of the highest occupied molecular orbital (HOMO) and the lowest unoccupied molecular orbital (LUMO) to achieve a small ΔE_{ST} [74, 75].

2- Using exciplexes (molecules with different electron affinity) (Fig. 2.19b) [76, 77].

3- TADF through space (Fig. 2.19c) that the donor and the acceptor are not conjugated, and electron sharing follows FRET or Dexter rules [78–81].

Fig. 2.19 Three ways to design TADF molecules.

It is noteworthy that the high torsion angle might shrink ΔE_{ST}, S1 → S0 radiative decay diminishes, albeit rISC occurs efficiently because of the small ΔE_{ST}. From the other point of view, having a large orbital overlap, a larger ΔE_{ST} leading to a high oscillator strength that determines fluorescence (k_f) also improves the photoluminescence quantum yield [82]. As a consequence, the key is how to design the molecules with a small ΔE_{ST} and a high oscillator strength.

The important criteria for OLED to be an efficient device are the need to apply low voltage and achieve high external quantum efficiency (EQE). The external quantum efficiency can be expressed as the following equation [83]:

$$EQE = \eta_{int}\,\eta_{out}$$

η_{out} = out-coupling constant efficiency
η_{int} = internal quantum efficiency (IQE)
η_{PL} = PL efficiency

In the device, EQE is the number of emitted photons per injected charges. Moreover, the internal quantum efficiency (IQE) is the number of the generated

photons within the OLED per injected charges. The equation of IQE is presented below [83].

$$IQE = n_{r,S} \, \Phi_{PF} + n_{r,S} \, \Phi_{TADF} + n_{r,T} \, \Phi_{TADF}/\Phi_T$$

$n_{r,S}$ = singlet excitons (0.25)
$n_{r,T}$ = triplet excitons (0.75)
Φ_{PF} = PL quantum yield of prompt fluorescence
Φ_T = quantum yield of ISC from S_1 to T_1
Φ_{TADF} = PL quantum yield of TADF

According to the aforementioned equation, high Φ_{TADF}/Φ_T and high Φ_{PF} are required to obtain high IQE. Whereas IQE with 100% is feasible, obtaining a good out-coupling constant still remains a challenge. In 2009 and 2011, Adachi and Yokoyama reported that the planar structure and the high degree horizontal orientation of emitters can enhance the electrical and optical characteristics of luminophores and may increase Φ_{out} by up to 45% [84, 85]. The orientation can be controled by either the synthesis of larger and planar structures or heating the substrate during the device fabrication.

In order to obtain a small ΔE_{ST} for giving efficient TADF, many molecules were synthesized and reported in [74]. Typically, the designed structures adhere to the following rules:
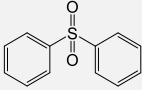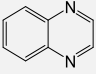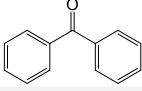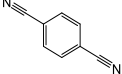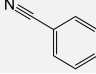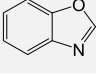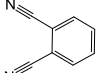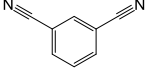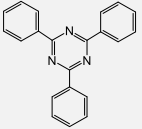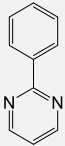
1- Steric hindrance between the donor and the acceptor [75];
2- Introduction of a bridge between the donor and the acceptor so that to enlarge the D/A separation distance [75, 86];
3- Meta-linked D-A architecture causes a spatial separation of HOMO and LUMO [86, 87];
4- Spiro compounds; by breaking the p-conjugation between the donor and the acceptor [88];
5- A strong acceptor or donor can descend the S-T energy band gap [75].

By possessing this knowledge, we need to know how to design and synthesize TADF molecules in the desired color region. Aside from their appealing applications in the visible range, in order to generate chromophores, we must define several criteria, such as the strength of the donor/acceptor, or HOMO/LUMO energy levels, and predict the created twist angle between D-A. Since the donor/acceptor pair usually was not investigated separately, the relevant data was obtained by molecular calculation. Besides, the behavior of coupled D-A in a chromophore is different from the individual unit. In brief, a strong donor and a strong acceptor cause a small S-T energy gap as well as shrinking of the HOMO-LUMO gap, and it consequently drives the emission towards longer wavelengths. Nevertheless, to date, many acceptors that have been introduced in TADF-OLED, electron donating groups are still restricted to carbazole, phenoxazine, phenothiazine, diphenyl amine, 9,9'-dimethyl acridine and their derivatives. Firstly, we need to take a general look at some common acceptors/donors and their singlet/triplet energy levels, then we shall briefly describe

the strategies developed to design the chromophores and the effect of moieties on the device efficiency.
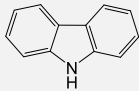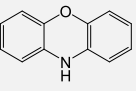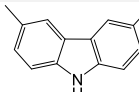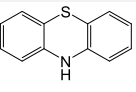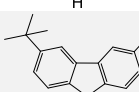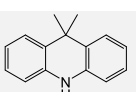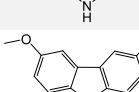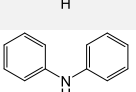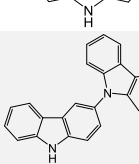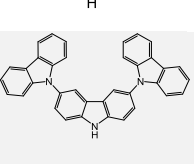
Table 2.1 demonstrates the lowest singlet and triplet energy levels of compounds. Among the acceptors, usually, quinoxaline and phthalonitrile derivatives are strong acceptors and drive the emission of the chromophore over the blue region.

Table 2.1 Acceptors and ST energies.

Acceptor	Chemical structure	E_S/E_T (eV)	Acceptor	Chemical structure	E_S/E_T (eV)
Sulfonyldibenzene		4.47/3.61	Quinoxaline		3.56/2.80
Benzophenone		3.57/2.94	Terephthalonine		4.89/3.08
Benzonitrile		5.05/3.44	Benzo[d]oxazole		5.10/3.53
Phthalonitrile		4.71/3.17	Isophthalonitrile		4.63/3.24
2,4,6-triphenyl-1,3,5-triazine		3.96/3.02	2-Penyl pyrimidine		4.04/3.11

As mentioned above, the torsion angle is a prominent factor to conduct a TADF molecule; therefore, it is worth to have a look at the influence of donors on it. These angles are in a wide range and depend on the substituents of the donor and the adjacent neighboring moieties. In general, diphenylamine and carbazole produce a dihedral angle in the range of 35–50°, with a phenyl group as the bridge. Meanwhile, stronger and bulky donors, such as phenoxazine and 9,9'-dimethyl acridine, lead to the observation of the twist angle around 80°. Phenothiazine, by having a large sulfur atom in the structure, can emerge as both quasi-axial and quasi-equatorial conformation, and, consequently, the dihedral angle is depend on the generated conformations. Evidently, incorporated bulky fragments cause steric hindrance between the donor and the adjacent moiety to effect the twist angle. In addition, bulky fragments may prevent molecular motions. As a consequence, rigidifyed molecular structure would reduce non-radiative transitions that have a profound impact on PLQY enhancement.

Table 2.2 Donors and ST energies.

Donor	Chemical structure	E_S/E_T (eV)	Donor	Chemical structure	E_S/E_T (eV)
9*H*-carbazole		3.63/2.95[a]	phenoxazine		3.66/2.81
3,6-dimethyl-9H-carbazole		4.05/3.15	phenothiazine		3.42/2.69
3,6-di-tert-butyl-9*H*-carbazole		4.01/3.17	9,9-dimethylacridine		3.78/3.19
3,6-dimethoxy-9H-carbazole		3.21/2.89[a]	diphenylamine		3.86/3.24
9*H*-3,9'-bicarbazole		3.33/3.16	9'*H*-9,3':6',9"-tercarbazole		3.34/3.08

2.5.1. Effect of donors

The synthesis of an efficient blue emitter is a big challenge in OLED; thus it has been in the focus of intense research recently. Owing to the wide band gap in the blue materials, operation of high voltage is needed to overcome the charge injection from adjacent layers to match the HOMO and LUMO levels of the layers. Besides, a large gap between the ground state and the excited state, and the mismatching of the adjacent layers have been poising problems both in terms of stability and device efficiency [90, 91]. In most reported cases, for blue emitters, a few fragments (triazine, benzophenone, sulfonyldibenzyle and benzonitrile moieties) have been used as the acceptor units which will be explained in detail below [92].

Triazine is one of the most promising acceptors in the blue region. In 2017, Kim and his team studied the effect of a bridge on the S-T energy gap and device efficiency [93, 94]. However, the enlarged bridge in compound **28** rendered a smaller ΔE_{ST}, and, on the contrary, EQE dropped from 22.3% to 4.7%.
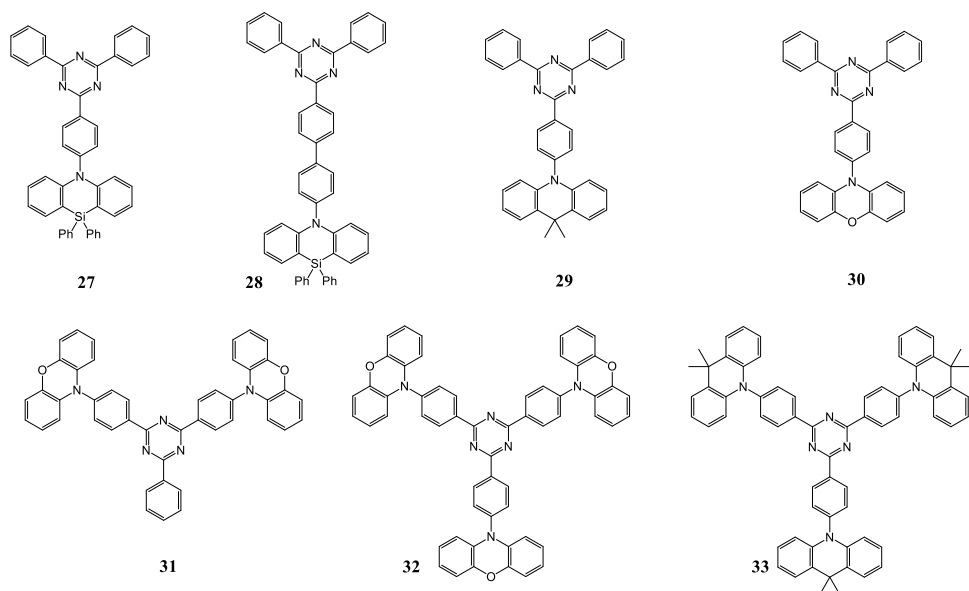
Fig. 2.20 Chemical structure of triazine containing materials.

Indeed, the reduction of the oscillator strength reflects the low PLQY. The weaker oscillator strength follows by an extended distance between the donor and the acceptor. Moreover, in this work, by using azasiline as the donor spectrum compared with 9,9'-dimethyl acridine (DMAC), the spectrum was blue-shifted. By using dimethyl acridine, chromophore **29** depicted a higher wavelength at 495 nm, and EQE went up to 26.5% [95]. The device efficiency decreased to 12.5% when phenoxazine was used as the donor, and for compound **30**, the spectrum shifted to 529 nm [96]. In addition, using phenoxazine as dyad **31** and triad **32** was also investigated, and red-shifted emissions, besides 9.1%, and 13.3% of EQE were observed, respectively. The addition of three DMAC (triad **33**) as an electron donating group that is weaker than phonoxazine represented an emission band peak at 511 nm and resulted in an EQE of 18.6%.

Due to the valuable features, such as chemical stability, high triplet level, and high thermal stability, carbazole derivatives have been considered as valuable donors [97, 98]. In the studies presented below, carbazole and triazine were combined without a bridge. The luminogens consist of carbazole derivatives which emerged in the sky blue and green spectra range with a ΔE_{ST} below 0.1 eV, while the maximum EQE was 14% [99–101]. Compounds **34**, **35** and **36** represented ΔE_{ST} of 0.05, 0.02 and 0.07 eV, respectively. The highest EQE was obtained for compound **35** at 14%, whereas compounds **34** and **36** demonstrated 11% and 6%, respectively. In the case of **35**, a higher steric repulsion of carbazole with a triazine unit shrank the orbital overlapping.
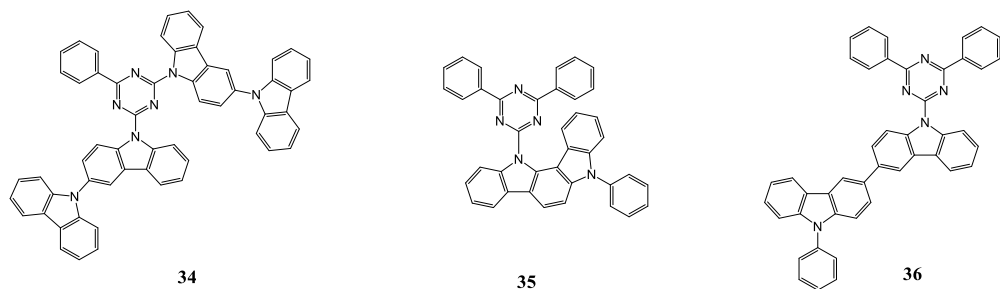
Fig. 2.21 Chemical structure of **34**–**39**, chromophores without bridge.

A substituent on the donor alongside the phenyl linkage resulted in further conjugation, which drove the spectrum towards a higher wavelength; the EQE thus increased. Therefore, the direct connection of D-A caused a lower efficiency of the device. Luminogens **37**, **38**, **39** and **40** contain the same acceptor, and a major difference from the previous compounds is the presence of the phenyl linkage [102, 103]. Besides, in this category of compounds, extra fragments are added on carbazole. With regard to compounds **37** to **40**, their emissions peaked at 477 nm, 478 nm, 487 nm and 492 nm, respectively. Aside from their influence on the wavelength, 14.6%, 16.8%, 20.6% and 21.7% device efficiencies were observed for compounds **37** to **40**, respectively. Consequently, closely looking at the structures disclose that the embedding bridge between D-A enhances EQE, plausibly because of the larger fluorescence oscillator strength. Additionally, extra moieties on the donor may lead to the restriction of motions for the donor and/or prevention of π-π stacking.
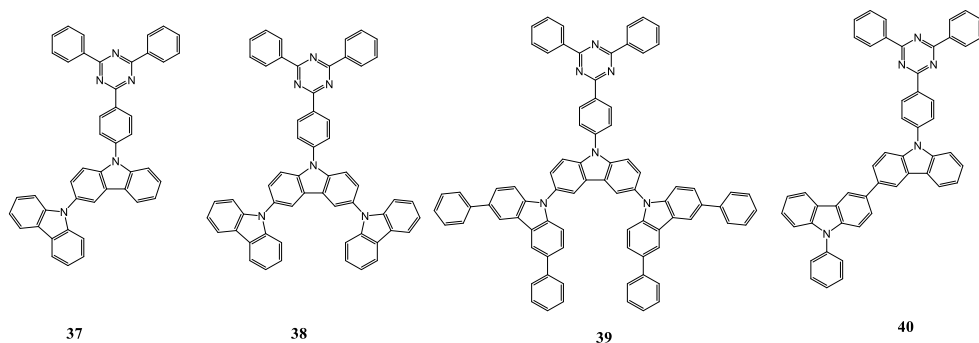
Fig. 2.22 Chemical structure of derivatives of triazine.

Benzophenone contains a twist angle in the center which prevents a planar structure and face-to-face aggregation. In 2014, a series of butterfly-shaped benzophenone derivatives were reported by Adachi *et al.* [104]. Blue emission with a peak at 446 nm and a ΔE_{ST} of 0.21 eV was detected for compound **42**; peaks at 484 nm and 539 nm (ΔE_{ST} of 0.14 eV and 0.03 eV) were exhibited by compounds **43** and **44**, respectively. Attaching another carbazole onto the 3rd position of carbazole enhanced the EQE from 8.1% to 14.3%. By using highly twisted phenoxazine, the EQE was 10.7%, which is higher than the values of compound **42**.

32
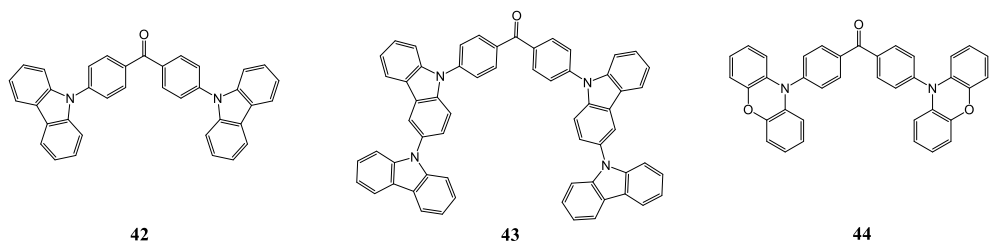
Fig. 2.23 Chemical structure of **42**–**44** with benzophenone as the acceptor.

Acceptors based on sulfone and its derivatives are commonly used in blue/green TADF emitters. Diphenyl sulfone involves a 5-membered ring core containing three aromatic rings, has a further conjugation and causes red-shifting. Through replacing di-*tert*-butylcarbazole (**45**) with di-methoxycarbazole (**46**), EQE was enhanced from 9.9% to 14.5%, and the emission was red-shifted up to 60 nm [105, 106]. The sky blue and green TADF with 19.5% and 17.5% EQE was reported with DMAC **47** and PXZ **48** as the electron donating groups [107, 108]. The singlet-triplet gap was demonstrated at 0.32 eV, 0.21 eV, 0.08 eV and 0.08 eV, respectively, for compounds **45**–**48**. Notably, studying diphenyl sulfone with a 5-membered ring (**49**, **50**) revealed that, in this planar acceptor, ΔE_{ST} increased to 0.35 eV for compound **49**, while for compound **50**, it is 0.19 eV [109, 110]. In addition, devices showed 14.0% and 14.3% EQE for compounds **49** and **50**, respectively. Therefore, the twisted acceptor shrinks ΔE_{ST} and yields blue-shifted emitters. Besides, stronger donors have more impact on the improvement of device efficiency.
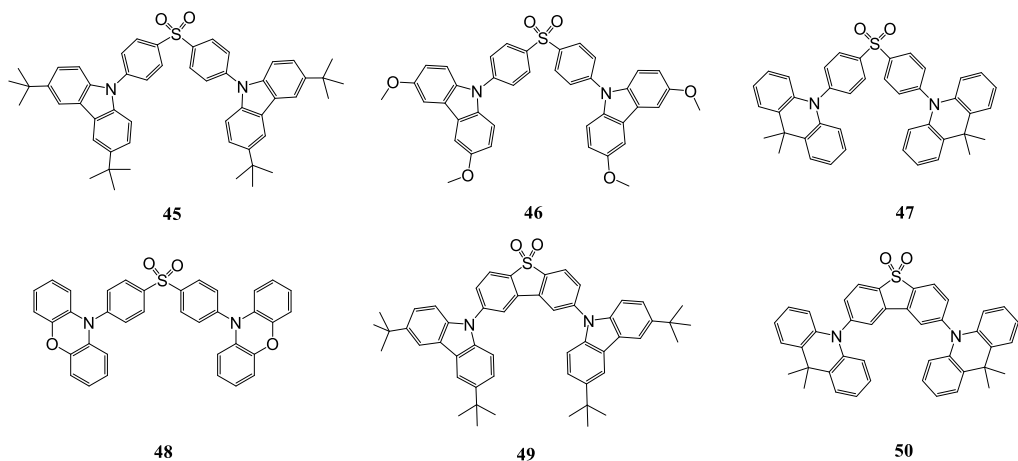
Fig. 2.24 Molecular structure of **45**–**50**.

In 2018, Yang *et al.* [111] studied the photophysical properties of quinoxaline-based acceptors with 9,10-dihydro-acridine or 10*H*-phenoxazine as the electron donating units (Fig. 2.25). Green emission with PL spectra at 532 and 534 nm for **51** and **52** and orange emission at 572 nm for both **53** and **54** were reported, respectively. Materials with three donors, **52** and **54**, demonstrated a higher EQE than chromophores with one donor. The highest EQE was observed for **52** at 22.4%, and

33

compounds **51**, **53** and **54** showed 13.0%, 11.1% and 14.1% of external quantum efficiency.
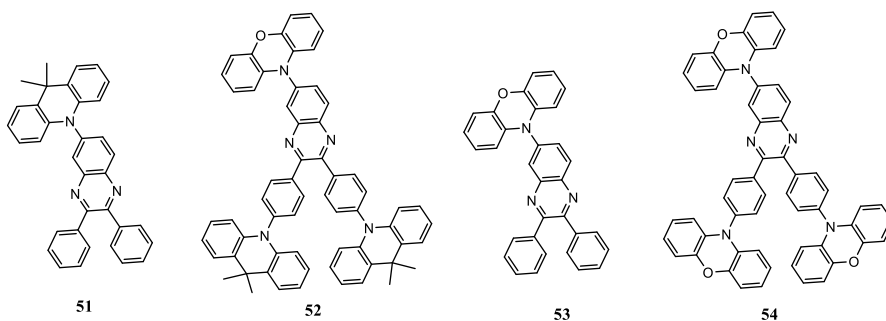
Fig. 2.25 Chemical structure of derivatives of quinoxaline.

2.5.2. Effect of acceptor

1,2-Dicarbonyle and dicyanopyrazine as acceptor units were combined with di-*tert*-butylcarbazole and 9,9-dimethylacridine with the objective to prepare TADF molecules. The HOMO/LUMO energy gap was decreased after replacing 2,3-diaminomalononitrile with 1,2-dicarbonyle. Green-emitting OLED based on compound **55** demonstrates the emission peak at 518 nm with 0.13 eV of ΔE_{ST}, which alters to a peak at 534 nm and 0.43 eV when using compound **56** [112]. The maximum EQE of 6.2% and 15.6% was reported respectively for compounds **55** and **56**. Acridine-based donors **57** and **58** represent emission peaks at 532 nm and 576 nm and EQE of 6.3% and 15.6%, respectively [111]. Moreover, smaller S-T gaps were obtained for DMAC compound **57** at 0.01 eV and for compound **58** $\Delta E_{ST} = 0.08$ eV. It can be claimed that, still, compounds **55** and **57** with bent conformations contain a smaller ΔE_{ST}, and their efficiency is lower, which implies that non-radiative transitions are suppressed in dicyanopyrazine. Furthermore, in the case of stronger acceptor, variation of the donor has a further impact on the alteration of the emission band.
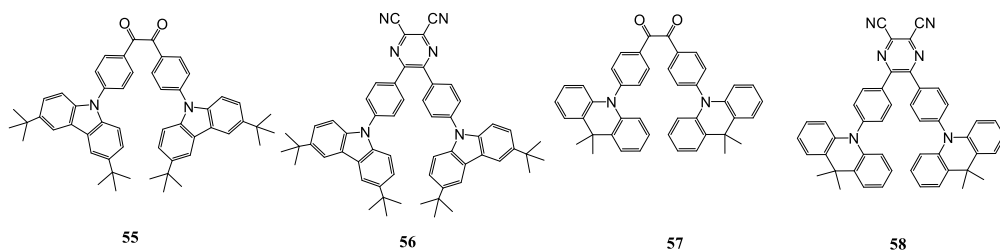
Fig. 2.26 Structures of 1,2-dicarbonyle and dicyanopyrazine derivatives.

2.5.3. TADF molecule with narrow emission

Although spectrum with a wide emission is advantageous in light applications. Nowadays, OLEDs are extensively applied in display screens which pursue narrow

emission with high color purity. In TADF molecules, emission arises from the charge transfer state (CT), and a highly twisted structure would achieve a wider peak. Therefore, in TADF molecules, the elimination of various emitting CT states to a few CT states is a desirable perspective.

Donor rotation around a single bond with the acceptor may broaden the emission spectra thus manifesting that the restriction of rotation may purify the color. There exists an approach that in order to sharpen the emission, we need to apply steric hindrance between D–A in the molecular design [113].

2.6.   Conclusions from literature review

The preceding subchapters addressed a brief overview of the most recently investigated and prominent luminogens with MCL and TADF characteristics. In the first section, we emphasized the chemical structure, the color variations and the applied ways to alter the luminescence in response to external stimuli. Multicolor luminescence variations under external stresses are usually obtained via applying high pressure or are observed for macromolecules with costly metal complexes. Therefore, simple, low-cost and small molecules which emerge as emitting materials are extremely rare.

Following on from the chemical structures for MCL materials, the parameter influence on the device efficiency and strategies in the TADF molecule architecture in the desired range of the spectrum was discussed. The effect of the phenyl linkage, the acceptor and the donors on the color emission, the variation of the singlet/triplet energy level and the device efficiencies were covered.

3. EXPERIMENTAL PART

3.1. General information

The starting materials, such as *o*-phenylenediamine (98%), 9*H*-carbazole (97%), 2-chloro-2-methylpropane (99%), $ZnCl_2$ (99%), CH_3COOH (99.9%), $Pd(OAc)_2$ (98%), $Pd_2(dba)_3$ (97%), XPhos (97%), 4,4′-dibromobenzil (90%), 2,3-diaminopyridine (98%), CuI (99%), PPh_3 (98%), 10,11-Dihydro-5*H*-dibenz[*b,f*]azepine (97%), 5*H*-Dibenz[*b,f*]azepine (97%), *t*-BuONa (98%) were purchased from *Sigma-Aldrich* and used without further purification. In addition, toluene was dried with a molecular sieve (4Å) and used for cross coupling reactions, while other substances were used without further drying.

^{1}H and ^{13}C NMR spectroscopy was carried out on a *Bruker Avance 400 NMR* spectrometer at 400 MHz and 100 MHz, respectively; δ in ppm. The residue signals of the solvents were used as internal standards. MS data was recorded on *UPLC-MS Acquity Waters SQ Detector 2*.

The absorption spectra of 10^{-4} M solutions or films were measured with a *Perkin Elmer Lambda 35* spectrometer or *UV-3600* double beam spectrophotometer (*Shimadzu*). Photoluminescence (PL) spectra of 10^{-5} M solutions, films, and powders were recorded by using *Edinburgh Instruments' FLS980 Fluorescence Spectrometer* or *FluoroMax-3* fluorescence spectrometer (*Jobin Yvon*). In these measurements, there is an associated uncertainty of about 1–3 nm involved, each measurement was repeated three times. Phosphorescence, prompt fluorescence (PF), and delayed fluorescence (DF) spectra and fluorescence decay curves were recorded by using nanosecond gated luminescence and lifetime measurements (from 400 ps to 1 s) by using either the third harmonics of a high energy pulsed Nd:YAG laser emitting at 355 nm (EKSPLA) or a N_2 laser emitting at 337 nm. In these measurements, the associated uncertainties are variable and are included in the relevant graphs. The emission was focused onto a spectrograph and detected on a sensitive gated iCCD camera (*Stanford Computer Optics*) having sub-nanosecond resolution. The PF/DF time resolved measurements were performed by exponentially increasing the gate and integration times. Temperature-dependent experiments were conducted by using a continuous flow liquid nitrogen cryostat (*Janis Research*) under nitrogen atmosphere, while measurements at room temperature were recorded in vacuum in the same cryostat. The uncertainty of the PL quantum yield is about 3–5%.

Power dependence data was fitted by using two expressions: $a \cdot x^b$ (I) for power laws and $a \cdot x$ (II) for linear relation. In the first attempt, we try to use linear expression (II) for fitting. If the data can be fitted by using a linear expression, then it is described as a linear fit. If the data cannot be fitted with expression (II), then we attempt to use power law expression (I) for fitting. In this case, the power law exponent is fitted, and its value is presented.

Thermogravimetric analysis (TGA) was performed on a *Metter TGA/SDTA851e/LF/1100* apparatus at a heating rate of 20 °C/min under nitrogen atmosphere. Differential scanning calorimetry (DSC) measurements were done on a *DSC Q 100 TA* Instrument at a heating rate of 10 °C/min under nitrogen atmosphere.

Cyclic voltammetry (CV) measurements were carried out with *Eco Chemie* Company's *AUTOLAB* potentiostat *PGSTAT20* and a glassy carbon working electrode in a three electrode cell. The measurements were performed in 0.1 M nBu$_4$NPF$_6$ solution in anhydrous dichloromethane at room temperature under nitrogen atmosphere. HOMO and LUMO levels were acquired by using equation [59] (Given ± 0.06 eV error in each measurement, repeated 3–5 times):

$E_{HOMO} = - (E^{1/0}_{1/2}$ (vs. Fc$^+$/Fc) +4.8);

$E_{LUMO} = - (E^{0/1}_{1/2}$(vs. Fc$^+$/Fc) + 4.8).

OLEDs were fabricated by employing the spin-coating/evaporation hybrid method. The hole injection layer (*Heraeus Clevios HIL 1.3N*), the electron blocking/hole transport layer (PVKH), and the emitting layer (PVK:PBD + dopant) were spin-coated, whereas the electron transport layer (TPBi) and the cathode (LiF/Al) were evaporated. Devices of 4x2mm pixel size were fabricated. PVK – poly(9-vinylcarbazole) (MW = 90 000, *Acros Organics*), PVKH – poly(9-vinylcarbazole) (MW = 1 100 000, *Sigma Aldrich*), PBD – 2-(biphenyl-4-yl)-5-(4-*tert*-butylphenyl)-1,3,4-oxadiazole (99%, *Sigma Aldrich*), TPBi – 2,2',2"-(1,3,5-Benzinetriyl)-tris(1-phenyl-1-*H*-benzimidazole) (sublimed, *LUMTEC*), LiF (99.995%, *Sigma Aldrich*), and Aluminum wire (99.9995%, *Alfa Aesar*) were purchased from the companies indicated in parentheses. OLED devices were fabricated by using pre-cleaned indium-tin-oxide (ITO) coated glass substrates after ozone plasma treatment with a sheet resistance of 20 Ω cm^{-2} and ITO thickness of 100 nm. *Heraeus Clevios HIL 1.3N* was spun-coated and annealed onto a hotplate at 200 °C for 3 min to yield 45 nm film. The electron blocking/hole transport layer (PVKH), was spun from chloroform:chlorobenzene (95:5 v/v) (3 mg/mL) and annealed at 50 °C for 5 min to obtain 10 nm film. The emitting layer was spun from a toluene solution of PVK:PBD (60:40 w/w) with the total concentration of the host 10 mg/mL. The dopant was dissolved in the host solution in order to obtain the final 5% w/w concentration of the emitting layer in PVK:PBD. The solution was spun onto the PVKH layer and then annealed at 50 °C for 5 min thus obtaining a 32 nm film. All the solutions were filtrated directly before application by using a PVDF or PTFE syringe filter with 0.45 μm pore size. All other organic and cathode layers were thermally evaporated by using *Kurt J. Lesker Spectros II* deposition system at 10^{-6} mbar. All the organic materials and aluminum were deposited at a rate of 1 Å s^{-1}. The LiF layer was deposited at 0.1–0.2 Å s^{-1}. The characterization of OLED devices was conducted in a 10-inch integrating sphere (*Labsphere*) connected to a Source Measure Unit.

The crystallographic nature of the powder materials was determined by using a *D8 Discover* X-ray diffractometer (*Bruker AXS GmbH*) with a Cu Kα (λ= 1.54 Å) X-ray source. Parallel beam geometry with 60 mm Göbel mirror (i.e., X-ray mirror on a high precision parabolic surface) was used. This configuration enables transforming the divergent incident X-ray beam from the line focus of the X-ray tube into a parallel beam that is free of Kβ radiation. The primary side also had a Soller slit with an axial divergence of 2.5 ° and a slit of 1 mm. The secondary side had a *LYNXEYE* (1D mode) detector with an opening angle of 2.160 ° and a slit opening of 6.0 mm. The X-ray

generator voltage and current were 40.0 kV and 40 mA, respectively. Coupled 2θ/θ scans were performed in the range of 3.0–60.0 ° with a step size of 0.065 °, time per step of 19.2 s and with the auto-repeat function enabled. Processing of the resultant diffractograms was performed with *DIFFRAC.EVA* software.

The single crystals of compounds were obtained from the mixture of solvents (DCM, acetone, hexane). Yellow color single crystals were mounted on the glass capillary by using glue. The crystallographic analysis was performed by employing *XtaLAB* mini diffractometer (*Rigaku*) with graphite monochromated Mo Kα (λ=0.71075 Å) X-ray source. The measurements were performed at a temperature of 293 K. The crystallographic data for structures IDBQx and ISBQx reported in this work has been deposited in *Cambridge Crystallographic Data Centre* with CCDC Nos. 1861441–1861442. The copies of our data can be obtained free of charge on application to CCDC (The Cambridge Structural Database (CSD) – The Cambridge Crystallographic Data Centre (CCDC), (http://www.ccdc.cam.ac.uk/solutions/csd-system/components/csd/). Calculations/visualizations were performed by using the OLEX2 crystallographic software package except for refinement which was performed by using *SHELXL*. For molecule, the ISBQx, solvent mask procedure was used. Anisotropic thermal parameters were assigned to all nonhydrogen atoms. The hydrogens were included in the structure factor calculation at idealized positions by using a riding model and refined isotropically.

3.2. Synthetic Procedure

2,3-Dichloroquinoxaline (I), 3,6-dimethoxy-9H-carbazole, 3,6-di-*tert*-butyl-9*H*-carbazole, 3-bromo-9*H*-carbazole and 3,6-dibomo-9*H*-carbazole were prepared according to the procedure reported previously [114–116].

3-Methoxy-9*H*-carbazole:
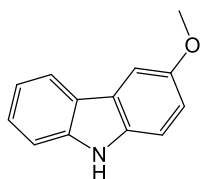
Na (2.2 g) was dissolved in dry MeOH (40 mL) under N_2, and then 3-bromo-9*H*-carbazole (2.23 g, 9.1 mmol), CuI (1.73 g, 9.1 mmol) and DMF (60 mL) were added and stirred at 125 °C for 12 h. After cooling to room temperature, the crude product was filtered through silica gel, washed in EtOAc and evaporated. The combined organic layers were purified by column chromatography on silica gel (n-hexane/DCM 1:2) to afford a white powder (1.23 g, 69%). Mp= 146–148 °C. ^{1}H NMR (400 MHz, CDCl3): δ_H = 3.83 (3H, s, MeO), 6.97 (1H, dd, [3]*J*= 8.7 Hz, [4]*J*= 2.5 Hz, CH), 7.11 (1H, t, [3]*J*= 7.8 Hz, CH), 7.17 (1H, d, [3]*J*= 8.7 Hz, CH), 7.25 (1H, d, [3]*J*= 7.9 Hz, CH), 7.31 (1H, t, [3]*J*= 7.9 Hz, CH), 7.46(1H, d, [4]*J*= 2.4 Hz, CH), 7.74 (1H, br s, NH), 7.93 (1H, d, [3]*J*= 7.7 Hz, CH) ppm. ^{13}C NMR (100 MHz, CDCl₃): δ_C = 56.1, 103.2, 110.7, 111.3, 115.1, 119.0, 120.2, 123.3, 123.7, 125.8, 134.4, 140.3, 153.9 ppm.

2,3-Di(9*H*-carbazol-9-yl)quinoxaline (CzQx):
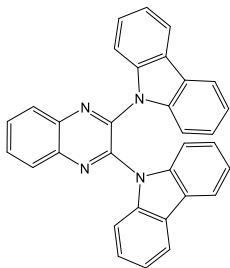
Procedure A: A mixture of carbazole (2.1 mmol) and K_2CO_3 (2.2 mmol) was dissolved in 7 mL DMSO and stirred for 20 min, then 2,3-dichloroquinoxaline (1 mmol) was added, and the reaction mixture was stirred at 90 °C for 7 h. After completion, the reaction mixture was cooled to room temperature, 100 mL of brine was added to the mixture and filtered. The crude compound was purified by flash column chromatography (n-hexane/ethyl acetate 10:1) to give green crystals. Mp= 295 °C. Yield (369 mg, 78%). ^1H NMR (400 MHz, CDCl$_3$): δ_H = 6.94 (4H, t, ^3J= 8.4 Hz, 4CH), 7.01 (4H, t, ^3J= 8.4 Hz, 4CH), 7.26 (4H, t, ^3J= 8.1 Hz, 4CH), 7.70 (4H, t, ^3J= 7.4 Hz, 4CH), 7.82 (2H, dd, ^3J= 6.3 Hz, ^4J= 3.4 Hz, 2CH), 8.2 (2H, dd, ^3J= 6.3 Hz, ^4J= 3.4 Hz, 2CH) ppm. ^{13}C NMR (100 MHz, CDCl$_3$): δ_C = 110.3, 119.8, 121.3, 124.3, 125.3, 128.6, 130.7, 138.7, 140.5, 141.9 ppm. MS, *m/z* = 461 ([M+H]$^+$, 45%).

2,3-Bis(3,6-di-*tert*-butyl-9*H*-carbazol-9-yl)quinoxaline (tCzQx):
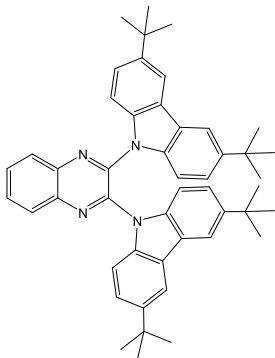
Procedure B: A mixture of 3,6-di-*tert*-butyl-9H-carbazole (720 mg, 2.6 mmol) and NaO*t*-Bu (260 mg, 2.7 mmol) was dissolved in 7 mL of DMF and stirred at room temperature for 20 min, then 2,3-dichloroquinoxaline (250 mg, 1.26 mmol) was added, and the reaction mixture was stirred at 90 °C for 7 h. After completion, the reaction mixture was cooled to room temperature, 50 mL of brine was added to the mixture, and it was extracted with EtOAc (3×15 mL). The combined organic layers were dried over Na$_2$SO$_4$ and evaporated to afford the crude product which was purified by column chromatography on silica gel (n-hexane/toluene 2:1) to afford a green powder. Mp= 326 °C. Yield (620 mg, 72%). ^1H NMR (400 MHz, CDCl$_3$): δ_H = 1.26 (36 H, s, 4CMe$_3$), 6.82 (4H, dd, ^3J= 8.6 Hz, ^4J= 1.9 Hz, 4CH), 7.00 (4H, t, ^3J= 8.6 Hz, 4CH), 7.52 (4H, d, ^4J= 1.8 Hz, 4CH), 7.80 (2H, dd, ^3J= 6.5 Hz, ^4J= 3.0 Hz, 2CH), 8.18 (2H, dd, ^3J= 6.5 Hz, ^4J= 3.0 Hz, 2CH) ppm. ^{13}C NMR (100 MHz, CDCl$_3$): δ_C = 31.8, 34.5, 109.6, 115.3, 123.3, 124.3, 128.5, 130.1, 137.0, 140.3, 142.2, 143.9 ppm. MS, *m/z* = 684 ([M+H]$^+$, 8).

2,3-Bis(3-methoxy-9*H*-carbazol-9-yl)quinoxaline (MeOQx):
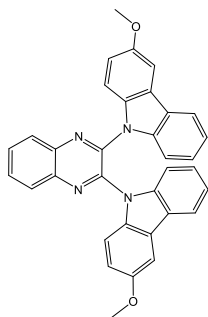
It was prepared from 3-methoxy-9*H*-carbazole by employing a procedure similar to procedure A. The crude product was purified by flash column chromatography (n-Hexane/DCM 4:1) to give a yellow powder. Mp= 262 °C. Yield (317 mg, 61%). ^{1}H NMR (400 MHz, CDCl$_3$): δ_H = 3.74 (6 H, s, 2MeO), 6.60 (2H, dd, ^3J= 8.9, ^3J= 2.5,2CH), 6.93–7.02 (4H, m, 4CH), 7.18–7.28 (6H, m, 6CH), 7.60 (2H, dd, ^3J= 7.7 Hz, ^4J= 4.1 Hz, 2CH), 7.78 (2H, dd, ^3J= 6.4 Hz, ^4J= 3.5 Hz, 2CH), 8.15 (2H, dd, ^3J= 6.4 Hz, ^4J= 3.5 Hz, 2CH) ppm. ^{13}C NMR (100 MHz, CDCl$_3$): δ_C = 55.8, 103.0, 110.4, 110.5, 111.2, 111.2, 114.4, 119.8, 121.0, 124.3, 125.1, 125.9, 128.4, 130.4, 133.4, 133.5, 139.2, 139.2, 140.3, 141.8 ppm. MS, m/z = 520 ([M]$^+$, 36%).

2,3-Bis(3,6-dimethoxy-9*H*-carbazol-9-yl)quinoxaline (MeO2Qx):
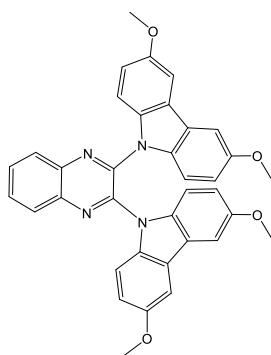
It was prepared from 3,6-dimethoxy-9*H*-carbazole as mentioned in procedure B. The crude compound was purified by flash column chromatography (n-hexane/DCM 2:1) to give the product which was ellow powder. Mp= 235 °C. Yield= (373 mg, 57 %). ^{1}H NMR (400 MHz, CDCl$_3$): δ_H = 3.75 (12 H, s, 4MeO), 6.61 (4H, dd, ^3J= 8.8 Hz, ^4J= 2.1 Hz, 4CH), 7.17–7.18 (6H, m, 8CH), 7.20 (2H, s, CH), 7.76 (2H, dd, ^3J= 6.4 Hz, ^4J= 3.4 Hz, 2CH), 8.11 (2H, dd, ^3J= 6.4 Hz, ^4J= 3.4 Hz, 2CH) ppm. ^{13}C NMR (100 MHz, CDCl$_3$): δ_C = 55.8, 102.8, 111.4, 114.7, 125.1, 128.3, 130.2, 134.0, 140.2, 141.8, 154.8 ppm. MS, m/z = 580 ([M]$^+$, 100).

Synthesis of 2,8-dibromo-10,11-dihydro-5*H*-dibenzo[*b,f*]azepine:
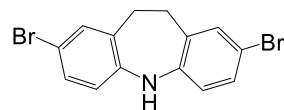
Iminodibenzyl (5 mmol) was added to a solution of DCM (15 mL) in silica gel (2 g). After stirring for 5 min, *N*-bromosuccinimide (NBS, 10 mmol, 1.78 g) dissolved in DCM:DMF (25:15 mL) was added dropwise and stirred for 1 h at room temperature. The reaction mixture was filtered and washed with DCM. The crude product was purified by column chromatography (n-hexane/EtOAc 10:1) to yield a white powder. Yield (1.10 g, 63%). ^{1}H NMR (400 MHz, DMSO-d$_6$): δ_H = 8.58 (1H, s, NH), 7.2 (2H, s, CH), 7.19 (2H, d, ^3J= 9.4 Hz, CH), 6.91 (2H, d, ^3J= 9.2 Hz, CH), 2.92 (4H, s, CH$_2$) ppm. ^{13}C NMR (100 MHz, DMSO-d$_6$): δ_C = 142.2, 132.8, 130.6, 129.6, 120.4, 110.1, 34.5 ppm. MS, m/z = 350 ([M-H]$^+$, 36%) 353 ([M+2, 100%]$^+$).

Synthesis of 2,8-dimethoxy-10,11-dihydro-5*H*-dibenzo[*b,f*]azepine:
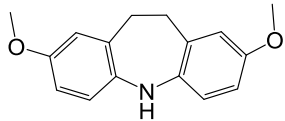
Na (3.2 g) was dissolved in dry MeOH (25 mL) under N_2 at 0 °C, and then 2,8-dibromo-10,11-dihydro-5*H*-dibenzo[*b,f*]azepine (1.1 g, 3.1 mmol), CuI (1.18 g, 6.2 mmol) and DMF (30 mL) at 125 °C for 12 h was stirred. After cooling to room temperature, the mixture was filtered through silica gel with EtOAc and evaporated, washed with water and dried over Na_2SO_4. The combined organic layers were purified by column chromatography on silica gel (n-Hexane/EtOAc 6:1) to afford a white product. Yield (616 mg, 78%). ^{1}H NMR (400 MHz, DMSO-d$_6$): δ_H = 7.66 (1H, s, NH), 6.85 (2H, d, ^3J= 8.6 Hz, CH), 6.64-6.59 (4H, m, CH), 3.66 (6H, s, OMe), 2.92 (4H, s, CH$_2$) ppm. ^{13}C NMR (100 MHz, DMSO-d$_6$): δ_C = 152.2, 138.0, 129.0, 119.1, 115.6, 112.8, 55.6, 34.7 ppm. MS, m/z = 254 ([M+H]$^+$, 100%). HRMS (ESI): calcd for $C_{16}H_{17}NO_2$ ([M+H]$^+$): 255.1259; found: 255.1253.

Synthesis of 2,3-bis(4-(10,11-dihydro-5*H*-dibenzo[*b,f*]azepin-5-yl)phenyl)quinoxaline (IDBQx):
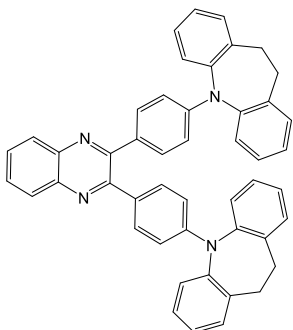
Procedure A: A two-neck flask was charged with Iminodibenzyl (468 g, 2.4 mmol), 2,3-bis(4-bromophenyl)quinoxaline (438 mg, 1 mmol) and NaO*t*-Bu (250 mg), evacuated and backfilled with N_2 for 3 times. Then, Pd(OAc)$_2$ (22 mg, 0.01 mmol, 10 mol%) and *t*Bu$_3$P (25 mg, 0.12 mmol, 12 mol%) were added under flow on nitrogen, and followed by charging with 10 mL of toluene. The reaction was stirred overnight at reflux. After cooling to room temperature, the mixture was filtered through silica gel by CHCl$_3$, and concentrated in vacuum. The crude product was isolated by column chromatography on silica gel (n-hexane/EtOAc 4:1) to afford a yellow powder. Mp= 286 °C. Yield (454 mg, 68%). ^{1}H NMR (400 MHz, CDCl$_3$): δ_H = 7.98 (2H, dd, ^3J= 6.1 Hz, ^4J= 3.3 Hz, CH), 7.54 (2H, dd, ^3J= 6.4 Hz, ^4J= 3.4 Hz, CH), 7.34 (4H, d, ^4J= 7.6 Hz, CH), 7.25 (4H, d, ^3J= 8.8 Hz, CH), 7.20–7.12 (12H, m, CH), 6.44 (4H, d, ^3J= 8.8 Hz, CH), 2.89 (8H, s, CH$_2$) ppm. ^{13}C NMR (100 MHz, CDCl$_3$): δ_C = 153.4, 149.6, 143.2, 140.7, 138.2, 130.9, 130.6, 129.9, 129.0, 128.7, 127.3, 127.1, 112.3, 30.7 ppm. MS, m/z = 668 ([M]$^+$, 19%), HRMS (ESI) calcd for $C_{48}H_{36}N_4$ ([M+H]$^+$): 669.3013; found: 669.3013.

Synthesis of 2,3-bis(4-(5*H*-dibenzo[*b,f*]azepin-5-yl)phenyl)quinoxaline (ISBQx):

Procedure B: A two-neck flask was charged with iminostilbene (340 mg, 1.76 mmol), 2,3-bis(4-bromophenyl)quinoxaline (365 mg, 0.83 mmol) and NaO*t*-Bu (354 mg, 3.8 mmol), evacuated and backfilled with N_2 for 3 times. Then, Pd$_2$(dba)$_3$ (56 mg, 0.06 mmol, 7 mol%) and XPhos (40 mg, 0.08 mmol, 10 mol%) were added under flow on
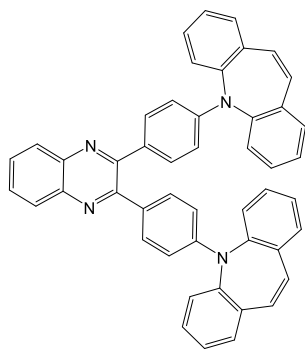
nitrogen, and followed by charging with 10 mL of toluene. The reaction was stirred for 6 hours at reflux. After cooling to room temperature, the mixture was filtered through silica gel by CHCl₃, and concentrated in vacuum. The crude product was isolated by column chromatography on silica gel (n-hexane/EtOAc 5:1) to afford a yellow powder. Mp= 294 °C. Yield (402 mg, 73%). ¹H NMR (400 MHz, CDCl₃): δ_H = 7.96 (2H, bs, CH), 7.54 (2H, dd, ^3J= 6.3 Hz, ^4J= 3.0 Hz, CH), 7.43 (2H, dd, ^4J= 3.8 Hz, CH), 7.36 (4H, d, ^3J= 7.6 Hz, CH), 7.32–7.28 (4H, m, CH), 7.13 (4H, d, ^3J= 8.8 Hz, CH), 6.70 (4H, s, CH) ppm. ¹³C NMR (100 MHz, CDCl₃): δ_C = 153.1, 149.5, 142.7, 140.3, 136.2, 130.5, 130.3, 130.2, 130.1, 129.7, 129.1, 128.4, 127.2, 111.8 ppm. MS, m/z = 664 ([M]⁺, 48%). HRMS (ESI) calcd for $C_{48}H_{32}N_4$ ([M+H]⁺): 665.2700; found: 665.2706.

Synthesis of 2,3-bis(10,11-dihydro-5*H*-dibenzo[*b,f*]azepin-5-yl)quinoxaline (AzQx):
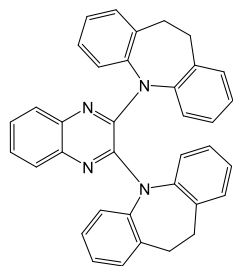
Due to twist boat conformation of IDB in this small molecule, desymmetrization resulted in exhibiting 18 carbon peaks in ¹³CNMR.

A mixture of iminodibenzyl (410 mg, 2.1 mmol) and 2,3-dichloroquinoxaline (198 mg, 1 mmol) dissolved in 7 mL DCE and added ZnCl₂ (286 mg, 2.1 mmol) at 90 °C for 12 h. After completion, the reaction mixture was poured into 30 mL of water, and organic products were extracted with DCM (3x15mL). The crude compound was purified by column chromatography (n-hexane/DCM 1:1) to afford a yellow powder. Yield (93 mg, 18%). ¹H NMR (400 MHz, CDCl₃): δ_H = 8.03 (2H, dd, ^3J= 6.3 Hz, ^4J= 3.4 Hz, 2CH), 7.61 (2H, dd, ^3J= 6.3 Hz, ^4J= 3.4 Hz, 2CH), 7.35 (2H, d, ^4J= 2.1 Hz, CH), 7.09 (2H, dd, ^3J= 8.3 Hz, ^4J= 2.1 Hz, CH), 7.03–6.96 (4H, m, CH), 6.07 (2H, t, ^3J= 7.4 Hz, CH), 6.67 (2H, d, ^3J= 8.3 Hz, CH), 6.54 (2H, d, ^3J= 8.3 Hz, CH), 6.06 (2H, s, CH), 2.99 (8H, s, CH₂) ppm. ¹³C NMR (100 MHz, CDCl₃): δ_C = 153.0, 142.9, 141.8, 140.9, 132.3, 130.6, 130.0, 129.2, 129.0, 128.8, 128.6, 128.0, 126.9, 119.9, 118.1, 117.4, 35.2, 34.9 ppm. MS, m/z = 516 ([M]⁺, 51%). HRMS (ESI) calcd for $C_{36}H_{28}N_4$ ([M+H]⁺): 517.2387; found: 517.2390.

Synthesis of 2,3-bis(4-(2,8-dimethoxy-10,11-dihydro-5*H*-dibenzo[*b*,*f*]azepin-5-yl)phenyl)quinoxaline (OIDBQx):
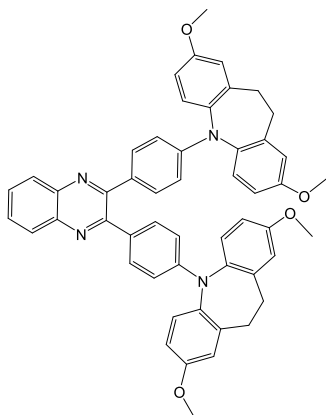
It was prepared according to procedure B, and organic products were extracted with DCM. The crude product was purified by column chromatography (n-hexane/DCM 1:1). Mp= 296 °C. Yield (490 mg, 75%). ^{1}H NMR (400 MHz, CDCl$_3$): δ$_H$ = 7.95 (2H, dd, ^3J= 6.3 Hz, ^4J= 3.4 Hz, CH), 7.54 (2H, dd, ^3J= 6.3 Hz, ^4J= 3.4 Hz, CH), 7.25–7.21 (8H, m, CH), 6.73–6.70 (8H, m, CH), 6.40 (4H, d, ^3J= 8.9 Hz, CH), 3.72 (12H, s, OMe), 2.84 (8H, s, CH$_2$) ppm. ^{13}C NMR (100 MHz, CDCl$_3$): δ$_C$ = 158.3, 153.5, 150.4, 140.8, 139.3, 136.7, 130.7, 130.5, 128.8, 128.4, 115.6, 112.4, 112.2, 55.4, 30.9 ppm. MS, m/z = 788 ([M]$^+$, 1%). HRMS (ESI) calcd for C$_{52}$H$_{44}$N$_4$O$_4$ ([M+H]$^+$): 789.3435; found: 789.3440.

3-bromo-6-(*tert*-butyl)-9*H*-carbazole:
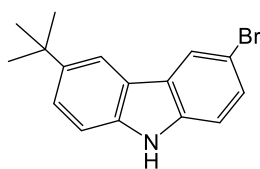
It was prepared under nitrogen atmosphere in a 100 mL round-bottom flask containing nitro methane (40 mL) and 3-bromo-9*H*-carbazole (3.43 g, 14 mmol), ZnCl$_2$ (2.84 g, 2.83 mmol) was added at room temperature. Then *tert*-butyl chloride (2.27 mL, 20.6 mmol) was added dropwise and stirred overnight. After completion, the reaction mixture was poured into 200 mL of water, and organic products were extracted with DCM (3x30mL). The crude compound was purified by column chromatography (n-hexane/ethyl acetate 1:20) to afford a white powder. Mp= 128–130 °C. Yield (2.44 g, 52%). ^{1}H NMR (400 MHz, DMSO): δ$_H$ = 8.12 (1H, d, ^4J= 1.9 Hz, 1CH), 7.93(1H, d, ^4J= 1.8 Hz, 1CH), 7.84 (1H, bs, NH), 7.44 (1H, d, ^3J= 8.5 Hz , ^4J= 1.9 Hz, 1CH), 7.37 (1H, dd, ^3J= 8.5 Hz, ^4J= 1.9 Hz, 1CH), 7.25 (1H, d, ^3J= 8.5 Hz, 1CH), 7.16 (1H, d, ^3J= 8.7 Hz, 1CH), 6.96 (1H, d, ^3J= 8.7 Hz, ^4J= 2.5 Hz, 1CH), 1.35 (9H, s, 3CH$_3$) ppm. ^{13}C NMR (100 MHz, DMSO): δ$_C$ = 143.0, 138.4, 137.9, 129.5, 128.2, 125.4, 124.6, 122.9, 122.1, 116.5, 112.0, 111.9, 110.3, 34.7, 31.9 ppm. MS, m/z = 302 ([M]$^+$, 23%), MS, m/z = 304 ([M+2]$^+$, 28%).

3-(*tert*-butyl)-6-methoxy-9*H*-carbazole (TOC):
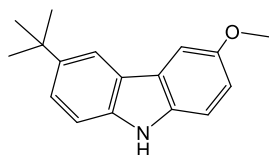
Na (4.8 g) was dissolved in dry MeOH (105 mL) under N$_2$ at 0 °C, and then 3-bromo-6-(*tert*-butyl)-9*H*-carbazole (6.8 g, 20 mmol), CuI (3.8 g, 20 mmol) and DMF (105 mL) at 125 °C for 12 h were stirred. After cooling to room temperature, the mixture was filtered through silica gel with EtOAc, evaporated, washed with water and dried over Na$_2$SO$_4$. The combined organic layers were purified by column chromatography on

silica gel (n-hexane/EtOAc 7:1) to afford a white product. Mp= 166–168 °C. Yield (3.48 g, 69%). ^{1}H NMR (400 MHz, DMSO): δ_H = 7.95 (1H, d, ^4J= 1.9 Hz, 1CH), 7.72 (1H, bs, NH), 7.48 (1H, d, ^4J= 2.4 Hz, 1CH), 7.40 (1H, dd, ^3J= 8.5 Hz, ^4J= 1.9 Hz, 1CH), 7.25 (1H, d, ^3J= 8.5 Hz, 1CH), 7.21 (1H, d, ^3J= 8.7 Hz, 1CH), 6.96 (1H, d, ^3J= 8.7 Hz, ^4J= 2.5 Hz, 1CH), 3.86 (3H, s, OMe), 1.37 (9H, s, 3CH$_3$) ppm. ^{13}C NMR (100 MHz, DMSO): δ_C = 153.7, 142.1, 138.4, 134.8, 124.0, 123.8, 123.0, 116.2, 114.9, 111.2, 110.2, 102.9, 56.1, 34.6, 32.0 ppm. MS, m/z = 253 ([M]$^+$, 100%).

Synthesis procedure C: A mixture of arylamine (2 mmol) and NaOt-Bu (2.3 mmol) was dissolved in 7 mL of DMSO and stirred at room temperature for 20 min, then 2,3-dichloropyrido[2,3-b]pyrazine/2,3-dichloroquinoxaline (1.0 mmol) was added, and the reaction mixture was stirred at 110 °C for 7 h. After completion, the reaction mixture was cooled to room temperature, 100 mL of brine was added to the mixture and filtered. The combined organic layers were dried to afford the crude product which was purified by column chromatography on silica gel to afford the desired product.

2,3-bis(3-(*tert*-butyl)-6-methoxy-9*H*-carbazol-9-yl)quinoxaline (TOCQx):
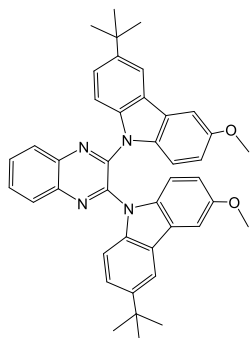
According to procedure C, a yellowish-green powder was obtained (455 mg, 72% yield). Mp= 243 °C. ^{1}H NMR (400 MHz, CDCl$_3$): δ_H = 8.13 (2H, dd, ^3J= 6.3 Hz, ^4J= 3.4 Hz, 2CH), 7.74 (2H, dd, ^3J= 6.3 Hz, ^4J= 3.4 Hz, 2CH), 7.59 (1H, s, CH), 7.53 (1H, s, CH), 7.32 (1H, d, ^3J= 8.8 Hz, CH), 7.18–7.10 (4H, m, 4CH), 6.91 (2H, t, ^3J= 8.5Hz, 2CH), 6.83 (1H, d, ^3J= 6.5 Hz, 2CH), 6.63 (1H, dd, ^3J= 8.5 Hz, ^4J= 2.2 Hz, CH), 6.53 (1H, dd, ^3J= 8.5 Hz, ^4J= 2.2 Hz, CH), 3.75 (6H, d, J= 10.2 Hz, 2OMe), 1.24 (18H, J= 10.2 Hz, 2t-Bu) ppm. ^{13}C NMR (100 MHz, CDCl$_3$): δ_C = 155.0, 144.0, 144.0, 142.1, 142.0, 137.4, 137.1, 134.0, 133.8, 130.2, 128.4, 125.8, 125.5, 124.2, 123.9, 123.8, 123.7, 115.7, 115.5, 114.4, 114.3, 111.3, 111.1, 110.1, 110.0, 102.7, 102.6, 55.9, 55.9, 34.6, 31.8 ppm. MS, m/z = 632 ([M]$^+$, 100 %).

9,9'-(pyrido[2,3-b]pyrazine-2,3-diyl)bis(3-(*tert*-butyl)-6-methoxy-9*H*-carbazole) (TOCPP):
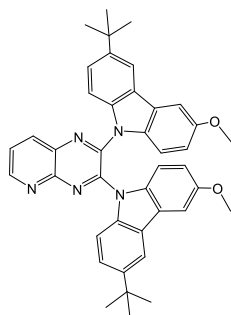
According to procedure C, an orange powder was obtained (424 mg, 67% yield). ^{1}H NMR (400 MHz, CDCl$_3$): δ_H = 9.10 (1H, d, ^4J= 2.4 Hz, CH), 8.45 (1H, d, ^3J= 8.2 Hz, CH), 7.69–7.36 (5H, m, 5CH), 7.24–7.13 (2H, m, 2CH), 7.08–6.50 (6H, m, 6CH), 3.78 (6H, s, 2OMe), 1.23 (18H, 2t-Bu) ppm. ^{13}C NMR (100 MHz, CDCl$_3$): δ_C = 155.4, 155.3, 155.2, 153.6, 148.6, 144.7, 144,5, 144.4, 144.1, 142.3, 137.0, 136.9, 136.6, 136.5, 135.1, 133.7, 133.4, 133.2, 126.12, 126.0, 125.7, 124.9, 124.4, 124.1, 124.1, 123.9, 123.9, 123.9, 123.8, 115.8, 115.5,

115.4, 114.5, 114.4, 114.3, 112.1, 111.8, 111.4, 111.1, 110.5, 110.3, 110.1, 109.9, 102.7, 102.5, 55.9, 55.8, 34.6, 34.5 ppm. MS, m/z = 634 ([M+H]$^+$, 100 %).

9,9'-(pyrido[2,3-*b*]pyrazine-2,3-diyl)bis(3,6-di-*tert*-butyl-9*H*-carbazole) (tCzPP):
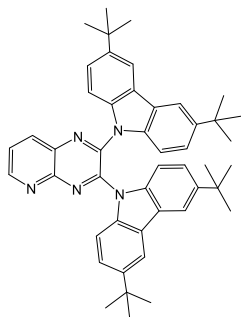
According to procedure C, a yellow powder was obtained (438 mg, 64% yield). Mp= 196 °C. ^{1}H NMR (400 MHz, CDCl$_3$): δ$_H$ = 9.14 (1H, s, 1CH), 8.51 (1H, d, ^3J= 8.3 Hz, CH), 7.71 (1H, s, CH), 7.51 (dd, ^3J= 9.6 Hz, ^4J= 1.9 Hz, CH), 7.16 (2H, d, ^3J= 8.2 Hz, 2CH), 7.04 (2H, d, ^3J= 8.5Hz, 4CH), 6.85 (2H, dd, ^3J= 8.5Hz, ^4J= 1.9 Hz, 2CH), 6.81 (1H, dd, ^3J= 8.5 Hz, ^4J= 1.9 Hz, 2CH), 1.26 (36H, ^4J= 4.3 Hz, 4*t*-Bu) ppm. ^{13}C NMR (100 MHz, CDCl$_3$): δ$_C$ = 153.4, 144.7, 144.5, 144.5, 142.6, 137.3, 136.6, 136.6, 124.7, 124.5, 123.4, 123.3, 115.4, 115.3, 110.2, 109.6, 34.5, 34.5, 31.8, 31.7 ppm. MS, m/z = 686 ([M]$^+$, 100%).

9,9'-(pyrido[2,3-*b*]pyrazine-2,3-diyl)bis(3,6-dimethoxy-9*H*-carbazole) (MeO2PP):
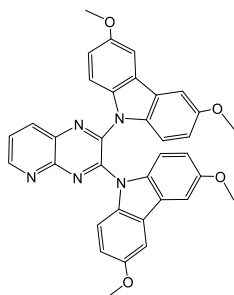
According to procedure C, a red powder was obtained (331 mg, 57% yield). Mp= 252 °C. ^{1}H NMR (400 MHz, CDCl$_3$): δ$_H$ = 9.09 (1H, d, ^4J= 2.5 Hz, 1CH), 8.42 (1H, d, ^3J= 8.2 Hz, CH), 7.76 (1H, m, CH), 7.35 (2H, d, ^3J= 8.9 Hz, 2CH), 7.22 (2H, d, ^3J= 8.9 Hz, 2CH), 7.15 (4H, dd, ^3J= 9.2 Hz, ^4J= 2.3 Hz, 4CH), 6.60 (4H, m, 4CH), 3.75 (12H, J= 3.4 Hz, 4O*Me*) ppm. ^{13}C NMR (100 MHz, CDCl$_3$): δ$_C$ = 155.2, 155.1, 153.7, 148.6, 143.8, 142.1, 136.8, 135.0, 133.6, 133.6, 125.5, 125.3, 124.9, 114.8, 114.7, 112.1, 111.5, 102.9, 102.7, 55.8, 55.8 ppm. MS, m/z = 582 ([M+H]$^+$, 100%).

4. RESULTS AND DISCUSSION

4.1. Mechanochromic and thermally activated delayed fluorescent materials
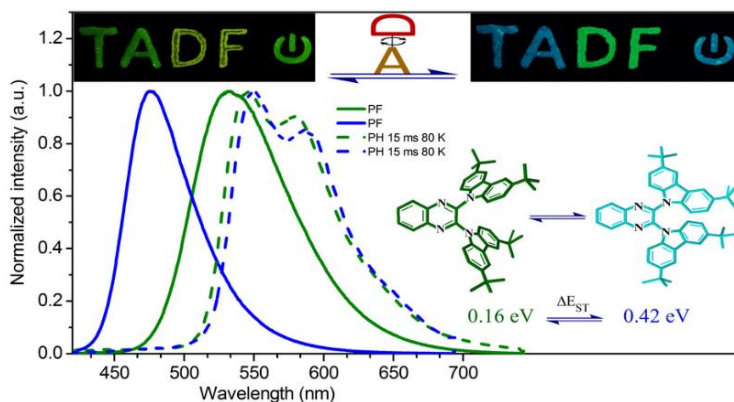
Scheme 4.1 Photoluminescence and phosphorescence of tCzQx in neat film and after heating of neat film.

This chapter is based on the paper published in *J. Phys. Chem. Lett*. **2018**, *9*, 1172–1177 [117]. In this chapter, we report a series of thermally activated delayed fluorescence (TADF) molecules with mechanochromic luminescence (MCL) properties and reversible TADF turn on/off properties in solid state that are induced by the transition between amorphous and crystalline states (Scheme 4.1). Additionally, multi-color altering through external stimulus is demonstrated. All the researched compounds exhibited recovery of the initial states associated with the narrower emission spectra. TADF OLEDs fabricated by solution processing rendered high external quantum efficiency up to 10.9% and luminance of 16760 cd m^{-2} .

4.1.1. Synthesis

Synthesis of the acceptor motif followed the procedure reported by Pfleiderer [114] and began with the reaction of *o*-phenylenediamine with oxalic acid in acidic condition, and then the obtained powders were dried and chlorinated with thionyl choride to generate 2,3-dichloroquinoxaline (I) (Scheme 4.2). In the next step, carbazole and its derivatives were added via nucleophilic aromatic substitution (S$_N$Ar) to the acceptor to afford target products (Scheme 4.4). Carbazole derivatives were prepared (Scheme 4.3) according to the procedure reported in the literature [115, 116]. The structures of the compounds were confirmed with ^{1}H NMR, ^{13}C NMR and mass spectrometry.
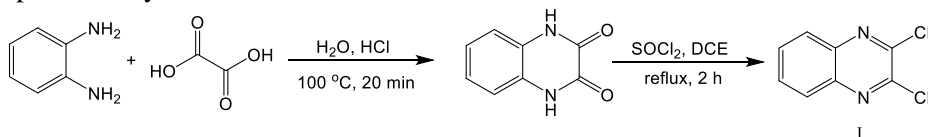
Scheme 4.2 Synthetic procedure for preparation of 2,3-dichloroquinoxaline.
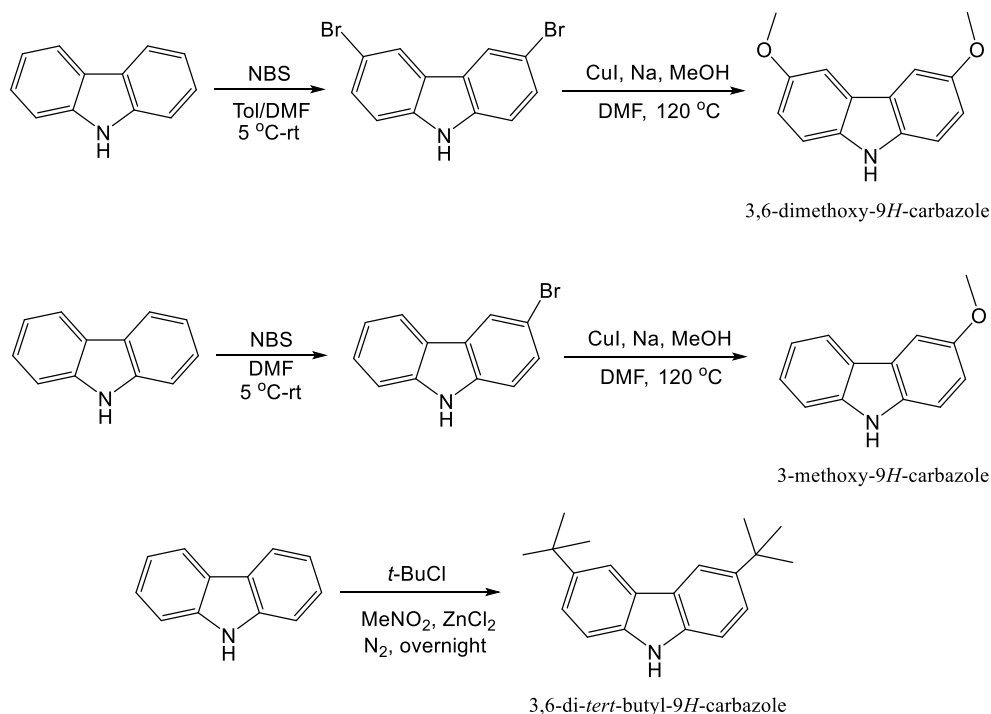
Scheme 4.3 Synthetic procedure for preparation of starting materials.

In the literature, 3,6-dimethoxy-9*H*-carbazole was reported as the donor [76]. By attaching methoxy groups to the carbazole moiety, its electron donating capability increases, which affects the HOMO/LUMO energy gap, the wavelength and the S-T energy gap. Typically, the dipole moment of a molecule increases with the incorporation of a strong donor, which causes the shrinking of ΔE_{ST}, mainly affects the excited singlet state, and, consequently, the rISC process and delayed fluorescence is achievable. One of the issues of the incorporation of this donor is red-shifted emission, which, compared with the emission of carbazole, shows up to 40 nm bathochromism. Taking these considerations into account, we were motivated to employ a methoxy group as the substituent of the carbazole moiety. We decided to synthesize 3-methoxy-9*H*-carbazole, which, to the best of our knowledge, had not yet been used in the synthesis of OLED materials. The goal was to compare the influence of methoxy groups on the properties of luminophore. Besides, one methoxy group can offer less bathochromic spectrum rather than two methoxy groups.
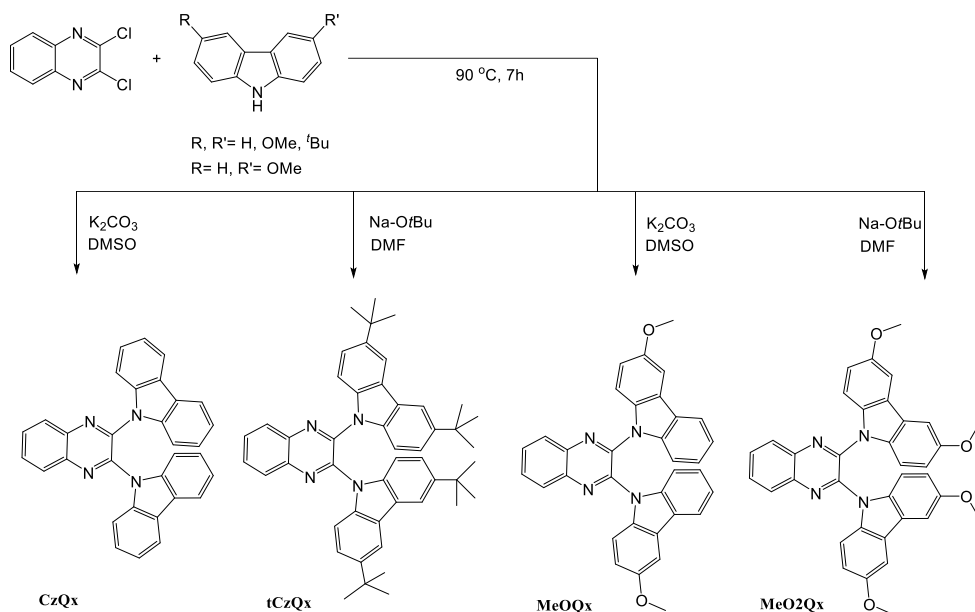
Scheme 4.4. Synthesis of derivatives of carbazole and quinoxaline.

4.1.2. Photophysical properties

4.1.2.1 Steady state photoluminescence spectra of solutions and neat films

The optical absorbance and photoluminescence (PL) spectra of neat films and toluene solutions are shown in Fig. 4.1. The PL spectra of the compounds were taken in solutions with different polarity (hexane, toluene, THF). Due to the solvatochromic behavior of compounds, the absorption bands around 420 nm are attributed to the charge transfer (CT) state. A look at the Fig. 4.1 shows that the fluorescence spectra of the compounds lie in the green-to-orange region, which reflects the impact of the electron donation ability of the substituents of the carbazole moiety.
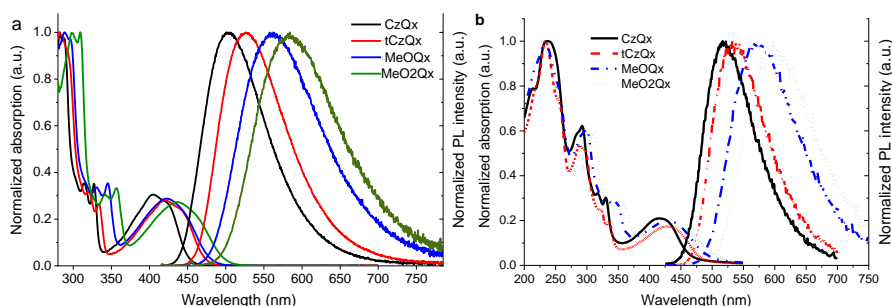
Fig. 4.1 Normalized UV-Vis absorption and PL spectra of investigated molecules in a) toluene and b) thin film.

In Figure 4.2, the PL spectra of the solutions and neat films of the compounds are compared. Generally, the emission of the solutions in polar solvents such as THF arises from CT. For our compounds, the emission spectra of the solutions in THF and neat films overlap or appear almost at the same wavelength, which implies that the emission of neat films apparently originates from the CT state. These results are in good agreement with the influence of the donor strength of carbazole moieties on the emission band: dimethoxy>methoxy>*tert*-butyl.
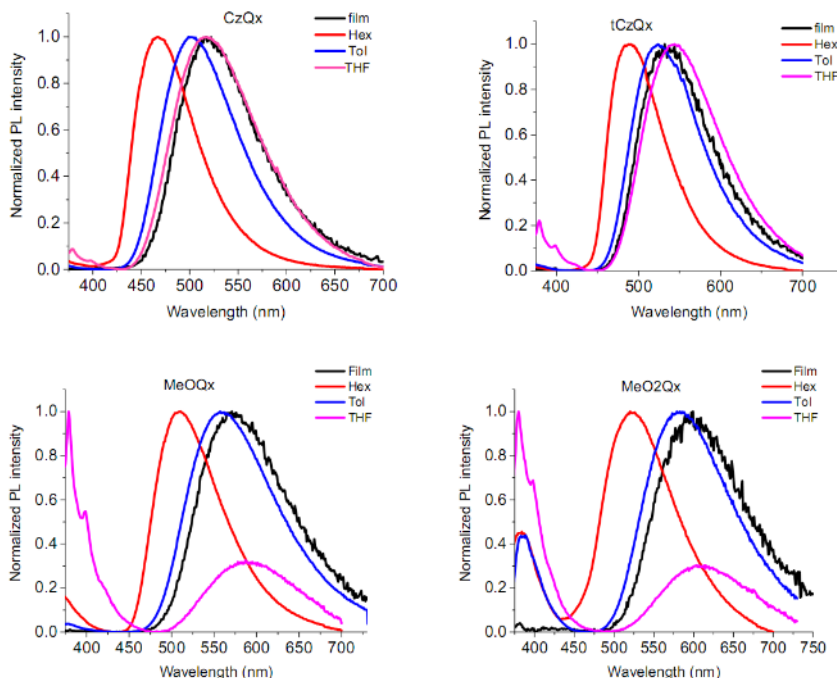
Fig. 4.2 Photoluminescence spectra of the solutions of the compounds in hexane (Hex), toluene (Tol), THF and of thin films (prepared from a chloroform solution).

4.1.2.2 Time-resolved photoluminescence study of dispersions in Zeonex (1% w/w)

PL decay curves of the dispersions of the compounds in zeonex as recorded at room temperature and at 80 K are shown in Figures 4.3–4.6 (graphs **a** and **b**). At low temperatures, the molecules do not have enough energy for rISC processes, and fluorescence is just prompt with the lifetimes in the order of nanoseconds. At room temperature, PF and DF components are denoted by longer PL lifetimes; they are in the order of milliseconds for CzQx and tCzQx, and in the order of microseconds for MeOQx and MeO2Qx. The intensity of DF was found to be temperature dependent: the intensity of delayed fluorescence was higher at RT compared to that recorded at 80 K. Shorter lifetimes of delayed fluorescence were observed for the dispersions of the compounds having substituents at the carbazole moiety. From these data it is

49

evident that the attachment of a stronger donor results in shorter delayed fluorescence lifetimes, which can be explained either by the difference in ΔE_{ST} or by the electron donating effect. In order to understand the origin of this behavior, fluorescence and phosphorescence spectra were taken at RT and at a low temperature (Figs. 4.3–4.6).
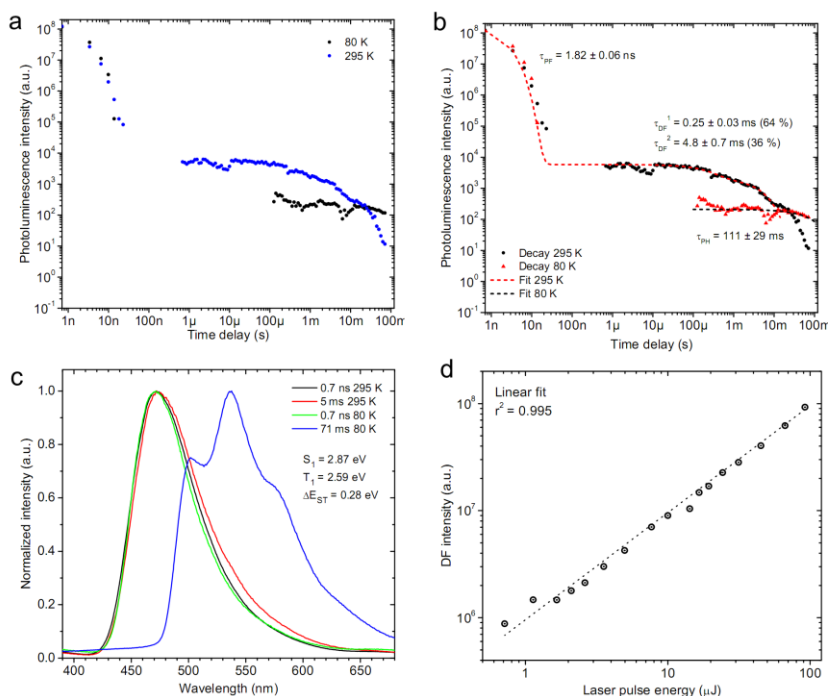
Fig. 4.3 PL decay curves of the dispersions of CzQx in Zeonex (1% w/w) recorded at 295 and 80 K (a); PL decay fits lifetimes (b); prompt and delayed fluorescence and phosphorescence spectra (c); power dependence of delayed fluorescence at 295 K (d). We should note that the power dependence denoted as linear is power law = 1.

Table 4.1 shows the singlet and triplet energies of the compounds. CzQx has ΔE_{ST} of 0.28 eV. ΔE_{ST} values of the other derivatives of carbazole and quinoxaline were found to be ca. twice lower. The causes of smaller ΔE_{ST} values of the compounds containing substituted carbazole moieties might be the stronger electron donation ability and the resonance along the carbazole ring. Because of having DF, the investigation of the power dependence of DF at room temperature for compounds was carried out (graph d). Linear dependence across all the compounds is indicative of thermally activated DF.

Table 4.1 Singlet and triplet energy levels of the dispersions in Zeonex.

Compound	S_1 (eV)	T_1 (eV)	ΔE_{ST} (eV)
CzQx	2.87	2.59	0.28
tCzQx	2.69	2.55	0.14
MeOQx	2.63	2.51	0.12
MeO2Qx	2.58	2.44	0.14
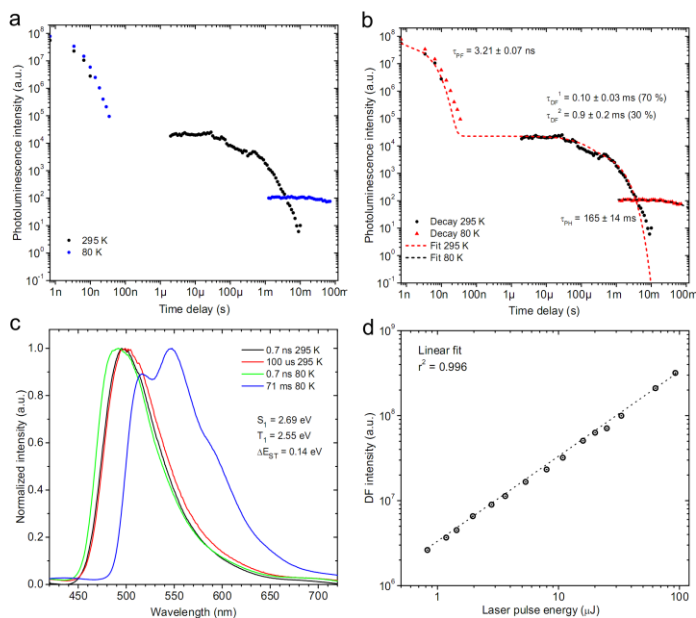
Fig. 4.4 PL decay curves of the dispersion of tCzQx in Zeonex (1% w/w) recorded at 295 and 80 K (a); PL decay with fits and lifetimes (b); prompt and delayed fluorescence and phosphorescence spectra (c); power dependence of delayed fluorescence intensity recorded at 295 K (d). We should note that the power dependence denoted as linear is power law = 1.
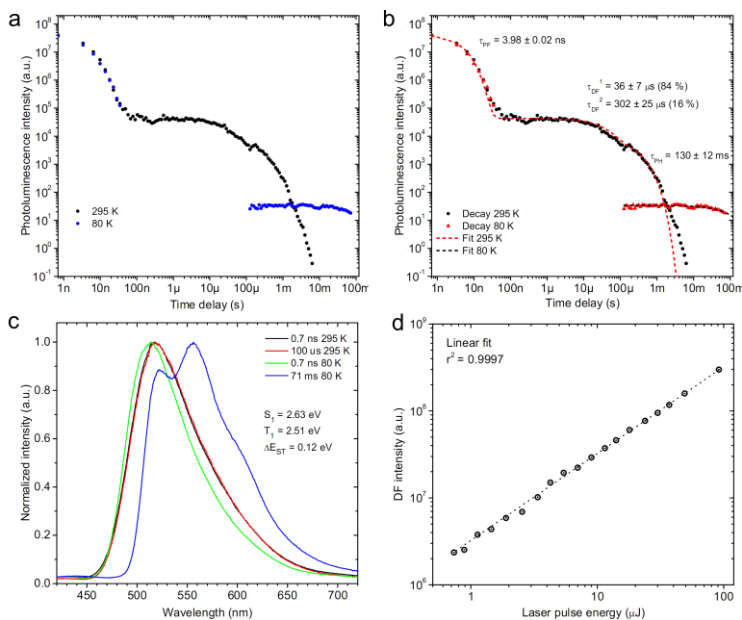
Fig. 4.5 PL decay curves of the dispersion of MeOQx in Zeonex (1% w/w) recorded at 295 and 80 K (a); PL decay with fits and lifetimes (b); prompt and delayed fluorescence and phosphorescence spectra (c); power dependence of delayed fluorescence intensity recorded at 295 K (d). We should note that the power dependence denoted as linear is power law = 1.
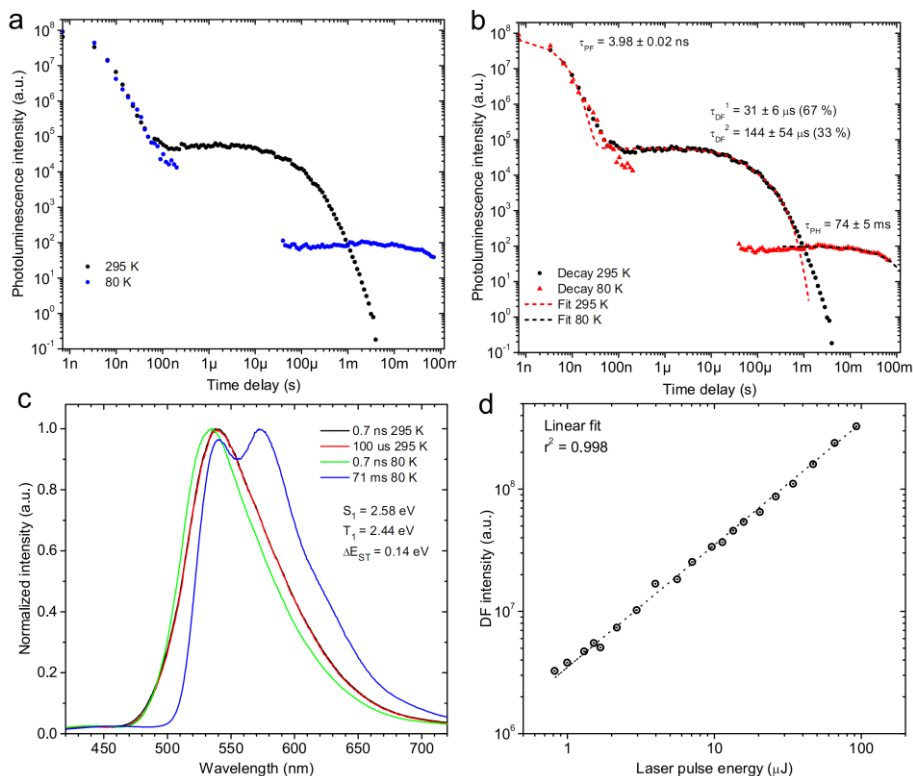
Fig. 4.6 PL decay curves of the dispersion of MeO2Qx in Zeonex (1% w/w) recorded at 295 and 80 K (a); PL decay with fits and lifetimes (b); prompt and delayed fluorescence and phosphorescence spectra (c); power dependence of delayed fluorescence intensity recorded at 295 K (d). We should note that the power dependence denoted as linear is power law = 1.

Figure 4.7 depicts the phosphorescence spectra of molecular dispersions of the compounds in Zeonex. For a comparison, the spectrum of the solid solution of quinoxaline in Zeonex is shown. The phosphorescence spectra of methoxy carbazole and dimethoxy carbazole dispersed in Zeonex are shown in Fig. 4.8. Based on these spectra, the lowest energy triplet state (^{3}LE) is localized on the acceptor, and the similar vibronic pattern and triplet energy of the donors are higher than the values shown by luminophores. As we see, in these compounds, the acceptor possesses the energy of the lowest excited triplet state, and the weaker is the donor, the stronger is the possession. These observations show that the substitution with a stronger donor results in more effective conjugation between the donor and the acceptor. The system is not fully decoupled, which results in increasing the oscillator strength and the radiative decay process. Thus electron donating substituents affect the electron density on the donor, which leads to the decrease of the triplet energy. Because of this, the triplet state in MeO2Qx is more affected than the CT state, and its ΔE_{ST} is larger than that of MeOQx; however, it is not smaller than that of tCzQx.
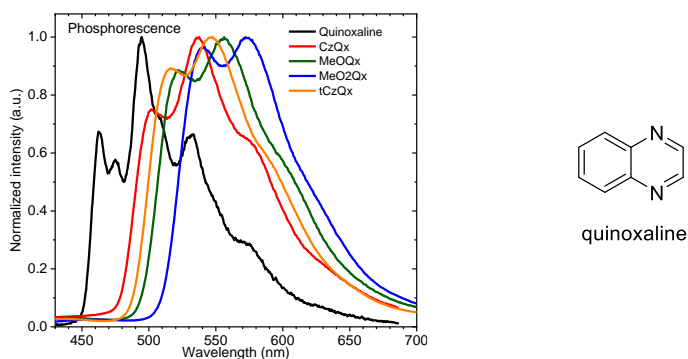
Fig. 4.7 Phosphorescence spectra of molecular dispersions of quinoxaline and of the studied molecules in Zeonex (1% w/w) at 80 K.
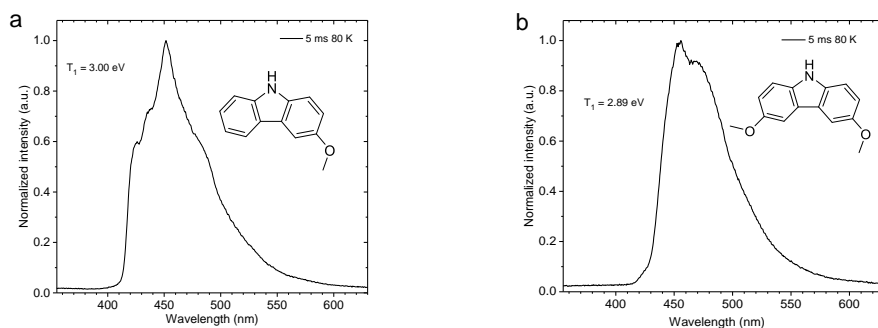
Fig. 4.8 Phosphorescence spectra of (a) 3-methoxy-9*H*-carbazole and (b) 3,6-dimethoxy-9*H*-carbazole dispersed in Zeonex (1% w/w).

4.1.2.3 Time-resolved photoluminescence study of solid solutions in the blend of PBD (5% w/w) and PVK

In principle, the molecules behave very similarly in the PVK:PBD mixed host as in Zeonex (Figures 4.9–4.13). The results of the study show that TADF is also present in OLEDs fabricated while using this host. The high EQE of OLEDs can be explained by the presence of TADF.

Table 4.2 Singlet and triplet energies of the molecular dispersions in PVK:PBD.

Compound	S_1 (eV)	T_1 (eV)	ΔE_{ST} (eV)
CzQx	2.73	2.53	0.20
tCzQx	2.66	2.50	0.16
MeOQx	2.62	2.47	0.15
MeO2Qx	2.53	2.39	0.14

The contribution of TADF is very similar for the systems containing tCzQx, MeOQx and MeO2Qx, but the solid solution of CzQx in PVK:PBD shows a significantly smaller extent of delayed fluorescence (Figure 4.9). It is worth noting that the delayed fluorescence lifetime of molecular dispersions of the compounds in PVK:PBD is lower by approximately an order of magnitude compared to those of the dispersions in Zeonex. The singlet (CT) and triplet energies of the dispersions in PVK:PBD are also lower by a very similar value. This in fact makes the singlet-triplet energy gap to be virtually identical in both PVK:PBD and Zeonex. The phosphorescence spectra of the dispersions in PVK:PBD are not only red-shifted, but their vibronic structure also becomes less evident, and the decay constants are lower. This suggests a relatively strong interaction of the acceptor with the host molecules. The phosphorescence lifetime of the dispersion of tCzQx is the longest among all the studied molecular dispersions both in PVK:PBD and in Zeonex. As the phosphorescence spectra and triplet energies are different for all the molecules dispersed in PVK:PBD, they reflect the respective triplet energy of the dopants rather than that of the host.

It is also of interest in CzQx-doped PVK:PBD blend (Figure 4.10) that the existence of relatively long-lived fluorescence, biexponential prompt component, has been observed. As CzQx shows the lowest solubility in toluene, this might be due to the formation of aggregates in microscale. Thus the shorter prompt fluorescence component could be attributed to excitonic emission, while the longer one could be ascribed to aggregate emission. These results explain why CzQx-based OLED is significantly less efficient than the other devices.
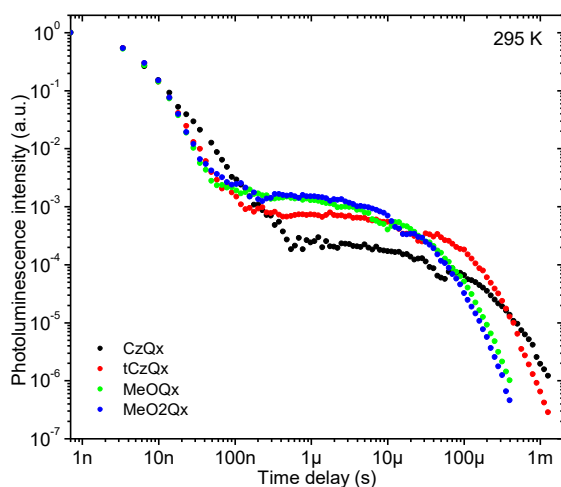
Fig. 4.9 Photoluminescence decays of the studied molecules dispersed in PVK:PBD (5% w/w).
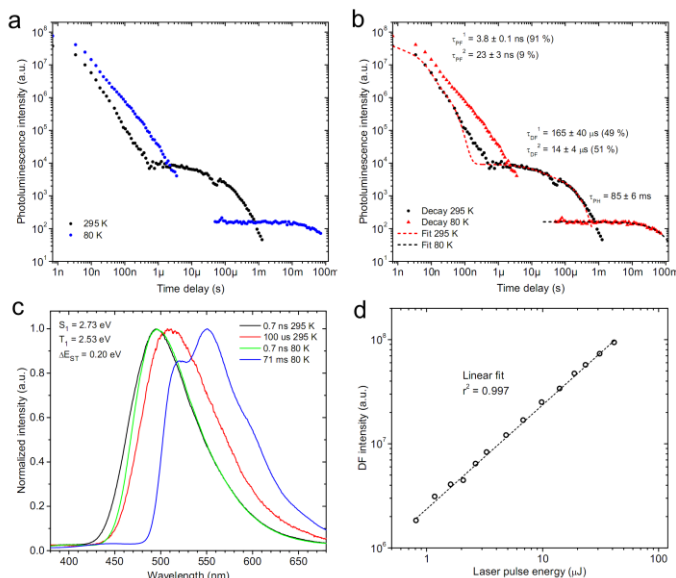
Fig. 4.10 Photoluminescence decay curves of the dispersion of CzQx in PVK:PBD 60:40 (5% w/w) recorded at 295 and 80 K (a); photoluminescence decay with fits and decay time constants (b); prompt and delayed fluorescence and phosphorescence spectra (c); power dependence of delayed fluorescence intensity at 295 K (d) . We should note that the power dependence denoted as linear is power law = 1.
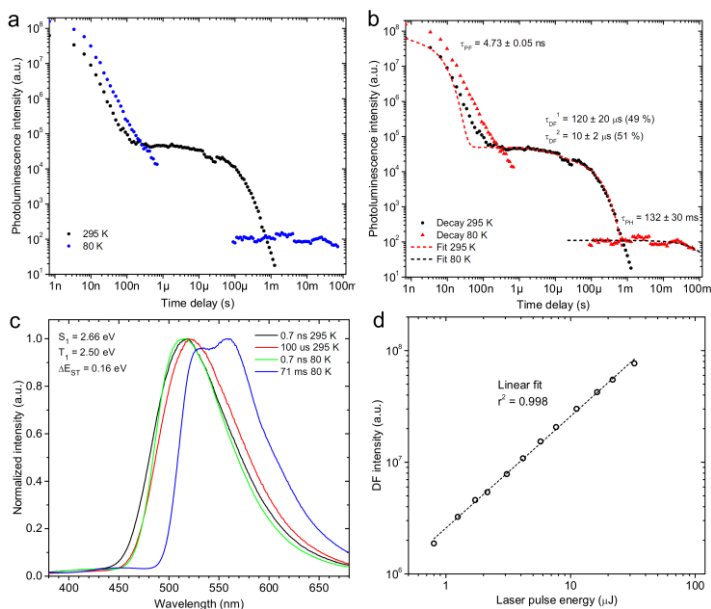
Fig. 4.11 Photoluminescence decay curves of the dispersion of tCzQx in PVK:PBD 60:40 (5% w/w): a) photoluminescence decay at 295 and 80 K; b) photoluminescence decay with fits and decay time constants shown; c) prompt and delayed fluorescence and phosphorescence spectra; d) power dependence of delayed fluorescence at 295 K. We should note that the power dependence denoted as linear is power law = 1.

55
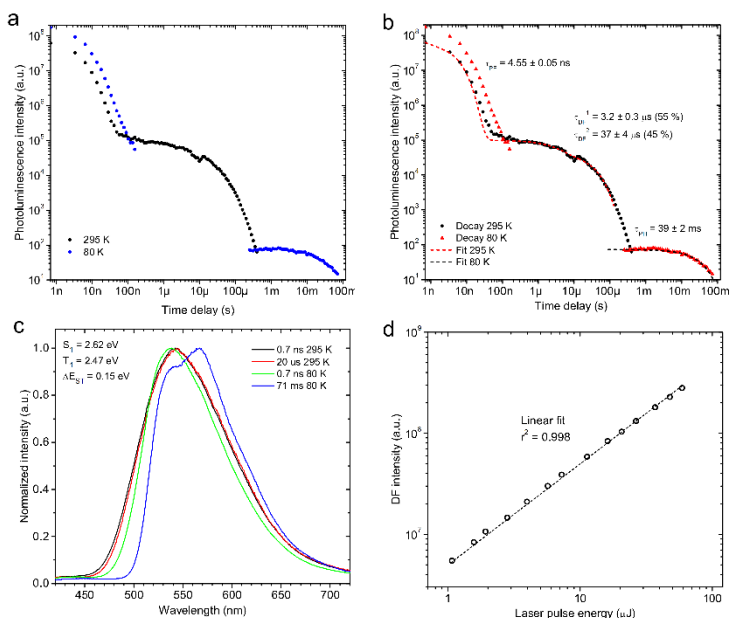
**Fig. 4.12** Photoluminescence decay curves of the dispersion of MeOQx in PVK:PBD 60:40 (5% w/w): a) photoluminescence decay at 295 and 80 K; b) photoluminescence decay with fits and decay time constants shown; c) prompt and delayed fluorescence and phosphorescence spectra; d) power dependence of delayed fluorescence at 295 K. We should note that the power dependence denoted as linear is power law = 1.
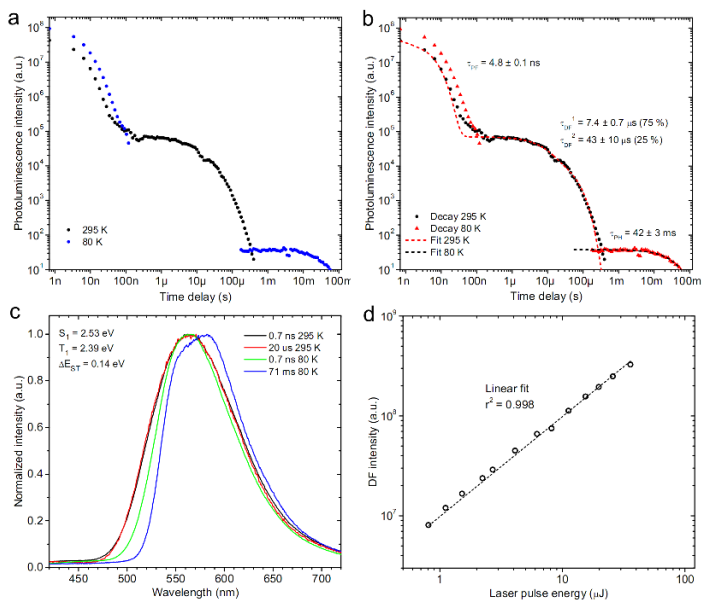

Fig. 4.13 Photoluminescence decay curves of the dispersion of MeO2Qx in PVK:PBD 60:40 (5% w/w): a) photoluminescence decay at 295 and 80 K; b) photoluminescence decay with fits and decay time constants shown; c) prompt and delayed fluorescence and phosphorescence spectra; d) power dependence of delayed fluorescence at 295 K. We should note that the power dependence denoted as linear is power law = 1.

4.1.3. Electrochemical characterization

The ionization potential and electron affinity demonstrate the necessary energies to pull and push an electron from HOMO and LUMO orbitals, respectively. These energies can be obtained from the cyclic voltammogram. In organic semiconductors, electrons and holes are transported via LUMO and HOMO, and knowing these energy levels is essential. Therefore, in this work, for the elucidation of the required values, we shall use the HOMO and LUMO for obtained energies from cyclic voltammetry (CV). All the molecules showed reversible oxidation and reduction in CV experiments (Fig. 4.14). This observation proved the electrochemical stability of the compounds.
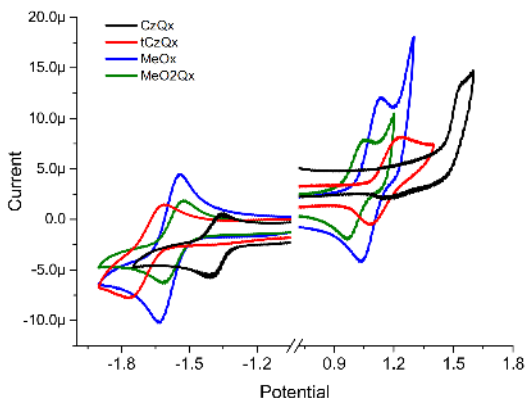
Fig. 4.14 CV curves of the solutions of the compounds in DCM.

Typically, for the molecules with the same acceptor, increasing the strength of the donor leads to an increase of the HOMO and LUMO energies. The highest HOMO energy was observed for MeO2Qx (-5.47 eV), whereas the lowest value was recorded for CzQx (-5.87 eV). As shown in Table 4.3, from CzQx to MeO2Qx, the increase of the electron donating capacity of carbazole moieties resulted in the increase of the HOMO energy levels. Since all the compounds contain the same acceptor, a close look at the LUMO energy levels (Table 4.3) reveals that, in the range from tCzQx to MeO2Qx, the attachment of electron rich donating moieties to the carbazole moiety caused a decrease of LUMO.

Table 4.3 Summary of electrochemical properties.

Compound	HOMO/LUMO (eV)[a]	E_g (eV)[b]
CzQx	-5.87/-3.11	2.75
tCzQx	-5.68/-2.97	2.63
MeOQx	-5.51/-3.03	2.60
MeO2Qx	-5.47/-3.05	2.49

[a] HOMO and LUMO energy determined by cyclic voltammetry in DCM; [b] energy gap of the solutions in toluene.

MeO2Qx containing dimethoxy strengthens the carbazole moiety and shows the lowest LUMO level. Thisese results implies that MeO2Qx increases the electron density on the acceptor having a further orbital overlap. Meanwhile, the optical energy band gap of the solutions of the compounds in toluene is the lowest one for MeO2Qx.

4.1.4. Mechanochromic properties

The mechanoresponsive behavior of compounds under external stimuli was investigated. The fluorescence spectra upon grinding, melting and for the neat films were taken, and the tuning of the emission color to the initial color by heating and/or fuming was performed.

4.1.4.1. Steady-state photoluminescence spectra and photographs
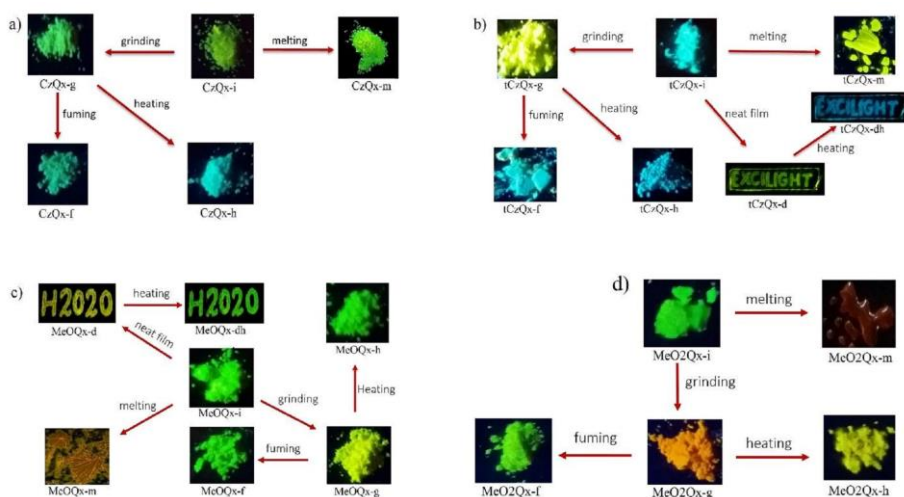
Fig. 4.15 Photoluminescence of (a) CzQx, (b) tCzQx, (c) MeOQx and (d) MeO2Qx forms obtained through various external stimuli (the images were taken under excitation wavelength of 365 nm).

The photophysical properties of the four compounds in their solid forms showed alterations that were induced by external stimuli and exhibited MCL behavior. MeOQx and MeO2Qx showed multicolor alteration in response to external forces (see Figure 4.15). The measurements of TADF emission were used as a complementary approach to clarify our understanding of the microstructure and phase transformation of the compounds alongside powder XRD analysis, (details are depicted in Fig. 4.19-4.26). The crystalline structures of the initial powders were disrupted upon grinding with a spatula thus creating the amorphous state. On the contrary, either upon heating or fuming of previously ground powders, clear diffraction peaks arose thus manifesting that the initially ground solids reassembled into new crystalline lattices. In contrast, the films obtained by melting and drop casting were amorphous, except for that of CzQx-m. The narrower PL spectra obtained from the crystalline samples,

58

in comparison with the amorphous ones, indicate a more local character of the emissive CT state (the so-called weak CT or hybrid local and CT state: HLCT). Moreover, melting causes a significant bathochromic shift of the PL spectrum.

For example, in the prepared form, tCzQx-i shows sky blue emission, which, upon grinding with the objective to form tCzQx-g, shifts towards yellow emission. Heating (tCzQx-h) and fuming (tCzQx-f) of tCzQx-g powder reproduces a powder of sky-blue fluorescence. Remarkably, PL of tCzQx-i, tCzQx-h, and tCzQx-f, is blue-shifted relative to the emission of the solution in hexane. This observation suggests that the emissive singlet state has a more localized character than the emissive state of the solution in a non-polar solvent, i.e., the intermolecular interactions present in the solid forms are less effective on relaxing the molecular structure than in the liquid solution. The red shift of the photoluminescence after grinding (tCzQx-g) also implies a transformation of the excited state from the LE (or HLCT) state into the intramolecular charge transfer (ICT) state, which indicates a relaxation of the D-A dihedral angle. This observation is consistent with less predominant intermolecular interactions in the amorphous state than in the crystalline form. Probably, a larger free space allows the molecules to adapt their conformation in order to stabilize the charge transfer state. Finally, annealing of the amorphous drop-cast film of tCzQx (tCzQx-d) results in the formation of a crystalline state (tCzQx-dh) which recovers the sky blue emission (Figure 4.15). Further, the time-resolved photoluminescence studies of prompt and delayed emissions from different forms were also performed. The amorphous form of tCzQx demonstrated strong TADF, whereas, in the crystalline phase, very little or none of delayed fluorescence was observed. This surprising behavior implies that the introduction of heavy substituents (*t*-Bu) rigidified the donor around the C-N bond thus restrivting the vibrational rotation and non-radiative decays. In the crystalline form, the weak delayed fluorescence most probably appears as the result of triplet-triplet annihilation (see Fig. 4.21 for details). This phenomenon is exceptionally important since it shows that the molecular assembly and external stimuli, along with the molecular design and host effects, are parameters that can control the formation of the CT state and influence the TADF behavior.

Since the amorphous phase is expected to be less dense, and as it is thus expected to carry more free space, the donor and acceptor moieties can rotate around the C-Nbond more freely. This results in a relaxed charge transfer conformation, probably with a larger donor-acceptor dihedral angle. Therefore, the PL spectrum red-shifts after transformation from the crystalline to the amorphous phase with the larger stabilization of the CT state. In the crystalline phase, the larger intermolecular interactions that are prevalent in the ordered packing reduce the free space and probably force spacious donor/acceptor units to adapt a relatively less twisted configuration. This decreases the donor-acceptor dihedral angle, and, consequently, leads to the weakening of the CT character, which, in turn, becomes of a more localized nature (such as a hybrid local and CT state). As in both forms the local triplet state (^{3}LE) is virtually not affected by the D-A dihedral angle (due to its localized nature), the change induced on the energy of the singlet CT state can either promote TADF (amorphous phase) or quench it (crystalline phase) due to a change in ΔE_{ST}.

This is evidenced by Figure 4.17 where prompt fluorescence and phosphorescence spectra of drop-cast films are presented. Clearly, in tCzQx-d and tCzQx-dh, the phosphorescence not only resembles the one observed from the dispersion in Zeonex, but it also remains virtually identical in both cases. Changes are only observed in terms of the CT energy, which serves as evidence that the observed alternations are driven entirely by the change in the D-A dihedral angle. A similar behavior is observed for powders, and, therefore, can be explained by the same mechanism. Interestingly, tCzQx in the powder form gives not only a switchable color of luminescence, but also reversible turn-on/turn-off TADF (Figure 4.21). For the CzQx powders, these results demonstrate the coexistence of amorphous and crystalline forms showing green and blue emissions. The introduction of stronger donors in the case of MeOQx and MeO2Qx resulted in a high-contrast emission change from green to red. The annealed form of MeO2Qx-h, showed yellow emission, and the fumed form of MeO2Qx-f resembled the emission of the initial form (Figure 4.15). Accordingly, the X-ray diffractogram of MeO2Qx-h shows significantly different patterns compared to those of other crystalline samples, e.g., MeO2Qx-f (Figure 4.26). This suggests that MeO2Qx may have distinct crystal structures with different D-A dihedral angles. It is particularly interesting that the heated form shows a relatively narrow emission band compared to those of MeO2Qx-i and MeO2Qx-f, which suggests a more rigid structure. In order to show the versatility of the presented molecules, their triplet harvesting properties are highlighted by their performance in OLEDs. Due to the excellent solubility of the compounds in toluene and the efficient TADF of the films, OLEDs were fabricated by solution processing.

Table 4.4 PL properties of compounds in solid films and powders in air.

Sample	solid states	initial (-i)	ground (-g)	heated (-h)	fumed (-f)	melted (-m)	neat film (-d)	heated film (-dh)
tCzQx	PL (nm)	482	527	477	479	544	534	482
	PLQY (%)	9	12	9	9	9	11	6
MeOQx	PL (nm)	516	543	511	514	582	592	519
	PLQY (%)	10	7	10	9	7	10	11
MeO2Qx	PL (nm)	534	586	559	523	618	598	
	PLQY (%)	6	4	7	5	2	6	
CzQx	PL (nm)	504	510	478	478	524	519	
	PLQY (%)	4	5	11	6	10	7	

Heating of MeO2Qx-d and CzQx-d did not result in a change of photoluminescence color, and no – dh form was obtained.
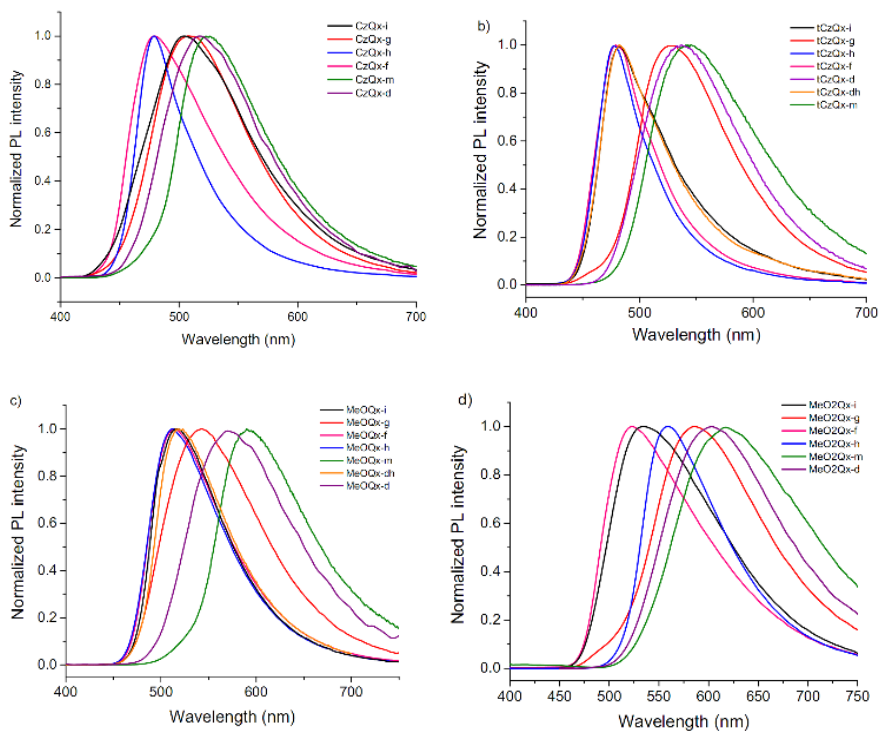
Fig. 4.16 PL spectra of the compounds in different forms.

4.1.4.2. Time-resolved photoluminescence spectrometry study
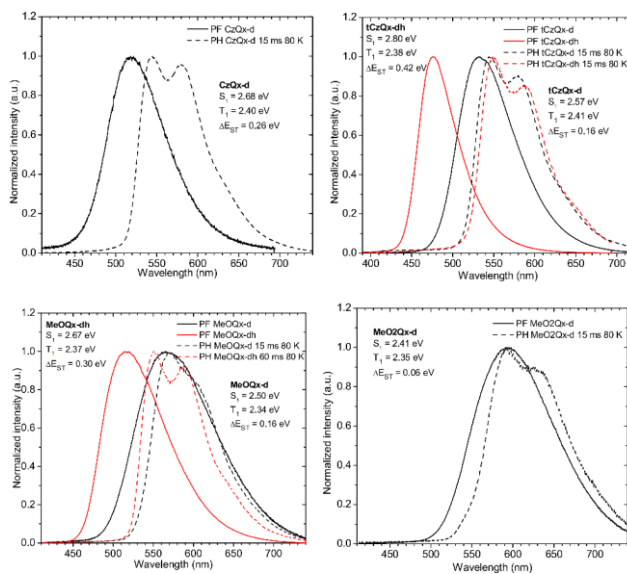
Fig. 4.17 Prompt fluorescence and phosphorescence spectra of the films of the compounds (-d and -dh forms).

It is worth noting that the phosphorescence spectra are affected by the emission of the CT state if S_1 and T_1 are close. In MeOQx-d, the PH spectrum is distorted by mixing with the emission of the CT state as it lies nearby. The distorted phosphorescence of MeO2Qx-d can apparently be explained by a similar effect. The fact that the phosphorescence spectra of tCzQx-d and tCzQx-dh are nearly identical indicates that there are neither signs of aggregation, nor excimer formation. Even in the neat film, the molecules behave as if isolated in the system, but D-A dihedral angles are different in the different states (Figure 4.17).

All the luminescent powders of CzQx are mixtures (Figures 4.18, 4.19). It is evident from the photophysical investigations that CzQx-g contains the majority of the amorphous phase, while CzQx-h and CzQx-f, which are in fact very similar, contain mostly the crystalline phase. As all the powders exhibit emissions from at least two distinct forms of CzQx, it is difficult to precisely determine their properties. CzQx-m is in principle very similar to CzQx-g, but CzQx-d is different. This shows that a film deposited from a chloroform solution and obtained *via* melt-casting show different packing. All the powders and films show delayed fluorescence. It is a mixture of the crystal/amorphous phase emissions with a dominating, red-shifted emission at longer delay times (i.e., > 10 µs). It is attributed to a relaxed CT-state emission of the molecules or excimer emission. As all the above discussed forms show a mixed contribution of emissive forms, the further analysis is inconclusive. It can be stated that, most likely, all the forms show the TADF emission as originating from the relaxed CT state/excimer, which is nearly identical in all of its forms, with a contribution of delayed fluorescence from other forms. CzQx-d shows a weak signal of the delayed fluorescence of crystal forms (blue-shifted in respect to prompt emission). This observation is consistent with the XRD results.
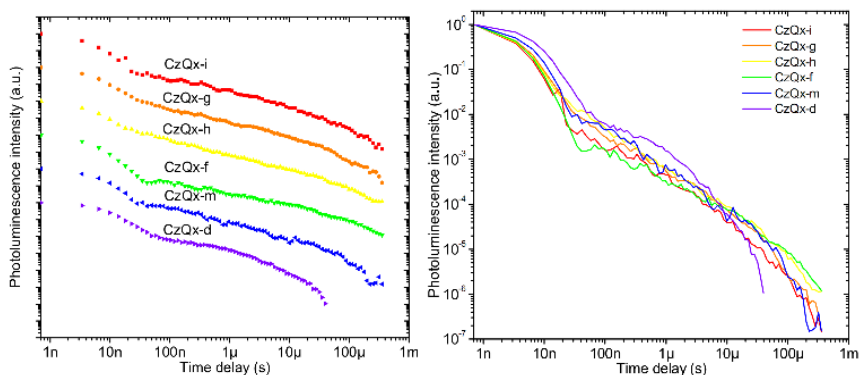
Fig. 4.18 Photoluminescence decays of different emissive forms of CzQx: (left) stacked, (right) normalized.
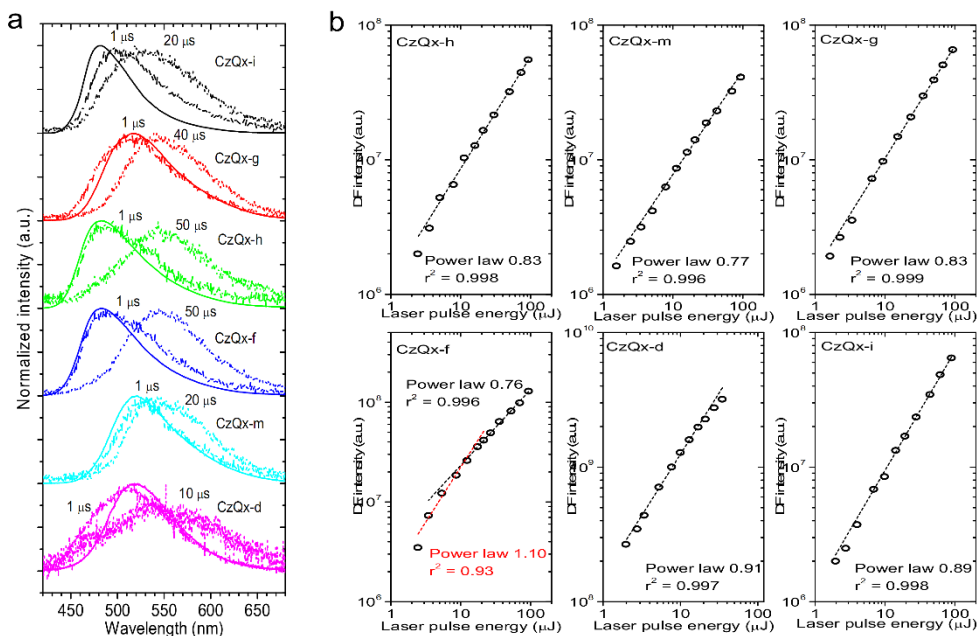
Fig. 4.19 (a) Time-resolved spectra of luminescent forms of CzQx. Solid line: prompt fluorescence; dotted and dashed lines indicate delayed fluorescence. Delay at which the delayed fluorescence spectrum was recorded is indicated in the figure next to the respective spectrum. (b) Power dependence of delayed fluorescence recorded for different photoluminescent forms of CzQx.
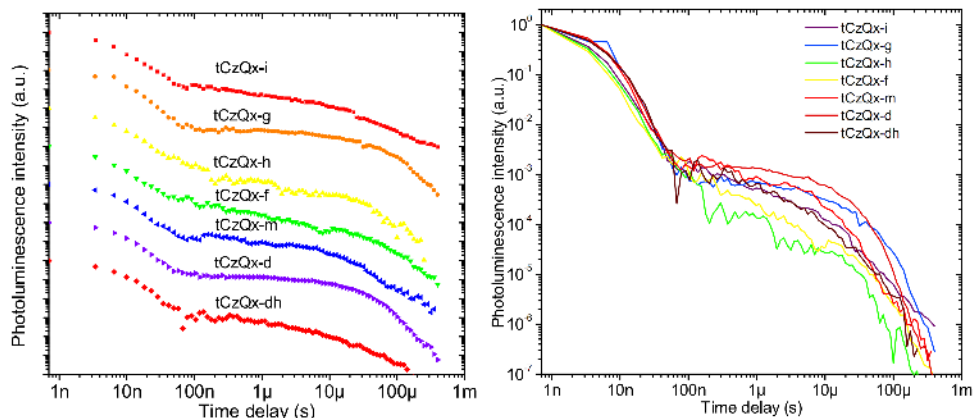
Fig. 4.20 Photoluminescence decays of different emissive forms of tCzQx: (left) stacked, (right) normalized.
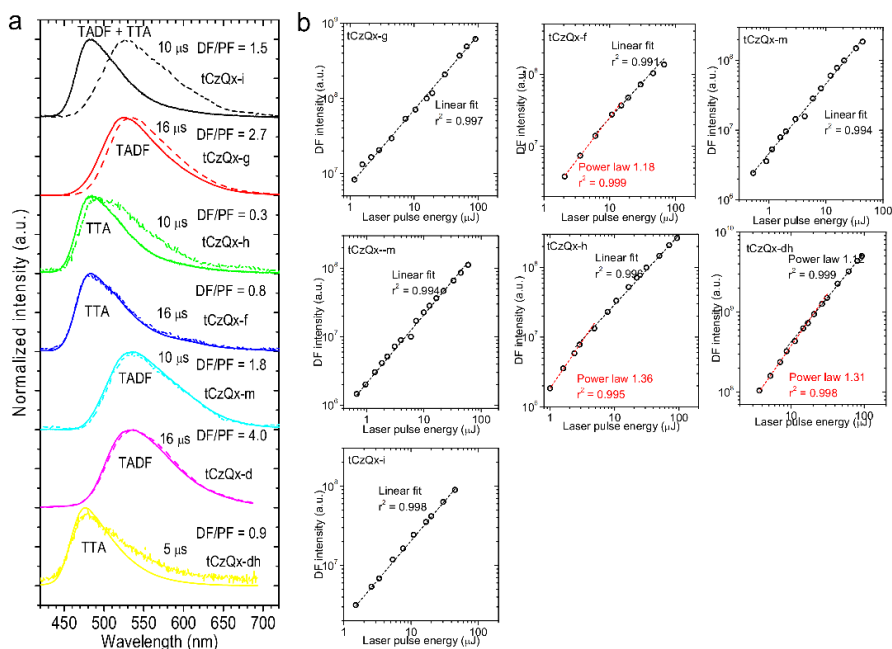
Fig. 4.21 (a) Time-resolved spectra of luminescent forms of tCzQx. Solid line: prompt fluorescence; dotted and dashed lines indicate delayed fluorescence. Delay at which the delayed fluorescence spectrum was recorded is indicated in the figure next to the respective spectrum. Delayed fluorescence to prompt fluorescence ratio (DF/PF) is shown next to each spectrum. We should note the visibly larger DF contribution in amorphous forms. (b) Power dependence of delayed fluorescence recorded for different photoluminescent forms of tCzQx.

tCzQx shows a definite distinction of photophysical properties between the crystal and amorphous forms (Figures 4.20, 4.21). In fact, tCzQx-g, tCzQx-d, and tCzQx-m are of a nearly identical amorphous phase, while tCzQx-f, tCzQx-h, and tCzQx-dh are of the same crystalline character. tCzQx-i is the mixture of amorphous and crystalline phases with the crystalline phase being predominant. In all the amorphous forms of tCzQx, a strong TADF can be observed, while the crystalline phase shows very little extent of delayed fluorescence, which is of triplet-triplet annihilation (TTA) origin (supralinear power dependence regime).

MeOQx behaves similarly to other materials (Figures 4.22, 4.23), however, no significant differences in the delayed fluorescence of the forms is observed (all of them show TADF with comparable intensity). Apparently, the differences of CT energy are less pronounced, thus S-T gap facilitates TADF emission in all cases. This is most likely due to the stronger electron-donating properties of the donor (compared to tCzQx), so the CT is less affected by the D-A dihedral angle than in the case of tCzQx.

MeOQx-i, MeOQx-h, and MeOQx-f appear to be crystalline, with prompt and delayed fluorescence spectra matching perfectly. On the other hand, MeOQx-g is amorphous, also showing TADF. MeOQx-m and MeOQx-d show a different, more red-shifted

emission than MeOQx-g. This shows that if the amorphous phase is produced directly from the liquid it contains more free volume than the sample of the crystalline powder being ground.
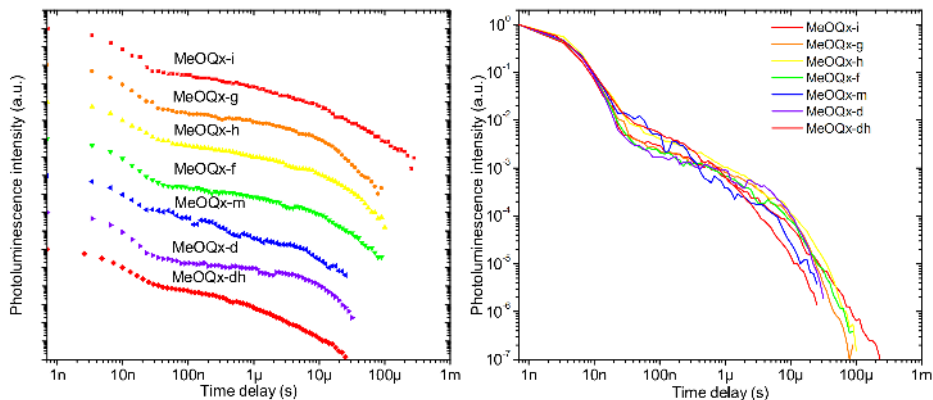
Fig. 4.22 Photoluminescence decays of different emissive forms of MeOQx: (left) stacked, (right) normalized.
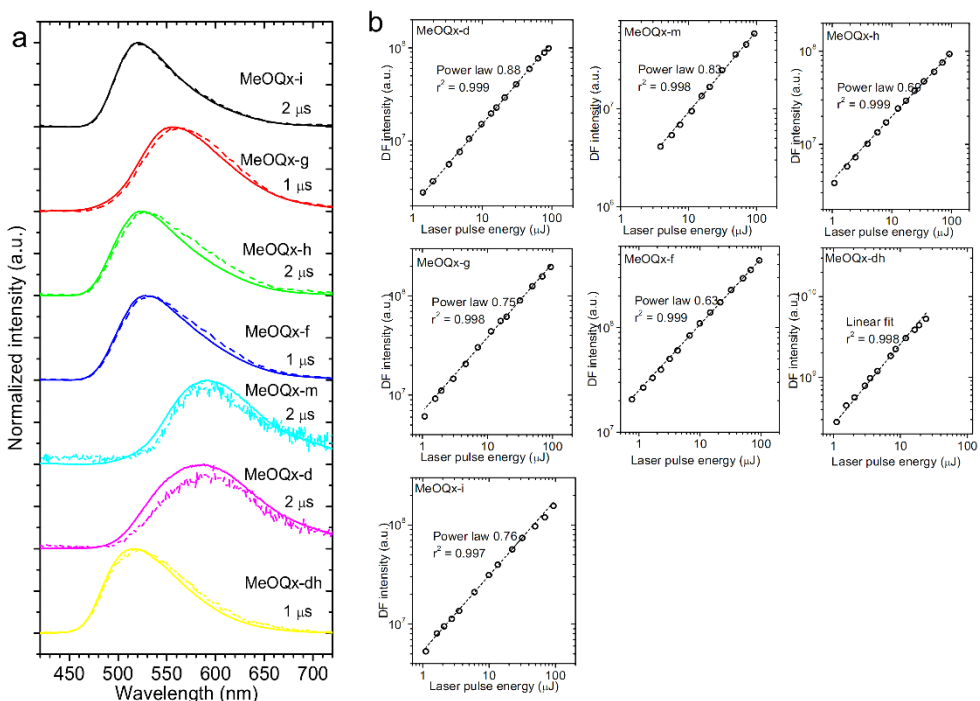
Fig. 4.23 (a) Time-resolved spectra of luminescent forms of MeOQx. Solid line: prompt fluorescence; dotted and dashed line indicate delayed fluorescence. Delay at which the delayed fluorescence spectrum was recorded is indicated in the figure next to the respective spectrum. (b) Power dependence of delayed fluorescence intensity is recorded for different photoluminescent forms of MeOQx.

MeOQx-m and MeOQx-d show lower CT emission energy than MeOQx-g due to the larger D-A dihedral angle (more free volume and more freedom of D-A orientation). MeOQx-d, when left on a hot plate, crystallizes to give MeOQx-dh with the crystal form similar to other crystal forms of MeOQx.

MeO2Qx-g, MeO2Qx-d and MeO2Qx-m are amorphous, while MeO2Qx-i, MeO2Qx-f, and MeO2Qx-h are crystalline. Like MeOQx, also MeO2Qx-d and MeO2Qx-m show more bathochromic emission than MeO2Qx-g.

MeO2Qx-i is similar to MeO2Qx-f, which can be explained by the same method of preparation. Both powders were obtained under influence of a solvent (Figures 4.24, 4.25). Interestingly, MeO2Qx-h, also being crystalline, shows completely different emission from the other crystalline forms. It is worth noting that the X-ray diffractogram of MeO2Qx-h shows significantly different patterns from the other two crystalline powders. This observation suggests that the compound can exist in two distinct crystal structures with different D-A dihedral angles. It is of particular interest that MeO2Qx-h shows a relatively narrow emission band compared to MeO2Qx-i or MeO2Qx-f, which suggests a very rigid structure. In fact, the D-A dihedral angle can be fixed in MeO2Qx-h, giving freedom only to minor oscillations of the donor unit, which makes the emission spectrum very narrow, but still of CT nature. In MeO2Qx-i and MeO2Qx-f, the donor has slightly more freedom to oscillate, which results in a broader (but blue-shifted) emission spectrum.
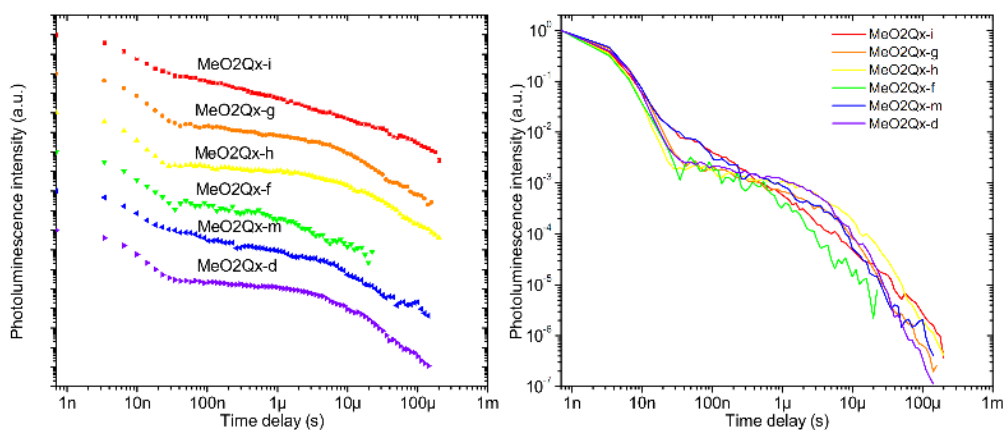

Fig. 4.24 Photoluminescence decays of different emissive forms of MeO2Qx: (left) stacked, (right) normalized.
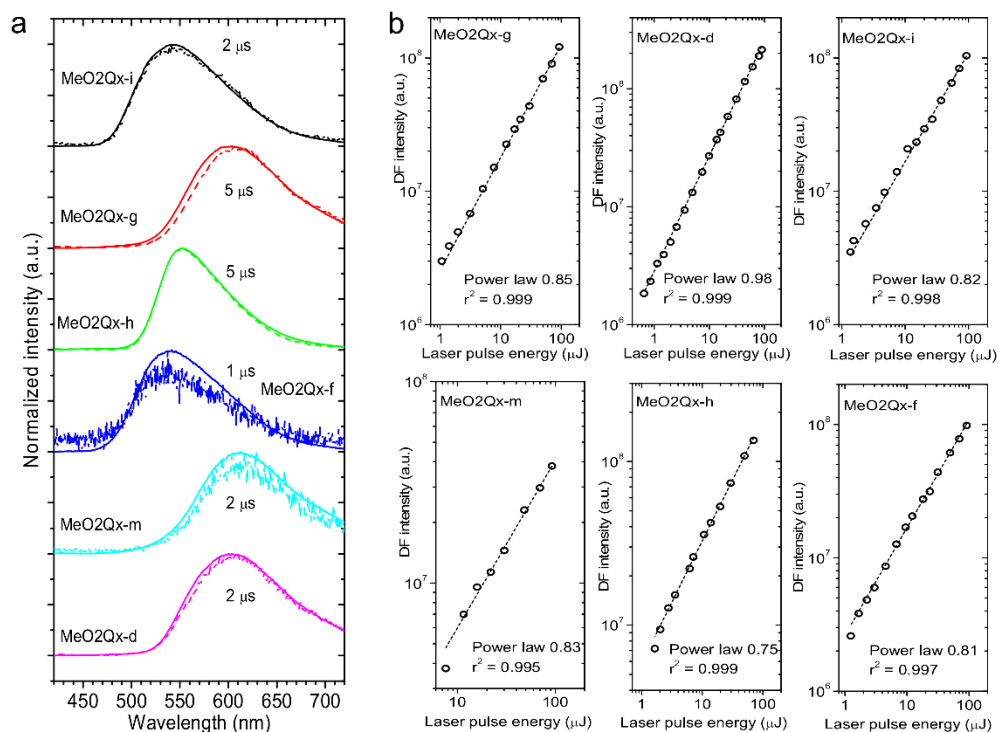
Fig. 4.25 (a) Time-resolved PL spectra of luminescent forms of MeO2Qx. The solid line depicts prompt fluorescence; the dotted-and-dashed line indicates delayed fluorescence. The delay at which the delayed fluorescence spectrum was recorded is indicated in the figure next to the respective spectrum. (b) Power dependence of delayed fluorescence is recorded in various photoluminescent forms of MeO2Qx.

4.1.5. PXRD study of different solid states

The powder XRD patterns of all the forms are depicted in Figure 4.26. The initial powders (-i) exhibited diffraction peaks demonstrating well-ordered and crystalline structures. However, after grinding with a spatula, their signals are either weaker or disappear, rendering the crystallinity of the starting forms disrupted by an external stimulus. Upon either heating (-h) or fuming (f) of ground powders (-g), new diffraction peaks arise; this is a manifestation that the ground solids reassembled from the amorphous form into a new crystalline lattice corresponding to a blue-shifted emission in relation to the ground form (-g). Melt- and drop-cast films are amorphous. The XRD patterns of MeO2Qx-h received by heating of MeO2Qx-g are different from the other crystalline forms, which suggests that a second crystalline form was obtained by heating. MeO2Qx-h thus shows a different crystal structure from the crystal form obtained by contact with a solvent (i.e., MeO2Qx-f).
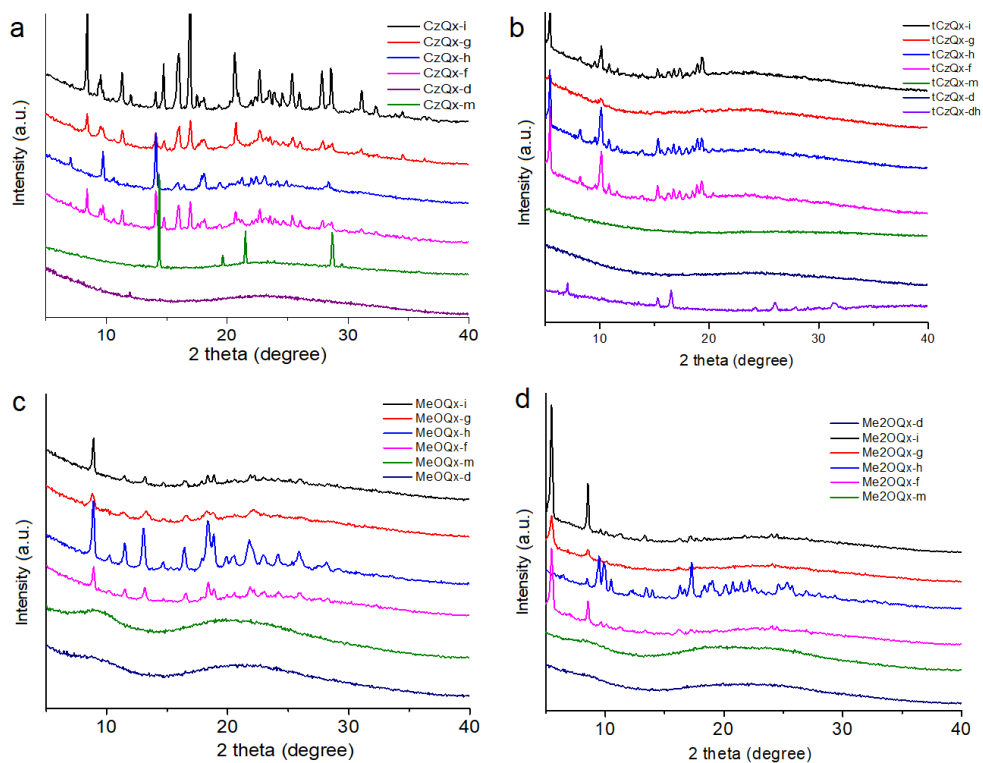
Fig. 4.26 XRD patterns of various forms of the compounds: a) CzQx, b) tCzQx, c) MeOQx, and d) MeO2Qx.

4.1.5.1 Summary of photophysical properties

The photophysical properties of the studied compounds in the solid state were altered by mechanical stimulation. They exhibited MCL behavior. Moreover, MeOQx and MeO2Qx exhibited multicolor altering in response to external forces. In all cases, grinding with a spatula perturbed solid forms. This led to red-shifted and broadened photoluminescence spectra, which reflected the conversion from crystalline to amorphous states. On the contrary, fuming by CH_2Cl_2 for 5 min or heating at 180 °C for 10 min resulted in blue-shifted and narrower photoluminescence spectra and typically higher PL quantum yields, except for tCzQx, for which, the opposite phenomenon was observed due to TADF contribution in amorphous forms. These observations imply a well-ordered and rigidified molecular structure upon heating and fuming. Consequently, a variation in the packing orientation and dihedral angles between the donor and the acceptor led to differences in the emission spectra due to the changes in CT energy. The alternation of the D-A dihedral angle resulted in switches between the charge transfer (CT) and/or the locally excited (LE) states. While CT always causes broadened spectra, the LE state provides narrower spectra. Melt-casting also causes a significant bathochromic shift of PL. These observations can be explained by the formation of excimer forms after melting or a further

relaxation of the CT due to a larger free volume. The drop-coast films demonstrate a red-shifted emission relative to that of the crystalline forms. The films of tCzQx and MeOQx can be transformed into the crystalline phase by heating and thus it results in blue-shifted photoluminescence (Table 4.4).

The pristine film of CzQx (CzQx-i) shows bluish-green emission with the intensity maximum located at 504 nm with Φ_{PL} = 3%. After mechanical grinding by using a spatula, the green emission red-shifts giving emission with the intensity maximum at 510 nm and Φ_{PL} = 5%. These changes are attributed to disarranging of the molecular assembly, which implies the decrease of the degree of crystallinity. After annealing at 180 $^{\circ}$C or vapor treating of the ground sample,DCM vapor for 5 min, the emission blue-shifts to sky blue with the maximum at 478 nm and 479 nm, and Φ_{PL} = 11% and 6%, respectively. The hypochromic shift and higher PL quantum yields imply that intermolecular interactions between adjacent molecules are suppressed. CzQx-h has a narrower PL spectrum and exhibits a higher Φ_{PL} than CzQx-f, which shows that CzQx-h has a higher degree of crystallinity, whereas CzQx-f still contains traces of the amorphous phase. The drop-cast film of CzQx exhibits emission with the maximum at 519 nm, and Φ_{PL} of 6% (Figure 4.26 and Table 4.4).

As-prepared tCzQx-i exhibits sky blue emission with the maximum at 477 nm; upon grinding (tCzQx-g), the fluorescence maximum shifts by 50 nm towards the red color with the PL intensity maximum of 527 nm. This is accompanied by the Φ_{PL} increase from 9% to 12%. Heating and fuming of tCzQx-g powder leads to sky-blue fluorescence. The emission bands of tCzQx-f and tCzQx-h have maxima of 477 nm and 479 nm.

The photoluminescence of tCzQx-i, tCzQx-h and tCzQx-f is more blue-shifted than that of hexane (488 nm). This may suggest that the singlet state emission has a more localized character than the emission of solution in a non-polar solvent. The red shift of photoluminescence after grinding (tCzQx-g) implies the transformation of the excited state from the LE (or HLCT) state into an intramolecular charge transfer (ICT) state upon relaxation of the D-A dihedral angle. In the amorphous phase, there is more free space, which allows the donor units to adapt a conformation promoting charge transfer. The drop-cast film (tCzQx-d) shows a similar emission to that of ground powder (tCzQx-g) with the maximum at 534 nm and a similar Φ_{PL} of 11%.

The PL intensity maximum of MeOQx-g is red-shifted by 27 nm (543 nm) compared to that of MeOQx-i (516 nm). Upon grinding, the Φ_{PL} and the full width at half maximum (FWHM) increases thus indicating CT state emission. The initial state can be recovered by thermal annealing (MeOQx-h) with Φ_{PL} of 10%. The fuming of MeOQx-g with DCM vapor turned its photoluminescence to green with the intensity maximum at 514 nm and the Φ_{PL} of 9%. We should note that the fluorescence spectra of drop-cast films emit orange photoluminescence (λ_{PL} = 576 nm) with Φ_{PL} = 10%.

MeO2Qx-i exhibits photoluminescence of λ_{PL} = 534 nm, Φ_{PL} = 6%. The photoluminescence color of MeO2Qx-i undergoes a change to orange-red through grinding (MeO2Qx-g), with λ_{PL} = 586 nm, and Φ_{PL} = 4%. The exposure of MeO2Qx-g to DCM vapor leads to MeO2Qx-f with λ_{PL} = 523 nm. Thermal annealing causes a slight blue shift and conversion to a yellow emissive powder (MeO2Qx-h) with the

PL intensity maximum at 559 nm, accompanied with the increase of Φ_{PL} to 7%. Thus MeO2Qx-h does not transform into MeO2Qx-f upon fuming, but can be recrystallized to obtain MeO2Qx-i.

A bathochromic shift occurs upon melt-casting. CzQx-m and tCzQx-m exhibit green and yellow emission with λ_{PL} = 524 nm, Φ_{PL} = 10% and λ_{PL} = 544 nm, and Φ_{PL} = 9%, respectively. The same treatment of MeOQx and MeO2Qx yields films with orange and red photoluminescence, with λ_{PL} of 582 nm and 618 nm, respectively (Figure 4.15).

4.1.5. Thermal transitions

The thermal stability of compounds was estimated by TGA. The results are shown in Fig. 4.27. The 5% weight loss was observed in the temperature range from 320 to 346 °C. The attachment of substituents to carbazole moieties increased the thermal stability. CzQx showed 5% weight loss temperature of 320 °C, tCzQx of 346 °C, MeOQx of 342 °C and MeO2Qx of 365 °C. These results imply that by using methoxy substituents, the intermolecular interactions between adjacent molecules increase.
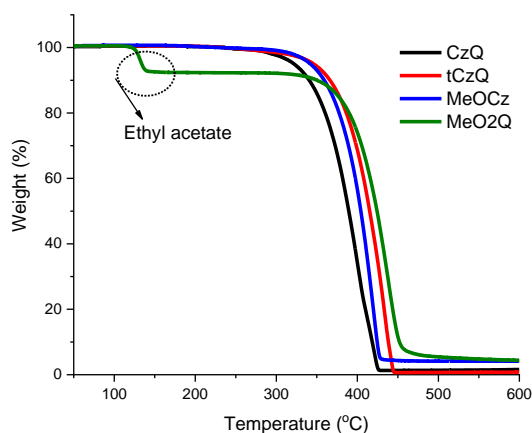
Fig. 4.27 The TGA thermograms of reported materials.

The DCS curves of the initial forms of the compounds were compared with those of their ground, heated and fumed forms (Fig. 4.28). The heating or cooling cycles that did not show any thermal dependence behavior were hidden for further clarifications. Our study discovered that, upon application of external stresses on compounds, the thermal properties of compounds changed because of the alteration in molecular packing. The glass transition, crystallization temperature and melting point of compounds in their different states after external stimulation are indicated in Figure 4.28. The highest and lowest melting points were observed for tCzQx and MeO2Qx at 326 and 235 °C, respectively, except for ground and fumed forms of CzQx. In general, methoxy substitution causes a decrease of the melting point: the more methoxy groups are attached to carbazole moieties, the lower is the melting point. Therefore, MeO2Qx has a lower melting point than MeOQx. This evidence implies that, in these molecules, methoxy units disrupt molecular assembly. The

70

higher melting point in tCzQx in comparison with CzQx can be attributed to the effect of heavy *tert*-butyl substitution, which results in locked and rigidified forms of the first substance. In the initial form of compounds, the highest glass transition temperature was observed for tCzQx (127 °C). Also, among these molecules in the initial form, the highest exothermic peak, corresponding to the crystallization temperature, occurred for MeOQx at 207 °C. In the cooling processes, neither endothermic nor exothermic peaks were observed, except for the initial and heated forms of CzQx. Cooling from the melts of CzQx-i and CzQx-h revealed their exothermic behavior. Usually, crystallization and glass transition signals are observed during the first and second heating or cooling scans; yet, CzQx was an exception. The glass transition of tCzQx observed for its initial form was lower than those of the other forms. This observation can be ascribed to changes in the molecular packing and enhancement of intermolecular interaction with the adjacent molecules.
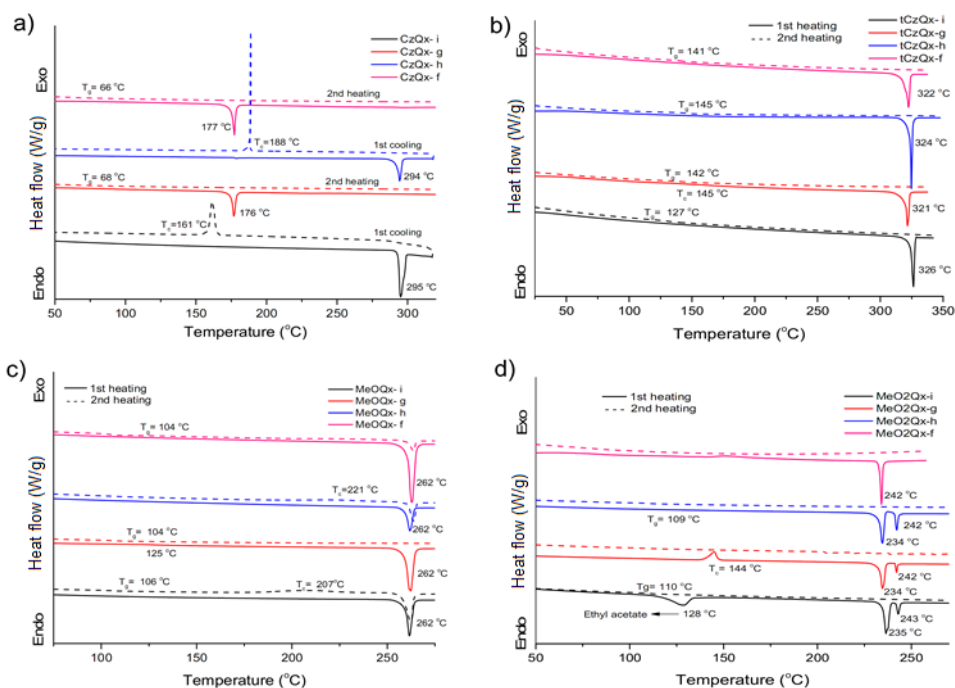
Fig. 4.28 DSC curves of differently treated solid samples.

4.1.6. Device fabrication

Due to the very good solubility of the compounds in toluene, OLEDs were fabricated by solution processing (Table 4.5). Due to their sufficient solubility in toluene, it was possible to use high molecular weight PVK (PVKH) as an electron blocking and hole transport material to improve the charge confinement. We should note that high molecular weight PVK (PVKH) is not soluble in toluene at room temperature. Therefore, PVKH was spun from the solution in chloroform-

Table 4.5 Summary of device characteristics.

| Device | Turn on at 5 cd m^{-2}, V | EQE (%) / Current efficiency (cd A^{-1}) | | | Max. cd m^{-2} | CIE (x,y) at max. brightness |
		max.	at 100 cd m^{-2}	at 1000 cd m^{-2}		
Dev 1	5.9	5.4 / 14.2	5.0 / 13.1	3.3 / 8.5	5397	0.22, 0.40
Dev 2	5.0	9.1 / 28.9	3.2 / 12.8	8.8 / 28.3	15290	0.29, 0.55
Dev 3	5.0	7.3 / 22.7	5.0 / 11.2	7.2 / 21.8	12910	0.36, 0.55
Dev 4	5.0	10.9 / 27.2	9.6 / 24.5	7.9 / 24.2	16760	0.41, 0.53

Device structure: ITO | HIL 1.3N (45 nm) | PVKH (10 nm) | PVK:PBD (60:40) co dopant 5% (32 nm) | TPBi (50 nm) | LiF (0.8 nm) | Al (100 nm). Where PVK denotes poly(*N*-vinylcarbazole) with average molecular weight of 90 000 g mol^{-1} while PVKH denotes poly(*N*-vinylcarbazole) with 1.1 • 10^6 g mol^{-1} average molecular weight. Dopants: Dev 1=CzQx, Dev 2=tCzQx, Dev 3= MeOQx, Dev 4= MeO2Qx

chlorobenzene (95:5) mixture, and PVK:PBD + dopant (5%) was spun from the toluene solution. The electron transporting layer of TPBi was then prepared by vacuum evaporation, LiF and Al layers were prepared by vacuum evaporation later in this order.
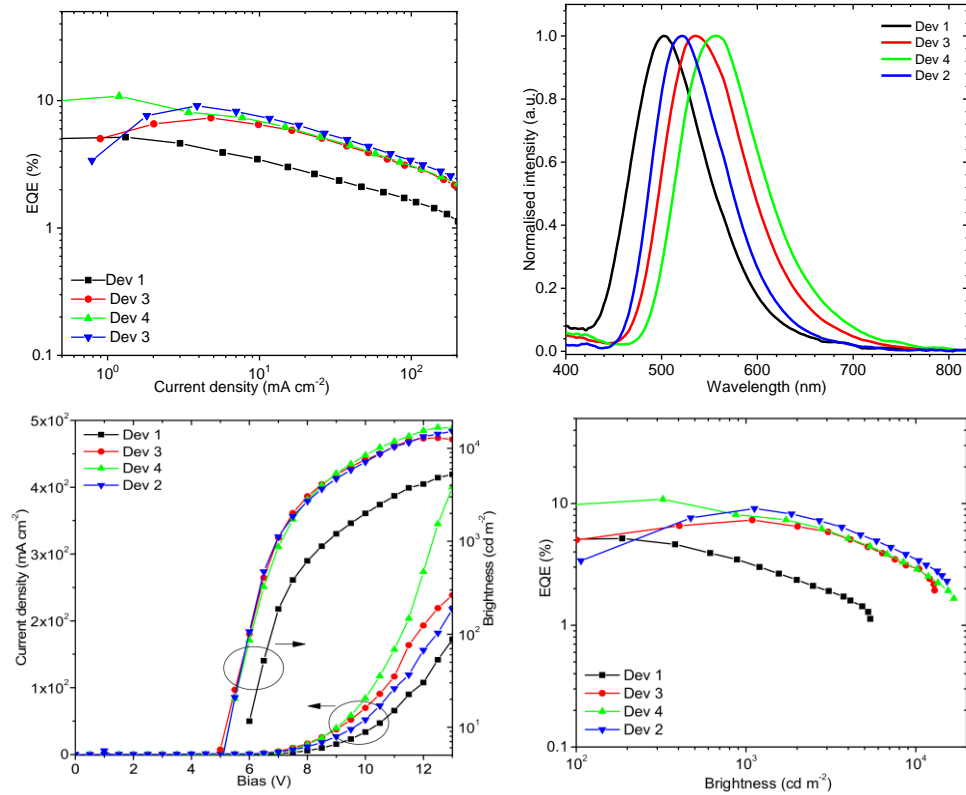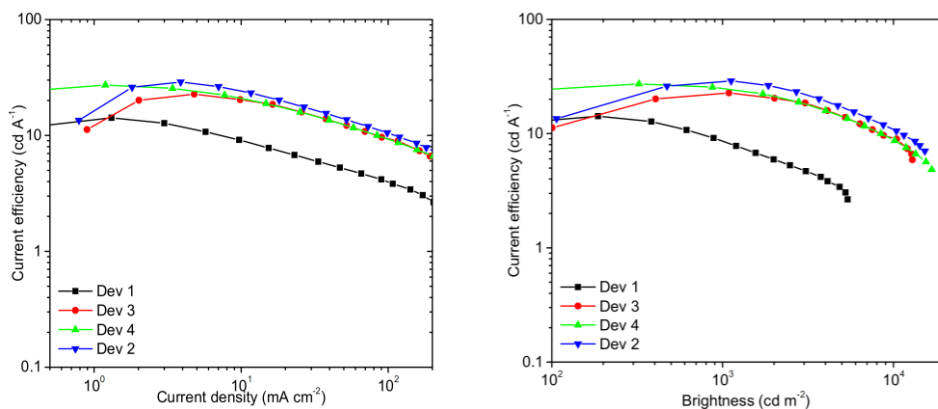
Fig. 4.29 OLED characteristics.

When using all the four compounds, efficient green-blue to green-yellow OLEDs were fabricated (Fig. 4.29). High-molecular-weight poly(9-vinylcarbazole) (PVKH) was used for an electron-blocking and hole-transporting material in order to improve charge confinement in the emitting layer. Since PVKH does not dissolve in toluene at room temperature, PVK:PBD blend was used as a host due to its superior film-forming and well-balanced charge transporting properties. The devices showed electroluminescence changing from blue-green (Dev 1) to yellow-green (Dev 4). The devices showed EQE over 5% and up to 10.9%, giving clear indication that triplet excitons are being harvested by the TADF mechanism. The best EQE was observed for Dev 4 which contained MeO2Qx as a dopant. Devices 2–4 were similar to each other, but Dev 1 was much less efficient and showed a higher turn-on voltage. The lower efficiency of Dev 1 is explained by the lower contribution and a longer lifetime of the TADF, while the higher turn-on voltage is a consequence of the highest HOMO energy of CzQx among the studied molecules.

4.2. Materials exhibiting room temperature phosphorescence, mechanochromic luminescence and delayed fluorescence properties:
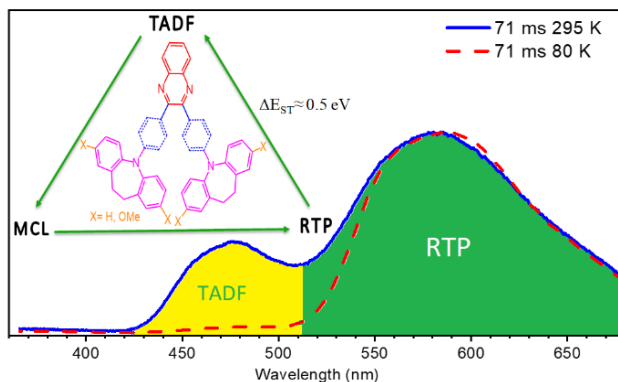
Scheme 4.5 Multifunctional behavior of shown molecules and their photoluminescence and phosphorescence at 80 K and 295 K.

This chapter is written based on the paper published in *Chem. Commun.* **2018**, *54*, 13857 [118]. Iminodibenzyl (IDB) and iminostilbene (ISB) are electron donating motifs with a 7-member ring in the core. The properties and applicability of IDB- and ISB-containing electroactive compounds previously were less investigated. In this part of the work, we designed new electroactive compounds by combining these donors with a quinoxaline moiety as an acceptor. Owing to the twisted and rigidified structure of iminodibenzyl, IDBQx exhibited both thermally activated delayed fluorescence and phosphorescence at room temperature even despite having a large energy gap between the excited singlet state and triplet state ($\Delta E_{ST} \approx 0.50$ eV). ISBQx with the same energy gap solely demonstrated prompt fluorescence. These results highlight iminodibenzyl as a promising donor capable to eliminate non-radiation transition.

4.2.1 Synthesis

The synthetic routes for the target compounds are described in the following Schemes 4.6–4.9. AzQx was prepared by the reaction of 2,3-dichloroquinoxaline and IDB in the presence of $ZnCl_2$. The synthesis of the luminogens with the phenylene bridges was conducted in two steps. Firstly, the reaction of *o*-phenylenediamine with 4,4'-dibromobenzil in the presence of HCl and AcOH gave the dibromoderivative of the extended quinoxaline acceptor. *N*-Arylation of the dibromoderivative through Buchwald-Hartwig reaction with IDB or ISB yielded the target products. The structures of the compounds were confirmed with ^{1}H NMR, ^{13}C NMR and mass spectrometry.
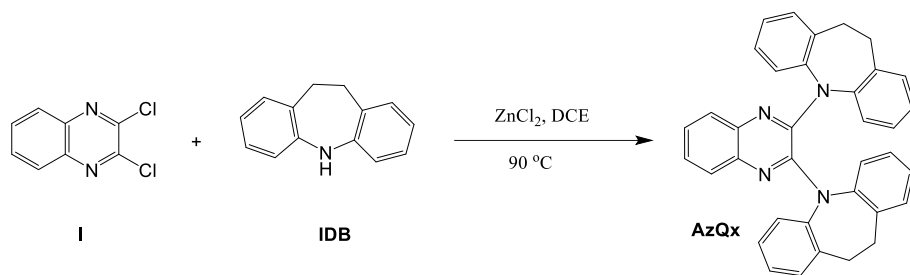
Scheme 4.6 Synthesis of AzQx.

OIDB was generated in two steps (Scheme 4.9). Firstly, iminodibenzyl was brominated via NBS in silica gel. Then, 3,6-dibromoiminodibenzyl was methoxylated by NaOMe in DMF in the presence of copper iodide in order to obtain the desired donor.
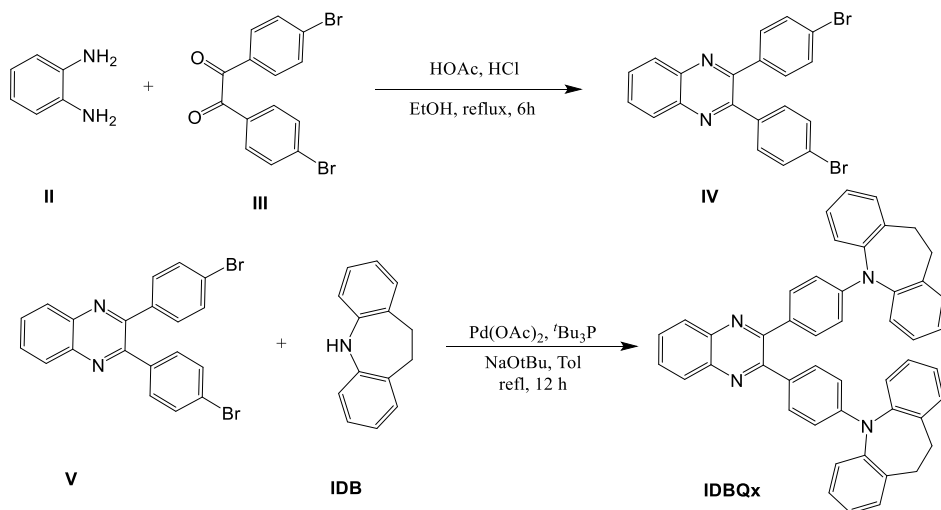
Scheme 4.7 Synthesis of IDBQx.
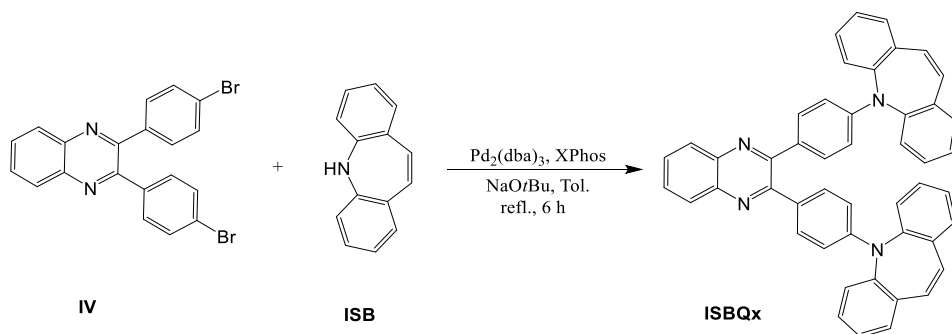
Scheme 4.8 Synthesis of ISBQx.

Scheme 4.9 Synthetic route for generation of OIDBQx.
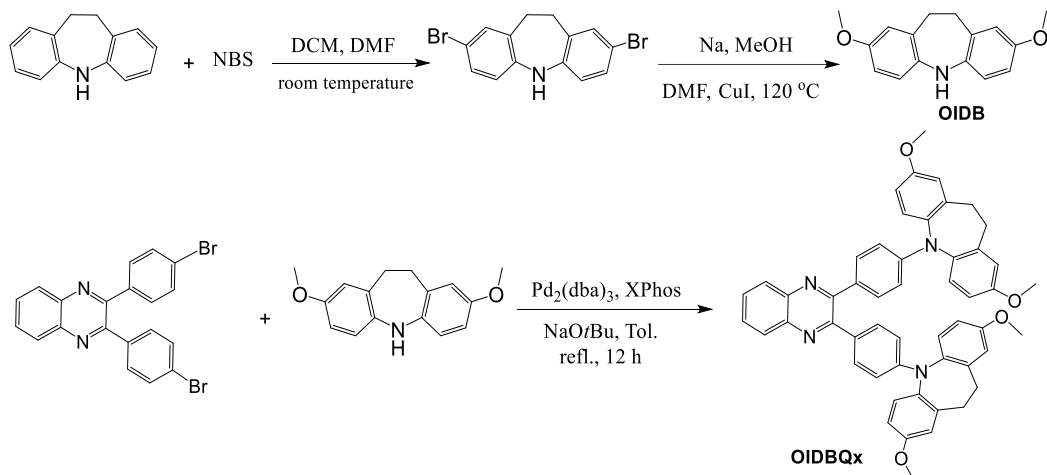
4.2.1. Electrochemical properties

Electrochemical measurements were conducted for DCM solutions while using Bu$_4$NPF$_6$ (0.1 M) as the supporting electrolyte and ferrocene as the standard couple. The compounds displayed a reversible oxidation wave as seen in Figure 4.30. Irreversible reduction waves were observed for all the studied derivatives of iminodibenzyl and iminostilbene.
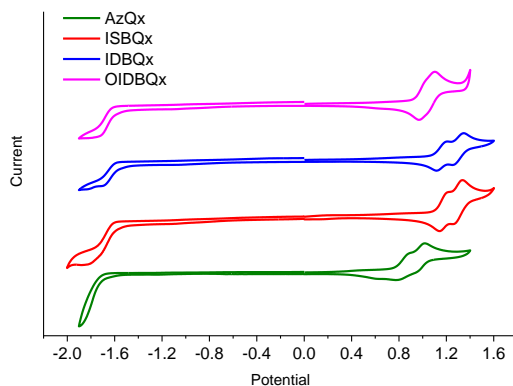
Fig. 4.30 CV curves of the solutions of the compounds in DCM.

All the molecules exhibited comparable LUMO energy values which can be attributed to the similar effects of donors on quinoxaline. The highest HOMO energy value was observed for AzQx, -5.23 eV, which implies good separation of HOMO and LUMO. Typically, a stronger donor indicates the increase of the energy level of HOMO and LUMO, and, conversely, a stronger acceptor results in a decrease of HOMO and LUMO. Therefore, methoxylation leads to increasing the HOMO energy level and to a slight enhancement in LUMO. Thus, whereas, IDBQx has -5.39 eV and -2.79 eV for HOMO and LUMO, respectively, OIDBQx in comparison indicates

higher HOMO and LUMO energy levels. The lowest HOMO was seen for ISBQx (-5.41 eV), which indicates that ISBQx contains the weakest donor, iminostilbene, among these four molecules.

Table 4.6 Summary of electrochemical properties.

Sample	HOMO (eV) [a]	LUMO (eV) [a]	E_g (eV) [b]
AzQx	-5.23	-2.77	2.68
IDBQx	-5.39	-2.79	2.71
ISBQx	-5.41	-2.76	2.68
OIDBQx	-5.26	-2.75	2.75

[a] HOMO and LUMO energy determined by cyclic voltammetry in CH_2Cl_2; [b] optical energy gap in CH_2Cl_2.

4.2.2. Thermal transitions

The results of thermal analysis show that the introduction of the phenylene linkage results in the increase of thermal stability. Differential scanning calorimetry of compounds was illustrated in Fig. 4.31. The second heating scan is different from the first as it did not show the melting point. Also, the DSC heating scan of AzQx did not show any melting signal. This observation shows that the compound was obtained in amorphous form. AzQx exhibited glass transition in its second and third heating scans at 111 °C and 117 °C, respectively.
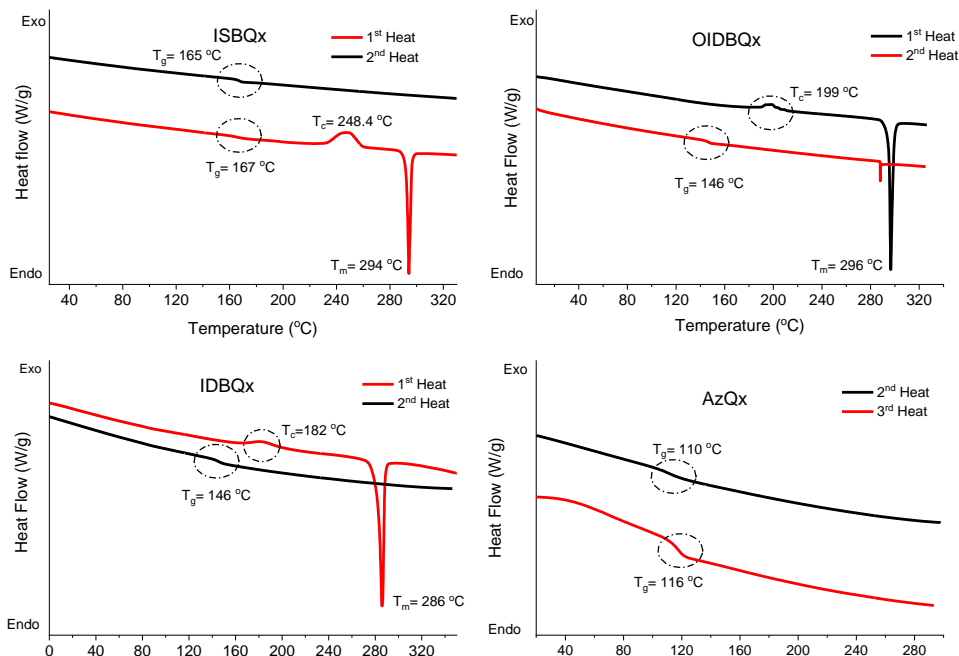
Fig. 4.31 DSC curves of the derivatives of iminodibenzyl and iminostilbene.

Whereas, in IDBQx, T_g increased to 146 °C, which manifested itself at second heating. These higher T_g temperatures for the compounds with a higher molecular weight can be explained by the enhanced intermolecular interactions which hindered molecular motions. Phenylene-bridged compounds exhibited crystallization signals in the first DSC heating scans (Fig. 4.31). Attaching a methoxy unit on iminodibenzyl led to an increase of the crystallization temperature and the melting point. So, as we see in Fig. 4.31, for T_c from 182 °C, (IDBQx) increases to 199 °C (OIDBQx), and the latter substance has a 10 °C higher melting point than the first substance.

As shown in Fig. 4.32, embedding the phenylene bridge causes an increase in the decomposition temperature. Thus the 5% weight loss for AzQx at 242 °C, and its low weight loss and several degradation implies that the molecule started to be polymerized. OIDBQx at 436 °C after losing about 25% of its weight started to be polymerized. OIDBQx and ISBQx exhibited higher thermal stability with 5% weight loss temperatures of 402, 398 and 418 °C, respectively. These results indicate the effect of intermolecular interactions.
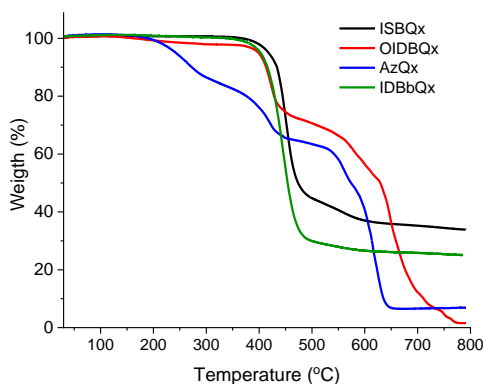
Fig. 4.32 TGA curves of the derivatives of iminodibenzyl and iminostilbene.

4.2.3. Single crystal XRD analysis

Single crystal XRD analysis of IDBQx and ISBQx revealed their molecular conformations. To minimize steric hindrance between the donor and the phenyl linkage, the 7-membered ring core of the donor is distorted by giving it a bent conformation. IDBQx demonstrated a twist-boat form, while the boat conformation was observed for ISBQx. Because of these adopted conformations, the donor-acceptor dihedral angles (Fig. 4.33) were found to be relatively small of *ca*. 11° and 12° for IDBQx and ISBQx, respectively.
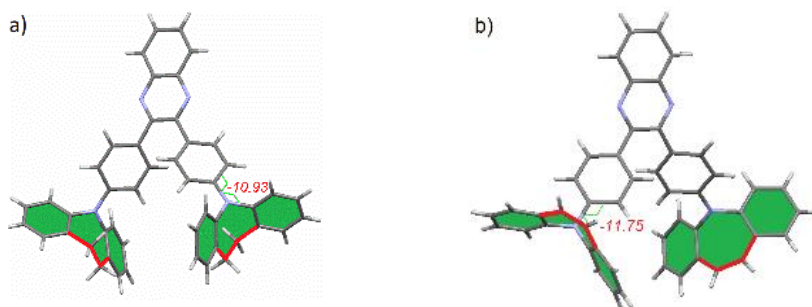
Fig. 4.33 Single crystal structures of a) IDBQx and b) ISBQx. Dihedral angles between the donor and the phenyl ring are depicted.

Figs. 4.34 and 4.35 showing the packing arrangement of molecules in the crystalline solid give an insight into intermolecular interactions. For IDBQx, the quinoxaline moiety is located close to another quinoxaline unit with edge-to-edge arrangement. Whereas, for ISBQx, ISB and quinoxaline are located next to each other.
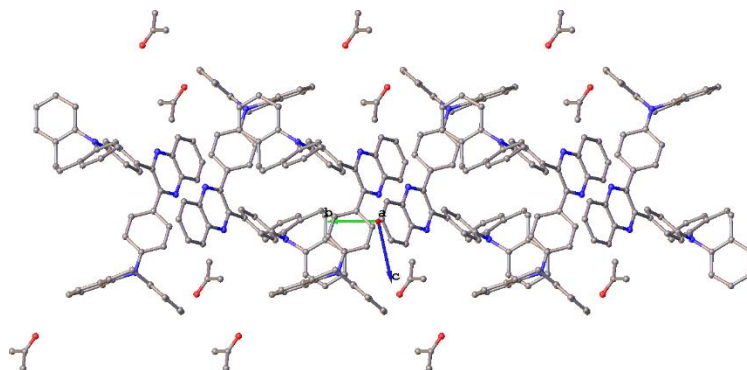
Fig. 4.34 Packing in the crystal structure of compound IDBQx viewed along the *a*-axis. Hydrogen atoms are removed for clarification.
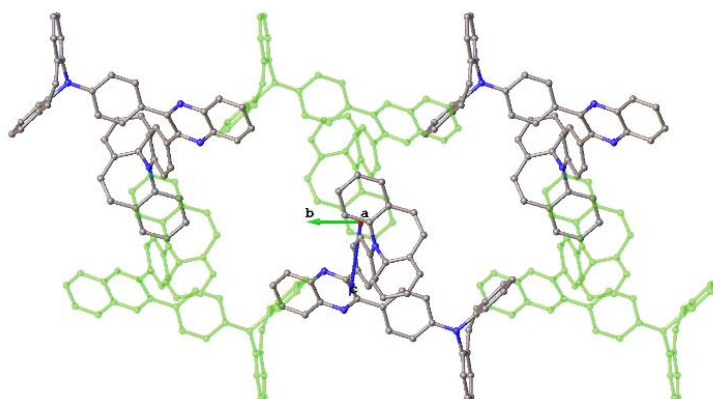
Fig. 4.35 Packing in the crystal structure of compound ISBQx viewed along the *a*-axis. Molecules are shown in two colors for clarity.

4.2.4. Photophysical properties

The studied molecules due to their bipolar, donor-acceptor structure showed pronounced solvatochromism (Fig. 4.36). For the molecules containing the phenylene spacer (IDBQx, ISBQx and OIDBQx), the CT character was found to be less expressed than for AzQx which contains no π-spacer. The emission color of IDBQx, ISBQx and OIDBQx varied from blue for the solutions in cyclohexane to green for solutions in highly polar acetonitrile. The solution of AzQx in cyclohexane showed blue emission while this substance in acetonitrile exhibited orange-red emission.
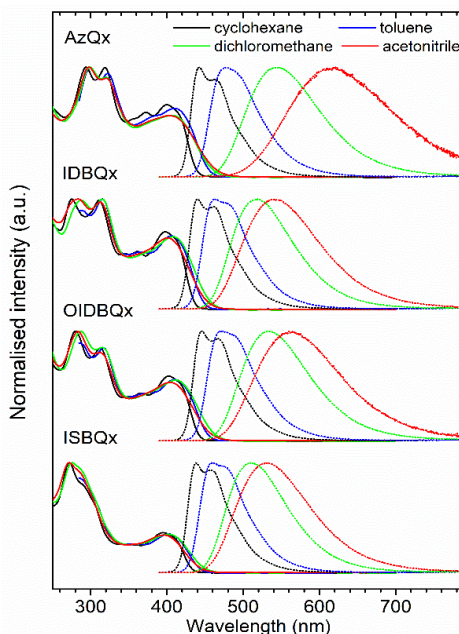
Fig. 4.36 Absorption and photoluminescence spectra of the solutions in various solvents.

In AzQx which has no spacer, spacious iminodibenzyl groups adopt twisted conformation in the quasi-orthogonal D-A orientation, thus the CT singlet excited state is further stabilized. The absorption band at *ca*. 400 nm in the spectra of all the molecules is attributed to ther CT-ππ* transition as indicated by positive solvatochromism. Although the molecules did not show delayed fluorescence in solutions, the films of their dispersions in Zeonex showed interesting properties (Fig. 4.37).

Due to the low polarity of Zeonex, the fluorescence spectra of the dispersions of iminodibenzyl and iminostilbene derivatives in this polymer were found to be similar to those observed for cyclohexane or toluene solutions which exhibit singlet emission in the blue region. This implies a large singlet-triplet gap of ≈0.5 eV (Table 4.7) thus preventing efficient thermally activated reverse intersystem crossing. For this reason, the molecules did not show significant contributions of TADF at room temperature.

Table 4.7 Photophysical characteristics of the derivatives iminodibenzyl and iminostilbene.

Sample	Abs (nm)[a]	PL (nm)[b]	$\Phi_{PL}{}^{c}$	$S_1 / T_1 (eV)^d$	$\Delta E_{ST} (eV)^e$
AzQx	299, 321, 406	545	0.41	2.92 / 2.41	0.51
IDBQx	288, 315, 408	518	0.38	2.93 / 2.41	0.52
OIDBQx	287, 315, 411	534	0.31	2.88 / 2.39	0.49
ISBQx	276, 402	511	0.35	2.91 / 2.40	0.51

[a]absorption maxima in CH_2Cl_2 solution; [b]emission maxima in CH_2Cl_2 solution; [c]PL quantum yield of degassed CH_2Cl_2 solution; [d]singlet and triplet energy of the dispersions in Zeonex 1% (w/w) film; [e]singlet-triplet energy splitting of the dispersions in Zeonex 1% (w/w) film.

However, unexpectedly, molecules containing IDB units showed strong room temperature phosphorescence (Figs. 4.38–4.41). In fact, only the iminodibenzyl-containing compounds demonstrated some delayed emission at room temperature, while the iminostilbene derivative was found to be a purely fluorescent system. This observation might be explained by the suppression of non-radiative decay which plays an important role in enabling the long-lived emissions. However, the singlet-triplet energy gap is still sufficient to allow thermal energy to partially up-convert the triplet states, and this is the reason why simultaneous TADF and RTP emissions were observed for derivatives of iminodibenzyl.
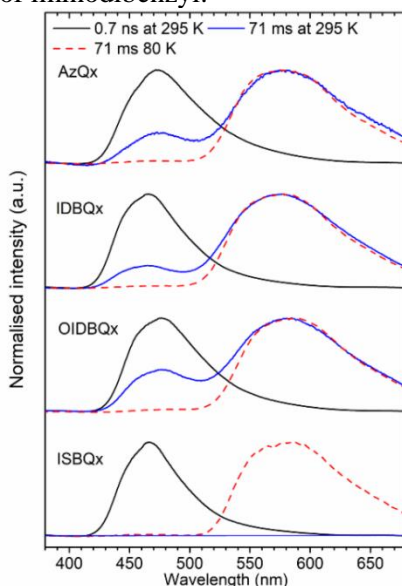
Fig. 4.37 Prompt fluorescence (black solid line), room temperature phosphorescence and TADF (blue solid line), low temperature phosphorescence (red dashed line) spectra of molecular dispersions of the compounds in Zeonex.
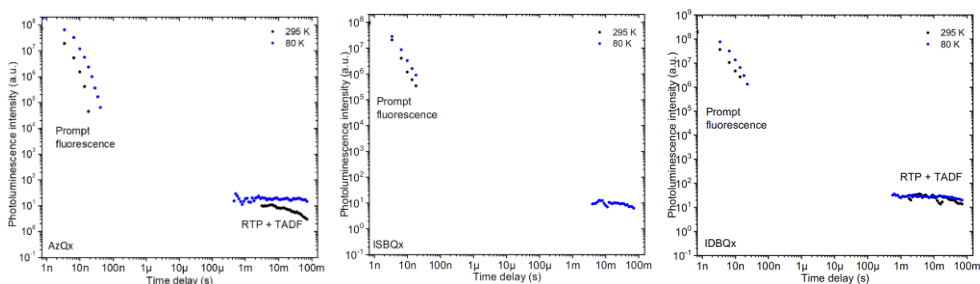
Fig. 4.38 Photoluminescence decay curves of IDBQx recorded at 80 and 295 K in Zeonex.

The existence of TADF and the absence of triplet-triplet annihilation was evidenced by the linear dependence of the intensity of the delayed fluorescence emission on the laser dose. The slope of DF intensity against excitation power was close to 1 in the log-log scale (see Fig 4.39a and Figs. 4.44, 4.45). In general, the ratio between TADF and RTP correlates with ΔE_{ST}, and, in this respect, the largest contribution of TADF was observed for OIDBQx.
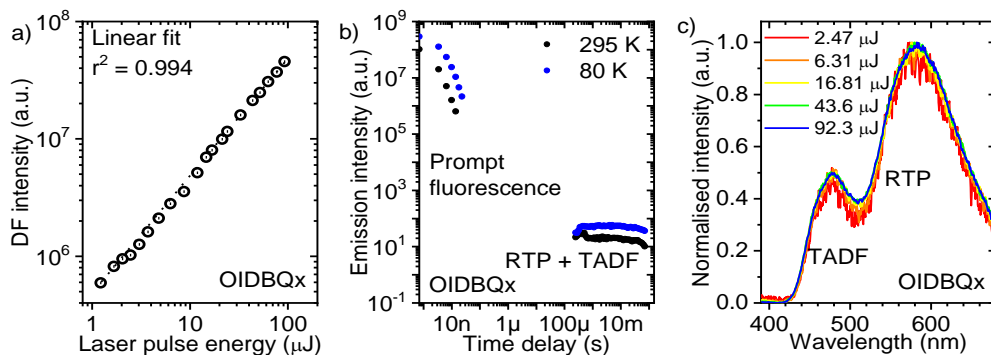
Fig. 4.39 a) Power dependences of delayed fluorescence for OIDBQx at 295 K; b) photoluminescence decay transients of OIDBQx recorded at 295 and 80 K; c) delayed fluorescence spectra and room temperature phosphorescence spectra recorded at 295 K with various excitation pulse energy.

The ratio of intensities of RTP and TADF did not change with the delay time for OIDBQx, which is also evidenced by monoexponential decay. This observation shows that both emissions originate from the same excited triplet state and both arrive from the same population of excited states (Fig. 4.44). TADF+RTP dual emission of the derivatives of iminodibenzyl is strong and easily noticeable as yellow-greenish afterglow. Furthermore, the lifetime of the TADF+RTP emission is relatively long, spanning from 51 ± 3 ms for AzQx up to a remarkable 128 ± 10 ms for OIDBQx (see Figs. 4.40–4.43).
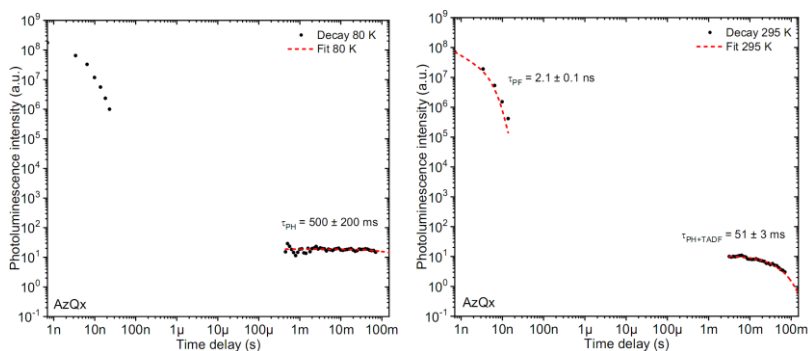
Fig. 4.40 Photoluminescence decay curves and fits for the dispersion of AzQx in Zeonex recorded at 80 and 295 K.
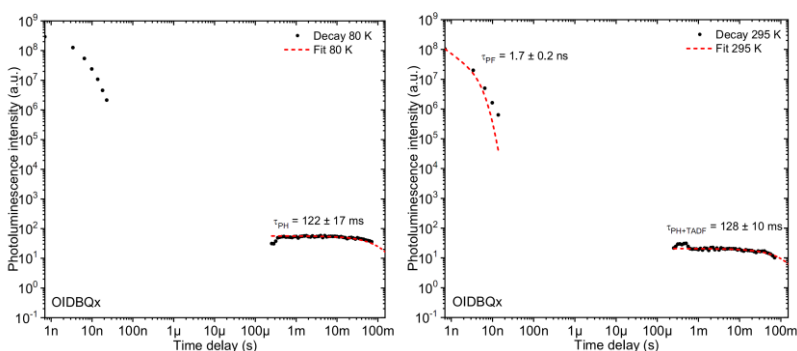
Fig. 4.41 Photoluminescence decay curves and fits of the dispersion of OIDBQx in Zeonex recorded at 80 and 295 K.

Such a behavior can be explained by the suppression of the non-radiative decay of the triplet state and by substantial triplet formation yields. The non-bonding orbitals, such as those present in the donor unit, predetermine high triplet formation yields due to the creation of n-π^* transitions which induce strong spin-orbit coupling according to El-Sayed's rule. However, the iminostilbene moiety does not support long-lived triplet emissions. This is likely to be caused by enhanced non-radiative decay. Both non-radiative decay and RISC process affect the iminodibenzyl derivatives, which is evidenced by substantially longer phosphorescence lifetimes observed at 80 K compared to the lifetime of TADF+RTP emissions recorded at 295 K. Remarkably, this is not the case for OIDBQx, which shows two emission lifetimes that are statistically insignificantly different at varying temperature (Fig. 4.41). The methoxy substitution not only stabilizes the triplet state but appears to induce the largest triplet formation yield. In turn, the TADF+RTP emission is the most efficient for OIDBQx. This can be caused either by inducing a larger contribution of the non-bonding pairs to the excited state, by the introduction of the methoxy groups or by the fact that the ΔE_{S-T} is the smallest (which improves the coupling of the S_1 and T_1 states).
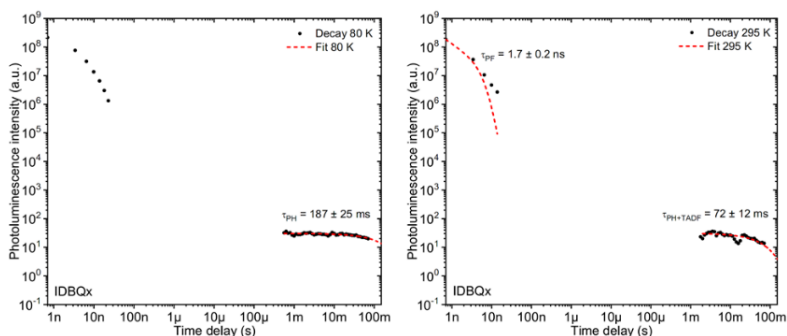
Fig. 4.42 Photoluminescence decay curves and fits of the dispersion of IDBQx in Zeonex recorded at 80 and 295 K.
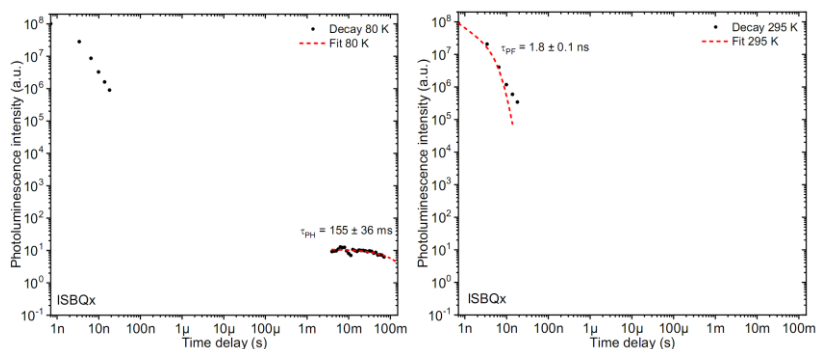
Fig. 4.43 Photoluminescence decay curves and fits of the dispersion ISBQx in Zeonex recorded at 80 and 295 K.

Laser fluence with various excitation pulse energy was used to assign the origin of emissions. The emission ratio of compounds was not dependent on the laser fluence (Fig. 4.44).
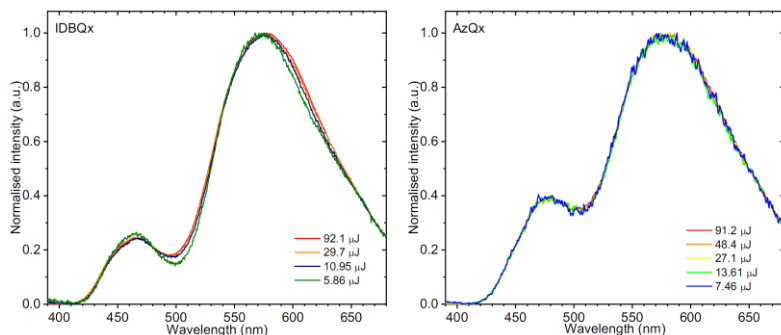
Fig. 4.44 Delayed fluorescence and room temperature phosphorescence spectra recorded at 295 K with various levels of excitation pulse energy.
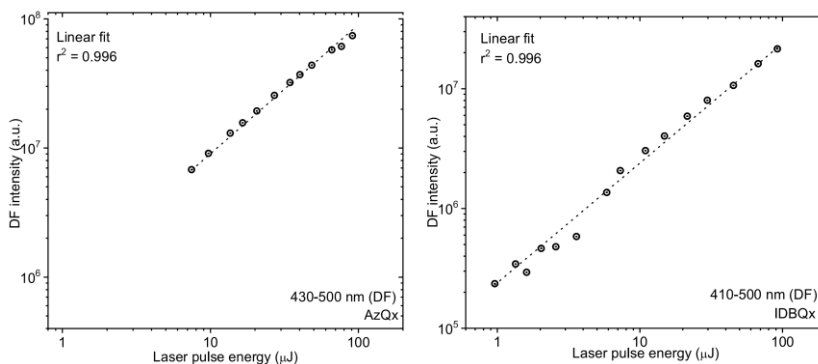
Fig. 4.45 Laser fluence dependence of delayed fluorescence intensity for the dispersions of AzQx and IDBQx in Zeonex recorded at room temperature.

4.2.5. Mechanochromic properties

In mechanochromic materials, increasing the strength of the acceptor leads to stronger mechanochromism. OIDBQx displayed reversible luminescence changes upon applying external stress (Fig. 4.46d). In the initial state, its powder demonstrated greenish-blue emission with the emission maximum at 494 nm. Through grinding the initial powder with a spatula, the emission broadened, and the intensity maximum red-shifted to 522 nm. The initial state was restored by exposure to CH_2Cl_2 vapor for 5 min. The vapor-treated form exhibited emission spectrum nearly identical to that of the initial powder ($\lambda_{max} = 495$ nm). A neat film showed a similar emission spectrum to that of the ground powder. In contrast, insignificant changes were observed in the emission of IDBQx after grinding. The photoluminescence maximum shifted from 495 nm to 499 nm (Fig. 4.46a). These results indicate that increasing the strength of the electron donor by methoxylation of IDB can increase the color contrast upon the application of external stimuli, which is in agreement with the previously described results. The luminescence of AzQx and ISBQx did not change after mechanical force (Fig. 4.46b and 4.46c).
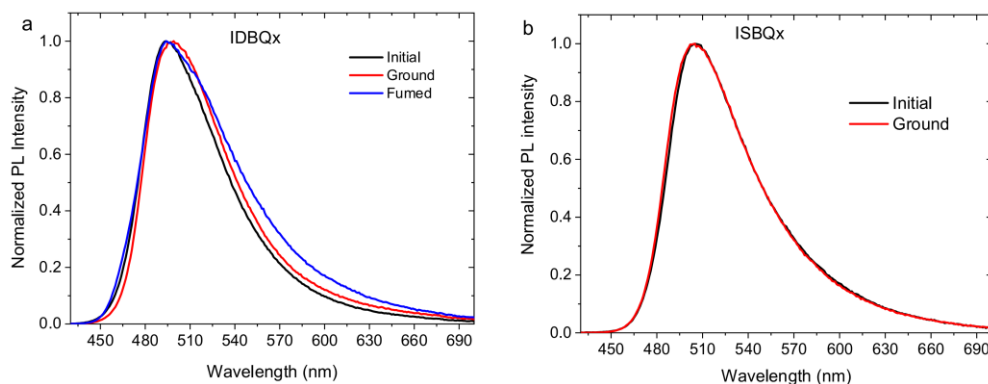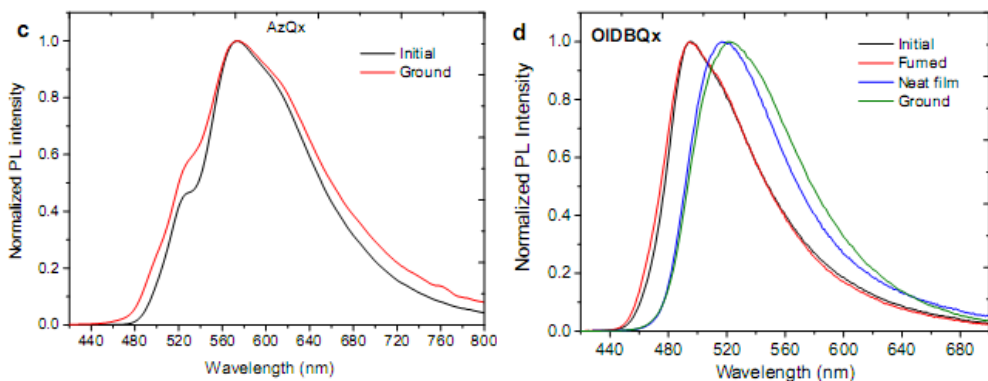
Fig. 4.46 PL spectra of a) IDBQx and b) ISBQx c) AzQx and d) OIDBQx after external stimuli in different forms. Neat film obtained by drop casting.

Powder XRD analysis of OIDBQx illustrated its morphological differences in different states. It can be seen in Figure 4.47 that the initial and fumed forms are crystalline, while, after grinding, it becomes amorphous. The drop-cast film was also amorphous.
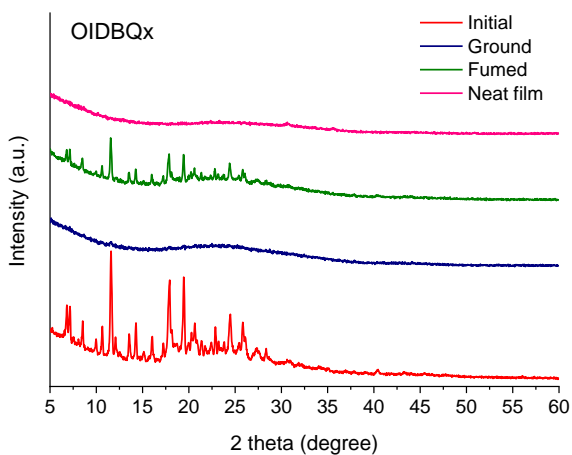
Fig. 4.47 Powder X-ray diffractogram of OIDBQx in the initial form (-i), ground (-g), drop-cast film (-df), and after fuming (-f).

4.3. Influence of acceptor and donor on mechanochromism and delayed fluorescence
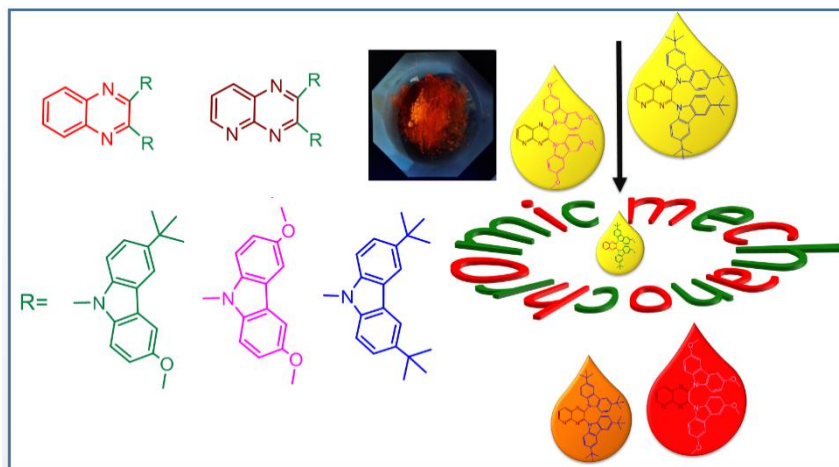
Scheme 4.10 Chemical structure of quinoxaline and pyridopyrazine containing compounds; their mechanochromic luminescence characteristics.

In this chapter, four new series of multifunctional materials are illustrated. A variety of MCL materials have been reported so far, and, as discussed in the introduction, there is no distinct architecture to synthesize materials aiming to tune their color upon environmental stimulation. After the preparation of the first series of MCL-TADF molecules, and because of their interesting properties, we decided to synthesize new series. In this part of the work, we explored new multifunctional materials that also revealed MCL-TADF. Four new luminophores were designed and synthesized, and their photophysical, electrochemical and MCL properties were studied. MCL was based on conformational variation and/or intramolecular interactions. Surprisingly, although the compounds have similar structures, MCL was observed only for three of them.

4.3.1. Synthesis

Taking into account the previously described results which revealed that the derivatives of methoxylated carbazole exhibited multichromism as well as a shorter excited life time, and that *tert*-butyl carbazole derivatives showed very good solubility, we designed new donor moieties containing *tert*-butyl and methoxy groups attached to a carbazole moiety (Scheme 4.11). In the first step of the synthesis, 3-methoxy-9*H*-carbazole was synthesized by bromination of carbazole. Then, by adding *t*-BuCl in the presence of zinc chloride, 3-bromo-6-(*tert*-butyl)-9*H*-carbazole was obtained. In the final step, methoxylation by methanol, Na and copper iodide generated the new donor TOC.
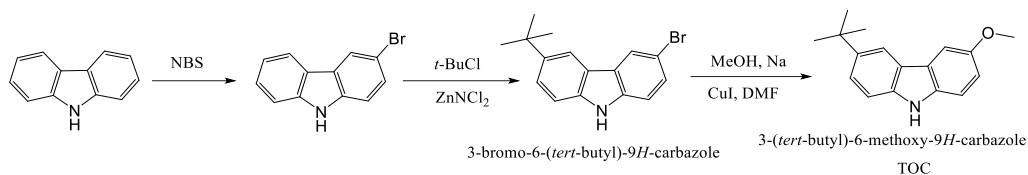
Scheme 4.11 Synthetic route for preparation of 3-(*tert*-butyl)-6-methoxy-9*H*-carbazole (TOC).

Two acceptors 2,3-dichloroquinoxaline and 2,3-dichloropyrido[2,3-*b*]pyrazine were used in the synthesis of the target compounds to compare the effect of the acceptor on the properties. The aim of the usage of a stronger acceptor, 2,3-dichloropyrido[2,3-*b*]pyrazine, was to decrease the ΔE_{ST} thus facilitating rISC, to study its effect on MCL properties and to obtain a more considerable contrast with the strong donor. We strove to understand whether the donor or the acceptor has more influence on MCL. The acceptor was prepared according the procedure reported in the literature [113]. The target products were obtained via S_NAr reaction in DMSO (Scheme 4.12), and characterized by NMR and mass spectroscopy. The reaction is not sensitive to air or moisture and was conducted without any drying of the solvent.
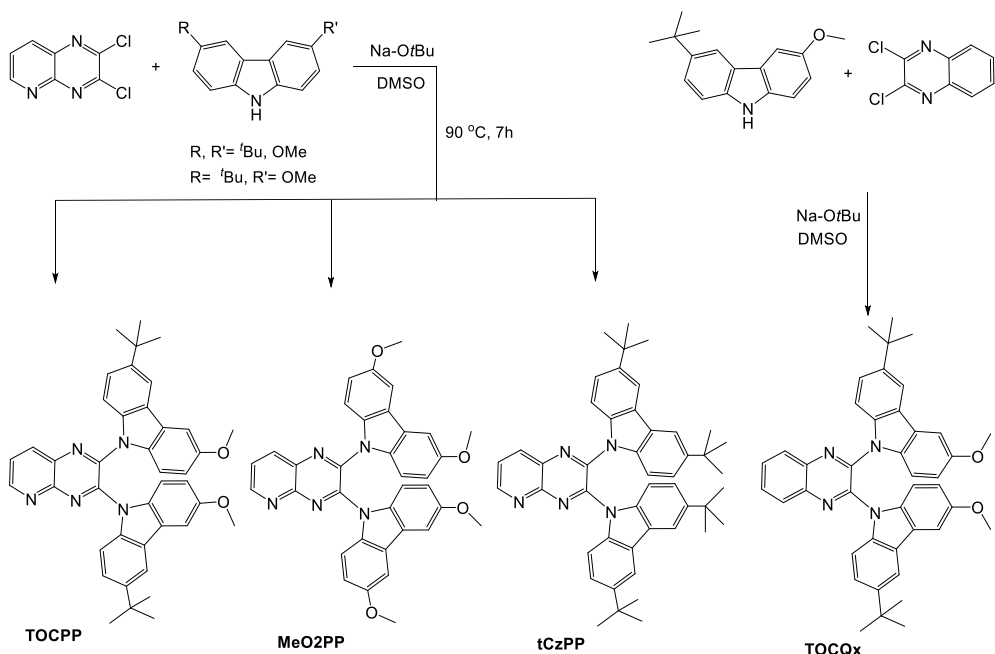
Scheme 4.12 Synthesis of derivatives of quinoxaline and pyrido[2,3-*b*]pyrazine.

4.3.2. Photophysical properties

The UV-Vis absorption and fluorescence spectra of the solutions of the compounds in toluene are depicted in Figure 4.48. The photophysical characteristics of the emitters are summarized in Table 4.8. The absorption bands peaking at 290 nm and 340 nm can be ascribed to π-π* and n-π* transitions, respectively. The absorption

bands at ca. 450 nm and their solvatochromic character can be attributed to the intramolecular charge transfer.
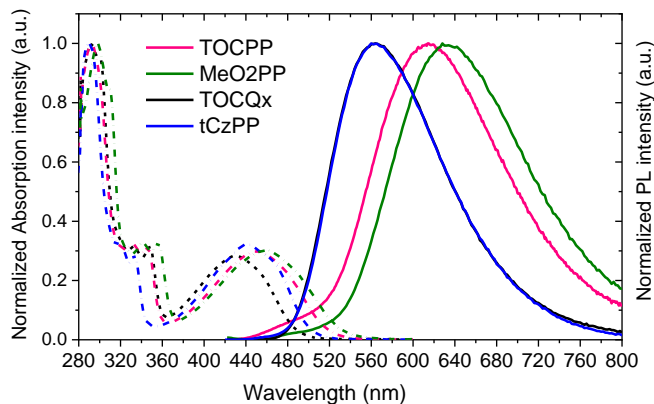
Fig. 4.48 UV-Vis and fluorescence of the solutions of the derivatives of quinoxaline and pyrido[2,3-*b*]pyrazine in toluene.

The photoluminescence spectra of the solutions of the compounds in solvents with different polarities disclosed their solvent-dependence behaviors (Fig. 4.49). The bathochromic shifts of the PL spectra and the wider emission bands observed with the increasing polarity of solvents indicate that dipole moments of the compounds in their excited states are larger than those in the ground states.
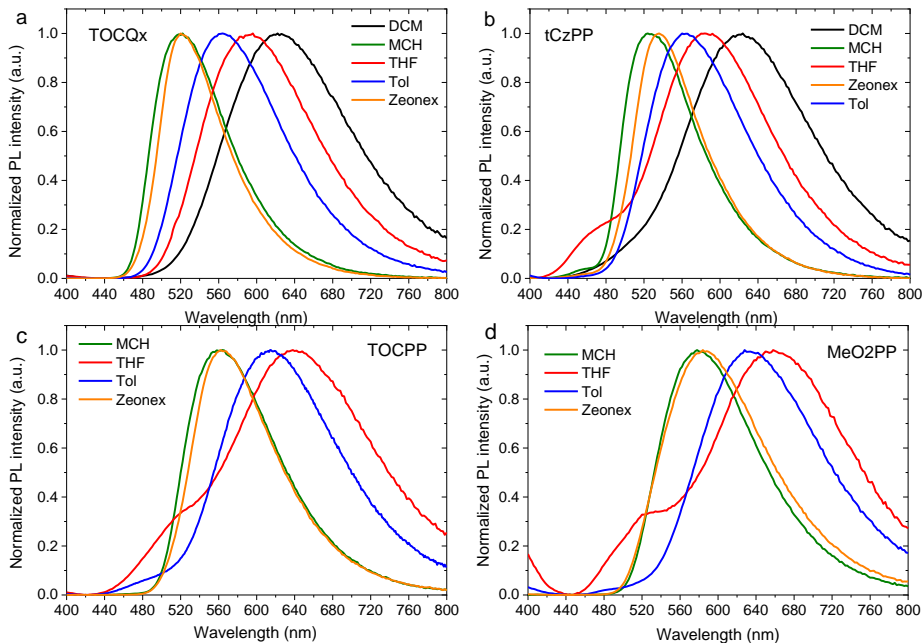
Fig. 4.49 PL spectra of the solutions of the derivatives of quinoxaline and pyrido[2,3-*b*]pyrazine in different solvents with λ_{ex}=350 nm.

The emission spectra of THF solutions of compounds tCzPP, TOCPP and MeO2PP containing a pyridopyrazine moiety demonstrate small peaks below 550 nm in addition to the main peaks (Figure 4.49). This observation implies that, apparently, in THF, local excited states of the acceptor begin to emit individually. In these cases, the electron donor affects the electron density of the acceptor and alters its PL spectrum.

To get insight into the effect of solvents on emission, the solutions of MeO2PP as the compound with the biggest dipole moment were selected for more profound investigations. Figure 4.50 demonstrates fluorescence spectra of MeO2PP in THF and toluene after application of different excitation energies. For the solutions in THF, emission in the yellow region is predominant after applying lower energies. This observation shows that, at a lower excitation energy, emission belongs to mainly LE states of the acceptor. This observation can be explained by a big energy gap between the donor and the acceptor that lower energies excite the ground state of the acceptor. Thus electrons do not flow from the donor to acceptor to obtain efficient CT.
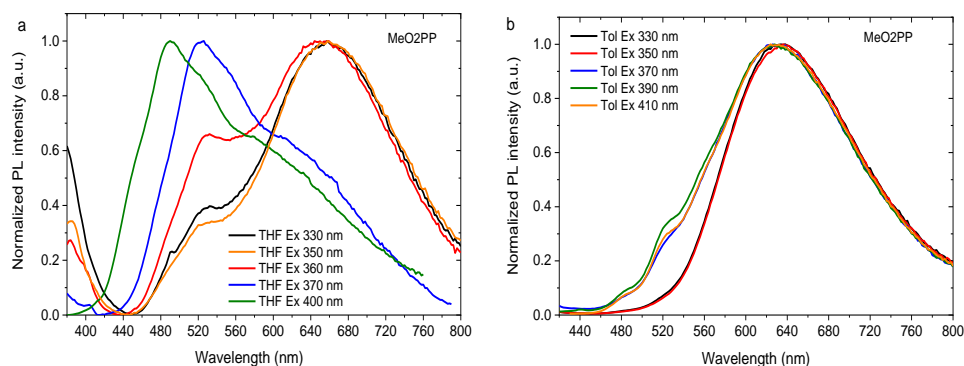
Fig. 4.50 PL spectra of the solution of MeO2PP in THF and in toluene recorded under application of different excitation energies.

Table 4.8 Photophysical characteristics of the derivatives of quinoxaline and pyrido[2,3-b]pyrazine.

Compound	Abs (nm)[a]	PL (nm)[b]	$\Phi_{PL}^{air\ c}$	S_1 / T_1 (eV)[d]	ΔE_{ST} (eV)[e]	E_g (eV)[h]
TOCQx	430	564	0.09	2.64 / 2.46	0.18	2.53
tCzPP	441	565	0.2	2.56 / 2.46	0.10	2.47
TOCPP	451	614	0.02	2.49 / 2.36	0.13	2.38
MeO2PP	459	632	0.01	2.48 / 2.33	0.15	2.33

[a] Wavelengths of CT band absorption maxima in toluene solution; [b] wavelengths of emission maxima in toluene solution; [c]photoluminescence quantum yield of air-equilibrated toluene solution; [d]singlet and triplet energies of the films of the dispersions in Zeonex 1% (w/w); [e]singlet-triplet energy splitting in of the films of the dispersions in Zeonex 1% (w/w); [f]energy gap in toluene.

4.3.3. Electrochemical characterization

CV measurements of the solutions of the compounds in DCM were conducted. They revealed reversible oxidation and reduction, which proves the electrochemical stability of compounds (Fig. 4.51).
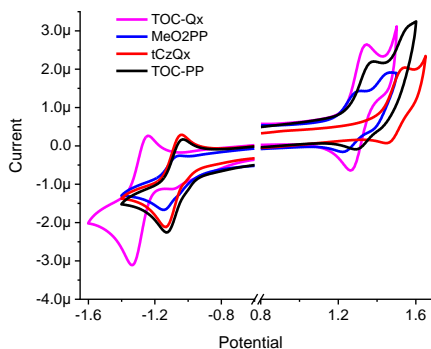
Fig. 4.51 Cyclic voltammetry of compounds in DCM.

The electrochemical properties of compounds by employing CV were collected in Table 4.9. By considering the electron donation abilities, it can be seen that the HOMO energy level is the highest for dimethoxylated carbazol, the strongest donor, which clearly leads to shrinking the energy bad gap. Moreover, the highest LUMO level is given for TOCQx, -3.12 eV, which contains quinoxaline as the electron withdrawing group, the weaker acceptor. The HOMO energy level of tCzPP is the lowest among these four molecules, which indicates a weaker electron donating ability in this molecule. Despite containing the same donor for TOCQx and TOCPP, the LUMO level of TOCPP is lower than TOCQx, which indicates a stronger electron withdrawing character of the acceptor in TOCPP and causes a decrease of the LUMO energy level. The LUMO energy level for the first three compounds is almost the same, which implies that HOMO/LUMO orbital overlapping is almost equal and also that the density of electrons in the acceptor, LUMO, is equal.

Table 4.9 Summary of electrochemical properties.

Sample	HOMO (eV) [a]	LUMO (eV) [a]	E_g (eV)
MeO2PP	-5.45	-3.36	2.09
tCzPP	-5.66	-3.38	2.28
TOCPP	-5.52	-3.37	2.15
TOCQx	-5.46	-3.12	2.34

[a] HOMO and LUMO energy determined by cyclic voltammetry in DCM; [b]energy gap in DCM.

4.3.4. MCL properties

The solid samples of compounds, except for TOCPP, showed obvious mechanoluminescencent properties (Fig. 4.52) by application of external stimuli (grinding, heating, fuming and melting). In all the cases, grinding led to red-shifted emissions which occur either via increasing the twist angle or via the enhancement of intermolecular interactions. On the contrary, fuming resulted in blue-shifted emissions towards the initial PL spectra.

Interestingly, the initial and ground forms of TOCQx, TOCQx-i and TOCQx-g, demonstrated the same full width at half maxima (FWHM) which were found to be equal to 80 nm. These results allow presuming that, in this case, MCL arises from variations in the molecular packing and orientation.
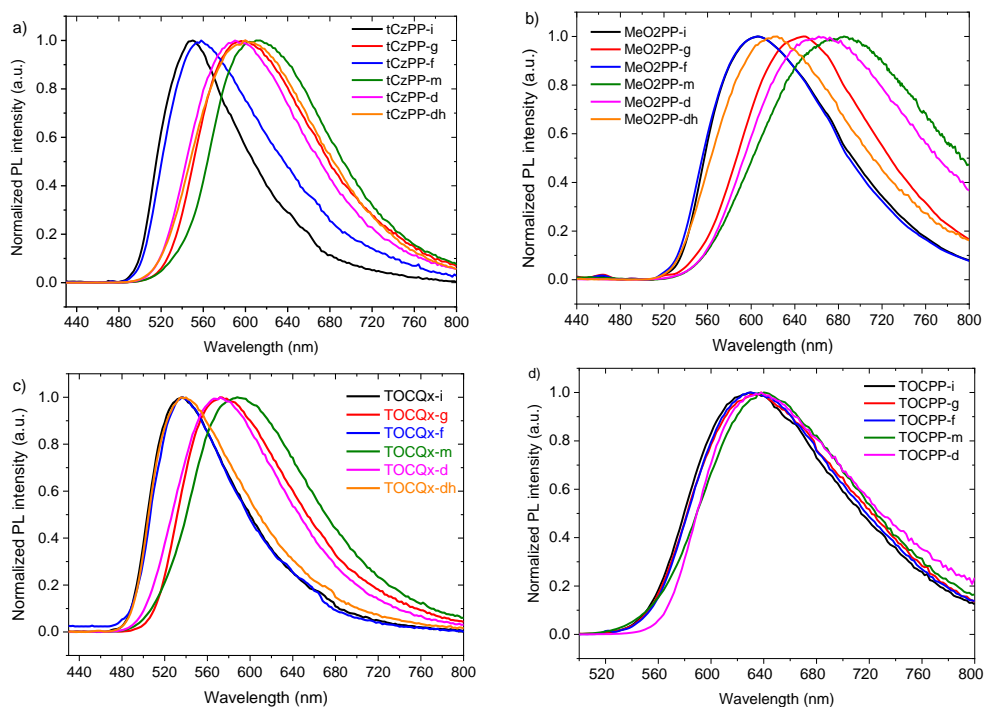
Fig. 4.52 PL spectra of various forms of condensed samples of of the derivatives of quinoxaline and pyridopyrazine.

The pristine sample of tCzPP showed a yellow emission with the intensity maximum at 550 nm. Upon mechanical grinding of the initial powder while using a spatula, the yellow emission turned to an orange emission with the intensity maximum at ca. 600 nm. After fuming the ground sample by exposure to the vapor of DCM for 5 min, the emission hypochromically shifted to the yellow region with the intensity maximum at 557 nm. The melting of the initial sample and cooling down to room temperature in air caused a bathochromic shift of luminescence to the reddish color with the intensity maximum at 612 nm. FWHM for ground and molten forms were

found to be 130 nm and 127 nm, respectively. These observations indicate that, for the molten form, bathochromism stems from the effect of intermolecular interactions.

The initial form of luminophore TOCQx exhibited a greenish-yellow emission at 536 nm, which, under grinding, shifted up to 41 nm to the orange region and peaked at 577 nm. The fuming of the ground form restored the initial state, and the emission centered at 537 nm. The thermal treatment by increasing the temperature above the melting point caused a further red shift to orange emission with the intensity maximum at 588 nm.

MeO2PP, which contains the strongest donor among the compounds of this series in the initial state, showed a reddish emission with the intensity maximum at 608 nm which shifted to 648 nm after mechanical treatment (Table 4.10). In this case, also, the exposure to DCM vapor led to the return to the initial state. The melting of the initial form caused a significant bathochromic shift of the PL maximum from 608 nm to 683 nm. A close look at the photophysical characteristics of the molten forms is given in Table 4.10, and their comparison with the corresponding characteristics of the ground forms reveals that, for TOCQx and tCzPP, melting resulted in 13 nm and 12 nm red-shifts of the emission maxima. The difference of the emission maxima wavelengths of MeO2PP-g and MeO2PP-m was 35 nm. These observations can be explained by the shorter distance between adjacent molecules in case of face-to-face intermolecular interaction and, consequently, excimer formation. The reason behind these differences might be the presence of bulky *tert*-butyl groups which enlarge the distance between neighboring luminophores; this results in weaker π-π stacking.

Table 4.10 Photophysical characteristics of different forms of condensed samples of derivatives quinoxaline and pyridopyrazine.

Sample	solid states	initial	ground	Fumed	Neat film	melted	Heated film
TOCQx	PL (nm)	536	577	537	572	588	537
	PLQY (%)	19	14	23	-	4	-
tCzPP	PL (nm)	550	600	557	590	612	601
	PLQY (%)	23	16	16	-	12	-
TOCPP	PL (nm)	630	636	632	637	642	-
	PLQY (%)	-	-	-	-	-	-
MeO2PP	PL (nm)	608	648	606	664	683	619
	PLQY (%)	3	1	2	-	0	-

Neat films prepared by drop-casting of tCzPP and TOCQx exhibited fluorescence spectra that were very similar to those of the ground form, which can be explained by strong π-π stacking. In the neat film, the PL spectra of tCzPP and TOCQx are blue-shifted by10 nm and 5 nm, respectively, relative to those of the ground states. In the neat film, the PL spectrum of MeO2PP is located between the spectra of ground and

molten forms. This observation implies that, in the film, the distances between the neighboring molecules are shorter than the ground form. On the other hand, the molecules that contain bulky *t*-Bu groups experience a longer intermolecular distance and weaker π-π interactions.

Heating the drop-cast film of MeO2PP (MeO2PP-dh) at 150 °C for 2 h results in a hypsochromic shift of the PL intensity maximum of 619 nm. TOCQx-dh recovered the initial color of the emission by annealing for 1 h at 170 °C. On the contrary, tCzPP-dh did not recover the initial emission color by annealing at 170 °C but instead exhibited the red shift up to 11 nm, and the PL of annealed sample peaked at 601nm, i.e., at the same wavelength as PL of the ground form. FWHM after heating changed from 126 nm to 135 nm, which can be attributed to the twist angle enlargement.

Surprisingly, TOCPP did not show any stimuli-responsive behavior. Its initial form showed a red emission with the maximum at 630 nm. This is the most red-shifted emission among condensed samples of the studied derivatives of quinoxaline and pyridopyrazine. After melting, its PL intensity maximum shifted by 12 nm to 642 nm. As it was already mentioned, a stronger donor-acceptor interaction leads to more pronounced mechanochromism. Usually, in the molten form, compounds experience H-aggregation with face-to-face interactions. Therefore, the unusual color emission of TOCPP-i arises form H-aggregation and, for this reason, the difference in wavelengths of emission of the initial and molten forms is 12 nm.

Table 4.11 shows the results of comparison of the emission of the solid forms discussed in this chapter with that of the first series of MCL materials (Chapter 4.1.4).

Table 4.11 PL comparison of 1st and 2nd series of MCL materials.

	Sample	Initial	ground	Fumed	Neat film	melted
	tCzQx	482	527	479	534	544
PL (nm)	*TOCQx*	536	577	537	564	588
	MeOQx	516	543	514	592	582
PL (nm)	*tCzPP*	550	600	557	590	612
	TOCPP	630	636	632	637	642
PL (nm)	*MeO2PP*	608	648	606	664	683
	MeO2Qx	534	586	523	598	632

Attachment of TOC instead of tCz/MeO leads to a bathochromic shift which can be attributed to either the stronger electron donation ability of TOC or to some sort of H-aggregation. The substitution of the quinoxaline unit with a pyridopyrazine moiety causes a bathochromic shift of the PL by 70 nm (cf. the data for tCzQx-tCzPP and MeO2Qx-MeO2PP). Therefore, upon these data, from TOCQx to TOCPP, we

could predict the emission of TOCPP at around 600 nm, which, as a consequence of the H-type orientation, is red-shifted to 630 nm.

4.3.5. Thermal transitions

The TGA curves of the compounds shown in Fig. 4.53 reflect the effect of substitutions of carbazole moieties on the thermal stability of the compounds. TOCQx and TOCPP contain bulky *t*-Bu groups, which leads to weaker intermolecular interactions resulting in sublimation. In the case of MeO2PP with the strongest intermolecular interactions, thermal decomposition is obvious. The highest and lowest decomposition temperature at 5% weight loss was observed for MeO2PP and TOCQx, which reflects the effect of molecular assembly and intermolecular attractions between neighboring molecules. The summary of thermogravimetric analyses is shown in Table 4.12.
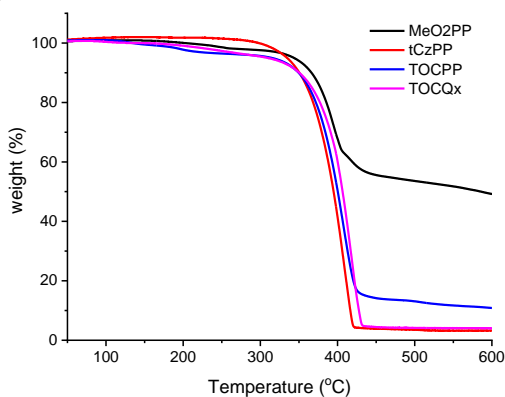
Fig. 4.53 TGA curves of the derivatives of quinoxaline and pyridopyrazine.

DSC cures shown in Fig. 4.54 revealed glass transition in the second heating scans and melting in the first heating scans. Cooling from melt did not show any transition. The thermal characteristics are collected in Table 4.12. The highest glass transition temperature was observed for tCzPP which contains heavy *tert*-butyl substituents.

Table 4.12 Thermal characteristics of the derivatives of quinoxaline and pyridopyrazine.

Sample	T_d^a	T_g/T_c (°C)	T_m
MeO2PP	343	122/-	252
tCzPP	334	157/-	196
TOCPP	314	129/-	-
TOCQx	309	107/-	243

[a] 5% weight loss; crystallization (T_c), glass transition (T_g) and decomposition (T_d) temperatures

Several parameters have an effect on increasing the melting point, such as rigidity, well-ordering of the molecular assembly and intermolecular interactions.

MeO2PP showed the highest melting point due to its shorter intermolecular distance between the neighboring molecules, which resulted in stronger intermolecular interaction as molecular motions were locked and consequently the structure is rigidified. Subsequently, tCzPP, by having bulky *t*-Bu units, had the lowest melting point because intermolecular interactions were weakened. Meanwhile, for heavy substituents, rigidity and stronger dipole moments led to a higher glass transition. Therefore, in the case of tCzPP, heavy *t*-Bu units led to a higher rigidity and resulted in the highest glass transition temperature. TOCPP that also contains one *tert*-butly unit on the carbazole yielded higher T_g than MeO2PP. Here, again, the effect of a heavy substitution, *t*-Bu, on the increase of glass transition was exhibited. In addition, the dipole moment in TOCPP is stronger than TOCQx, which implies higher glass transition for the TOCPP. Interestingly, TOCPP did not demonstrate the melting point and is in amorphous form.
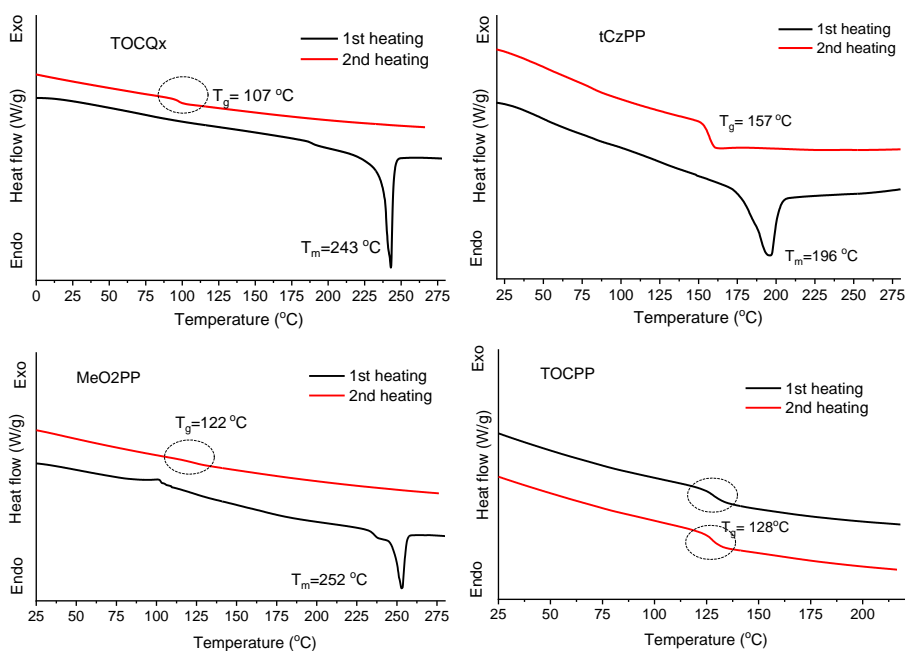
Fig. 4.54 DCS curves of the derivatives of quinoxaline and pyridopyrazine.

5. CONCLUSIONS

1. New luminophores based upon quinoxaline and pyridopyrazine as electron withdrawing units and various derivatives of carbazole, iminodibenzyl iminostilbene as electron donating moieties were synthesized and studied as multifunctional materials. Color altering through external stimuli, delayed fluorescence and phosphorescence at room temperature were demonstrated.

2. Solution processed organic light emitting diodes based on derivatives of carbazole and quinoxaline exhibited high external quantum efficiency. The device containing 2,3-bis(3,6-dimethoxy-9H-carbazol-9-yl)quinoxaline as an emitter showed external quantum efficiency of 10.9%, luminance of 16760 cd m-2.

3. Derivatives of quinoxaline and pyridopyrazine showed efficient thermally activated delayed fluorescence with the singlet-triplet energy gap ranging from 0.10 eV to 0.28 eV.

4. It was established that derivatives of quinoxaline/pyridopyrazine and carbazole exhibit mechanochromic properties.
   - It was shown that inserting a stronger donor results in a higher emission color contrast observed upon application of external stimuli.
   - Through the estimation of intensity of thermally activated delayed fluorescence of different states of compounds obtained upon applied stresses, it was shown that the driving mechanism of mechanochromic behavior arises from conformational variation.
   - A material with heavy tert-butyl groups attached to the carbazole moiety under external stresses showed reversible turn on/turn off thermally activated delayed fluorescence.
   - Replacement of a quinoxaline moiety with a pyridopyrazine unit as a stronger acceptor resulted in the shift of the fluorescence spectrum towards the red region of the spectrum.

5. Thermally activated delayed fluorescence was observed for the derivative of iminodibenzyl and quinoxaline despite the large energy gap between the excited singlet and the triplet states (ca. 0.5 eV).

6. Derivatives of iminodibenzyl having a non-aromatic structure and a twisted boat conformation and quinoxaline, blended with inter cyclo-olefin polymer Zeonex exhibited phosphorescence at room temperature. The most considerably red-shifted emission was recorded for the compound without a phenylene bridge which exhibited the shortest triplet emission lifetime (51 ms) at room temperature. The introduction of phenylene between the donor and acceptor moieties resulted in a prolonged emission lifetime. The highest phosphorescence lifetime of 128 ms was observed for the derivative of quinoxaline with the strongest donor, dimethoxy-substituted iminodibenzyl.

6. SUMMARY

6.1. ĮVADAS

Spalvos mūsų kasdieniniame gyvenime daro įtaką nuotaikai, jausmams, emocijoms. Dėl to dedamos didelės pastangos kurti dirbtinius, pigius ir prieinamus chromoforus. Dažų molekulės, turinčios konjuguotų dvigubų ryšių sistemas, absorbuoja šviesą. Elektronai p orbitalėse gali būti bendri konjuguotose molekulėse, konjugacijai didėjant, elektronai lengvai delokalizuojasi visose gretimose p orbitalėse, o energijos skirtumas tarp didžiausios užimtos molekulinės orbitalės ir mažiausios neužimtos molekulinės orbitalės mažėja.

Pradedant 1990 m., pažangiosios medžiagos ir organiniai šviesos diodai (toliau – OLED) sulaukė didelio akademinės bendruomenės bei pramonės tyrėjų susidomėjimo. Pažangios medžiagos, galinčios keisti spalvą esant išoriniams dirgikliams, pritaikomos indikatoriuose, jutikliuose bei atspindint aplinkos pokyčius. Mechanochrominės, pažangiosios, medžiagos (toliau – MCL) keičia savo mechanines ir / arba optines savybes, reaguodamos į aplinkos pokyčius bei išorinį poveikį, pvz., slėgį, temperatūrą, drėgmę, pH, gniuždymą, ultragarsą, elektros / magnetinius laukus ir kita [1]. Šie procesai yra grįžtami ir vyksta dėl morfologinių, konformacinių ar cheminės struktūros pokyčių. Nepaisant dedamų pastangų, mechanoreaguojančių medžiagų kūrimas vis dar išlieka sudėtingas, o daugiaspalvių grynų organinių junginių sintezė kol kas mažai paplitusi [1].

Šiuo metu OLED-ai yra plačiai paplitę visame pasaulyje, jie naudojami išmaniuosiuose telefonuose bei didelio ploto ekranuose, įskaitant televizijos ekranus. Pirmasis pranešimas organinių elektroliuminescuojančių (toliau – EL) medžiagų tema buvo paskelbtas Bernanose grupės 1953 metais [2]. Didžiulę įtaką OLED-ų plėtrai padarė Tang ir VanSlyke, pagaminę prietaisą, kurio išorinis kvantinis efektyvumas (toliau – EQE) siekė 1 %, o įsijungimo įtampa buvo 10 V [3]. Šis prietaisas buvo greitos pažangos kuriant bei sintetinant EL medžiagas pradžia. Fosforescuojantieji OLED-ai atstovauja antrosios kartos elektroliuminescenciniams prietaisams, kuriuose eksploatuojami tripletiniai eksitonai. Šiuose prietaisuose brangiųjų tauriųjų metalų kompleksai palengvina virsmą iš sužadintos singletinės būsenos į tripletinę būseną [4]. Naujosios kartos OLED-ai paremti termiškai aktyvuota uždelstąja fluorescencija (toliau – TADF) [5]. TADF medžiagos yra organiniai junginiai, kurių sudėtyje nėra

tauriųjų metalų. Jos panaudoja tiek singletinius, tiek tripletinius eksitonus, išspinduliuodamos fotonus iš singletinės būsenos. Vienas didžiausių tokių organinių junginių privalumų yra jų įvairovė, todėl TADF pagrindu sukurti OLED-ai yra labai perspektyvūs.

Paprastai, gaminant OLED-us, naudojamas vakuuminio terminio nusodinimo metodas, tačiau termiškai užgarinti OLED-ai yra brangūs ir reikalauja specialių sąlygų, kad erdvuose vakuuminėse kamerose būtų palaikomas aukštas vakuumas [6]. O tirpalų liejimo principu pagaminti prietaisai pasižymi mažomis gamybos sąnaudomis bei galimybe gaminti didelio ploto prietaisus. Deja, tirpalų liejimo principu pagaminti OLED-ai vis dar nepasižymi dideliu efektyvumu [7].

Brangių tauriųjų metalų alternatyva tapo vis didėjantis organinių luminogenų paplitimas bei jų puslaidininkinės ar mechanochrominės savybės. Organiniai elektroaktyvūs junginiai, kuriuose nėra brangių tauriųjų metalų, populiarūs dėl didelio galimų molekulinių dizaino ir taikymo sričių įvairovės.

Šio darbo **tikslas** – pigi ir paprasta naujų organinių junginių, turinčių akceptorinius chinoksalino arba piridopirazino fragmentus, sintezė ir jų savybių tyrimas.

Tikslui pasiekti buvo iškelti šie **uždaviniai**:
- Susintetinti naujus chinoksalino darinius, turinčius donorinius karbazolo, iminodibenzil ar iminostilbeno fragmentus.
- Susintetinti junginius, turinčius stiprų akceptorinį piridopirazino fragmentą.
- Sukurti, susintetinti ir charakterizuoti naujus elektronų donorinius junginius: 3-(*tret*-butil)-6-metoksi-9*H*-karbazolą ir 2,8-dimetoksi-10,11-dihidro-5*H*-dibenzo[*b*,*f*]azepiną.
- Ištirti fenileno tiltelio tarp donorinio ir akceptorinio fragmentų įtaką spinduolių fotofizikinėms savybėms.
- Ištirti junginių donorinių fragmentų prigimties įtaką optinėms, fotofizikinėms, mechanochrominėms ir elektrocheminėms savybėms.
- Suformuoti ir charakterizuoti OLED-us, panaudojant naujai susintetintus junginius.

Darbo naujumas

- Susintetinti keturi nauji organiniai spinduoliai, turintys karbazolo ar chinoksalino fragmentus, pasižymintys mechanochrominėmis savybėmis ir uždelstąja fluorescencija kambario temperatūroje.
- Pakeitus chinoksalino fragmentą pirido[2,3-*b*]pirazinu, susintetinti junginiai, pasižymintys mechanochromine liuminescencija ir termiškai aktyvuota uždelstąja fluorescencija.
- Susintetinti ir charakterizuoti trys donoriniai nauji junginiai: 3-(*tret*-butil)-6-metoksi-9*H*-karbazolas, 3-metoksi-9*H*-karbazolas ir 2,8-dimetoksi-10,11-dihidro-5*H*-dibenzo[*b*,*f*]azepinas.
- Sukurti trys nauji kambario temperatūroje fosforescuojantys junginiai ir ištirta donorinio fragmento ir tiltelio įtaka jų savybėms. Nustatyta, kad

iminodibenzilfragmentas efektyviai slopina nespindulinį sužadintų būsenų gesimą.

Darbo praktinė vertė

Susintetinti junginiai panaudoti OLED-ams formuoti. Junginiai, pasižymintys mechanochromine liuminescencija, gali būti panaudojami kaip išoriniams dirgikliams jautrios medžiagos.

Autoriaus indėlis

Pateiktoje lentelėje nurodytas autoriaus ir kitų tyrėjų indėlis. Gautus rezultatus analizavo autorius, išskyrus fotofizikinius ir elektrocheminius rezultatus, kurie tirti bendradarbiaujant su Piotr Pander. 2.2 skyriuje aprašytų junginių branduolių magnetinio rezonanso (toliau – BMR) spektroskopijos tyrimus atliko autorius.

Indėlis	Autorius	Piotr Pander	Algirdas Lazauskas	Audrius Bučinskas	Laura Pečiulytė	Jūratė Simokaitienė	Greta Ragaitė
Dizainas	■						
Sintezė	■						
Charakterizavimas	■						
CV	■						
MCL analizė	■	■					
PL tyrimai	■	■					
Prietaisų formavimas		■					
BMR	■						■
Monokristalo XRD				■			
Miltelių XRD			■				
Terminiai tyrimai					■	■	

6.2. TYRIMŲ REZULTATAI

6.2.1. Junginiai, pasižymintys mechanochrominėmis savybėmis ir termiškai aktyvuota uždelstąja fluorescencija
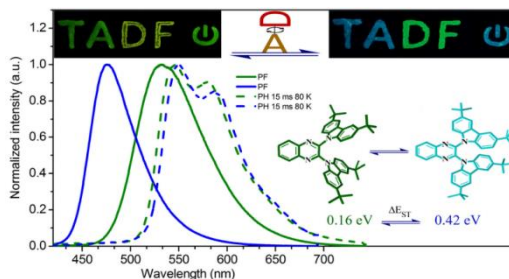
1 schema. tCzQx sluoksnių ir pakaitintų sluoksnių fotoliuminescencijos ir fosforescencijos spektrai

Šiame skyriuje aprašyti TADF junginiai, pasižymintys MCL savybėmis ir grįžtamosiomis TADF įsijungimo / išsijungimo savybėmis jiems esant kietos būsenos, kurias sukelia virsmas tarp amorfinės ir kristalinės būsenų (1 schema). Taip pat aprašyti emisijos spalvos pokyčiai, sukelti išorinių dirgiklių. Tirpalų liejimo būdu suformuoti TADF OLED-ai pasižymi aukštu EQE, siekiančiu 10,9 % ir skaisčiu, siekiančiu 16760 cd m^{-2}.

6.2.2. Sintezė

Karbazolo ir chinoksalino darinių sintezės eiga pavaizduota 2 schemoje. Junginių struktūros įrodytos ^{1}H BMR, ^{13}C BMR ir masių spektrometrijos metodais.
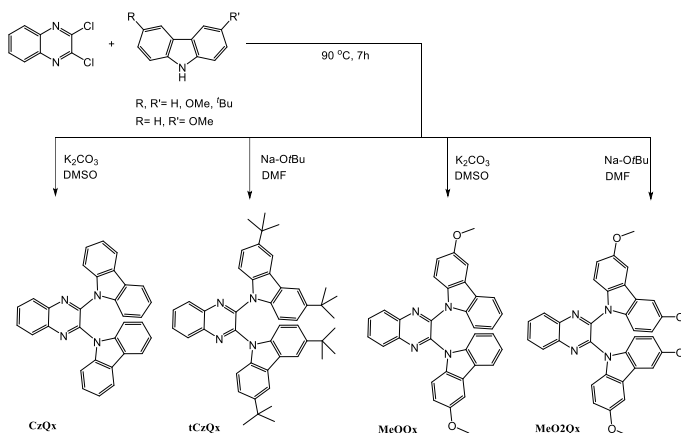
2 schema. Karbazolo ir chinoksalino darinių sintezė

6.2.3. Fotofizikinės savybės

Karbazolo ir chinoksalino darinių praskiestų tolueno tirpalų ir sluoksnių absorbcijos bei fotoliuminescencijos (toliau – PL) spektrai pateikti 1 pav. Fotofizikinės šių junginių charakteristikos pateiktos 1 lentelėje.

Visi aptariamų junginių kietieji tirpalai Zeonex pasižymi TADF savybėmis. Junginiai MeOQx ir MeO2Qx pasižymi trumpiausia uždelstosios fluorescencijos (toliau – DF) gyvavimo trukme ir didžiausiu DF intensyvumu. DF gyvavimo trukmė palaipsniui mažėja pereinant nuo CzQx iki MeO2Qx. Galima teigti, kad padidėja grįžtamos interkombinacinės konversijos (toliau – rISC) greičio konstanta. Tai lemia didėjantis donoro stipris serijoje CzQx < tCzQx < MeOQx < MeO2Qx.
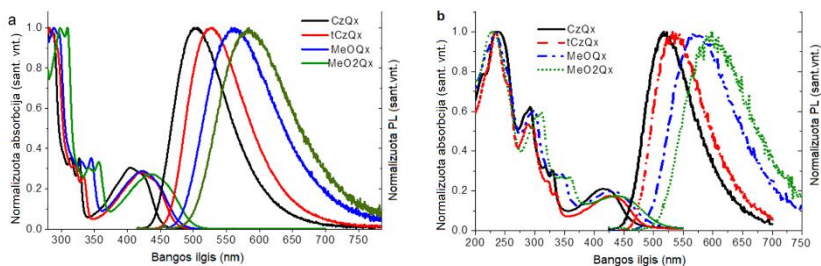
1 pav. Tirtų junginių a) tolueno tirpalų ir b) sluoksnių normalizuoti UV-Vis absorbcijos bei PL spektrai

1 lentelė. Karbazolo ir chinoksalino darinių fotofizikinės charakteristikos

Junginys	Abs (nm)[a]	PL (nm)[b]	S_1 / T_1 (eV)[c]	ΔE_{ST} (eV)[d]	HOMO/LUMO (eV)[e]
CzQx	404	503	2.87 / 2.59	0.28	-5.87/-3.11
tCzQx	419	527	2.69 / 2.55	0.14	-5.68/-2.97
MeOQx	423	560	2.63 / 2.51	0.12	-5.51/-3.03
MeO2Qx	437	582	2.58 / 2.44	0.14	-5.47/-3.05

[a]Tolueno tirpalo krūvio pernašos (toliau – CT) sugerties juostos maksimumo bangos ilgis; [b]Tolueno tirpalo emisijos maksimumo bangos ilgis; [c]kietųjų tirpalų Zeonex 1% (m/m) matricose singletinė ir tripletinė energija; [d]kietųjų tirpalų Zeonex 1% (m/m) matricose singletinės-tripletinės energijų skirtumas; [e]HOMO ir LUMO energijos, nustatytos ciklinės voltamperometrijos (toliau – CV) metodu dichlorometane

6.2.4. Mechanochrominės savybės

Ištirtas junginių PL spektrų jautrumas išoriniams dirgikliams. Junginių įvairių formų PL savybės, užfiksuotos paveikus išoriniams dirgikliams, pateiktos 2 lentelėje. MeOQx ir MeO2Qx pasižymėjo emisijos spalvos kitimu veikiant išoriniams dirgikliams (žr. 2 pav.). Miltelių rentgeno spindulių difrakcinė (toliau – XRD) analizė atskleidė, jog pradinės miltelių kristalinės struktūros suardomos bandinius trinant mentele, jiems transformuojantis į amorfinę būseną. Kita vertus, sutrintus miltelius kaitinant ar veikiant tirpiklių garais, atsiranda difrakcijos smailės. O junginių sluoksniai, gauti lydant ir tirpalų liejimo būdu, buvo amorfiniai, išskyrus CzQx-m sluoksnį. Kristalinių mėginių PL spektrai yra siauresni, palyginti su amorfinių mėginių spektrais, tai rodo, kad emisinė CT būsena yra labiau lokalinio pobūdžio (vadinamoji silpna CT arba hibridinė lokalinė ir CT būsena: HLCT). Be to, išlydžius mėginius, PL spektro juostos smarkiai pasislenka batochromiškai kitų mėginių spektrų atžvilgiu.
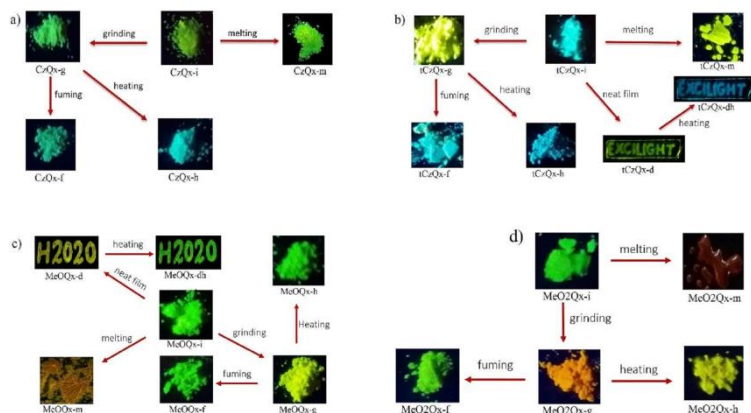
2 pav. (a) CzQx, (b) tCzQx, (c) MeOQx ir (d) MeO2Qx fotoliuminescencija, paveikus įvairiais išoriniais dirgikliais (sužadinimo bangos ilgis 365 nm)

Pavyzdžiui, CzQx-i pradinė forma pasižymi dangaus žydrumo emisija, o sutrynus (CzQx-g) emisija pasikeičia į geltoną. CzQx-g miltelių kaitinimas (CzQx-h) ir veikimas tirpiklių garais (CzQx-f) atkuria dangaus žydrumo fluorescenciją. Pažymėtina, kad tCzQx-i, tCzQx-h ir tCzQx-f PL spektrų juostos yra pasislinkusios trumpesnių bangų pusėn, palyginti su atitinkamomis heksano tirpalų PL juostomis. Tai leidžia manyti, kad emisinė singletinė būsena yra labiau lokalizuota nei atitinkama būsena tirpalo nepoliniame tirpiklyje, t. y. intermolekulinės sąveikos kietojoje būsenoje yra mažiau efektyvios nei tirpale.

Miltelius sutrynus (CzQx-g), fotoliuminescencijos poslinkis ilgesnių bangų kryptimi leidžia manyti, kad sužadinta būsena transformuojama iš lokalinio sužadinimo (LE arba HLCT) būsenos į intramolekulinę krūvio pernašos (ICT) būseną, tai rodo D-A dvisienio kampo relaksaciją. Šis rezultatas dera su amorfinėje būsenoje mažiau dominuojančiomis intermolekulinėmis sąveikomis nei kristalinėje būsenoje. Tikriausiai didesnė laisva erdvė leidžia molekulėms adaptuoti savo konformacijas, kad stabilizuotų krūvio pernašos būseną. Palietas CzQx amorfinis sluoksnis (CzQx-d) kaitinant kristalizuojasi (CzQx-dh) ir atgauna dangaus žydrumo emisiją (2 pav.).

2 lentelė. Junginių sluoksnių ir miltelių savybės ore

Junginys	kieta būsena	pradinė	trinta	kaitinta	veikta tirpiklių garais	lydyta	sluoksnyje	kaitintame sluoksnyje
tCzQx	PL (nm)	482	527	477	479	544	534	482
	PLQY (%)	9	12	9	9	9	11	6
MeOQx	PL (nm)	516	543	511	514	582	592	519
	PLQY (%	10	7	10	9	7	10	11
MeO2Qx	PL (nm)	534	586	559	523	618	598	
	PLQY (%	6	4	7	5	2	6	
CzQx	PL (nm)	504	510	478	478	524	519	
	PLQY (%	4	5	11	6	10	7	
MeO2Qx-d ir CzQx-d kaitinimas nesukėlė fotoliuminescencijos pokyčių								

6.2.5. Prietaisų formavimas

Visi keturi karbazolo ir chinoksalino dariniai pasižymi TADF efektu ir yra tinkami OLED-ams formuoti (3 lentelė). Didelės molekulinės masės poli(9-vinilkarbazolas) (PVKH) buvo naudojamas elektronų blokavimo ir skylės transportavimo sluoksniams, siekiant pagerinti krūvio izoliavimą emituojančiame sluoksnyje. Prietaisai pasižymėjo elektroliuminescencija regimosios šviesos intervale nuo mėlynai žalios (Dev 1) iki geltonai žalios (Dev 4).

3 lentelė. Prietaisų charakteristikos

Prietai-sas	Įjungimo įtampa ties 5 cd m^{-2}, V	EQE (%) / Srovės efektyvumas (cd A^{-1})			maks. skaistis cd m^{-2}	CIE (x,y) esant maks. skaisčiui
		maks.	esant 100 cd m^{-2}	esant 1000 cd m^{-2}		
Dev 1	5,9	5,4 / 14,2	5,0 / 13,1	3,3 / 8,5	5397	0,22, 0,40
Dev 2	5,0	9,1 / 28,9	3,2 / 12,8	8,8 / 28,3	15290	0,29, 0,55
Dev 3	5,0	7,3 / 22,7	5,0 / 11,2	7,2 / 21,8	12910	0,36, 0,55
Dev 4	5,0	10,9 /27,2	9,6 / 24,5	7,9 / 24,2	16760	0,41, 0,53

Prietaiso struktūra: ITO | HIL 1,3N (45 nm) | PVKH (10 nm) | PVK:PBD (60:40) emiteris 5% (32 nm) | TPBi (50 nm) | LiF (0,8 nm) | Al (100 nm), PVK – poli(N-vinilkarbazolas), kurio vidutinė molekulinė masė 90 000 g mol^{-1}, PVKH – poli(N-vinilkarbazolas), kurio vidutinė molekulinė masė $1,1 \cdot 10^{6}$ g mol^{-1}, emiteriai: Dev 1=CzQx, Dev 2=tCzQx, Dev 3= MeOQx, Dev 4= MeO2Qx

6.3. Junginiai, pasižymintys fosforescencija kambario temperatūroje, mechanochromine liuminescencija ir uždelstąja fluorescencija
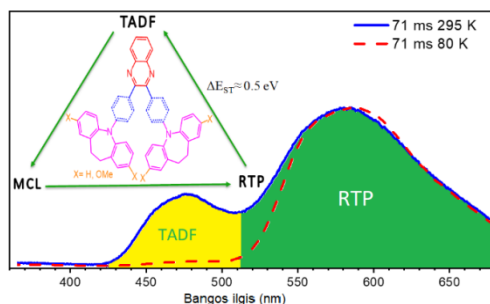
3 schema. Pavaizduotų molekulių daugiafunkcis elgesys bei jų fotoliuminescencija ir fosforescencija 80 K ir 295 K temperatūroje.

Šioje darbo dalyje susintetinti nauji chinoksalino dariniai, turintys iminodibenzil ar iminostilbeno fragmentus. Dėl susuktos ir standžios iminodibenzilo fragmento struktūros IDBQx pasižymėjo tiek TADF, tiek fosforescencija kambario temperatūroje, nepaisant didelio energijos tarpo tarp sužadintos singletinės ir tripletinės būsenų ($\Delta E_{ST} \approx 0,50$ eV). ISBQx, turėdamas tokį patį energetinį tarpą, pasižymėjo tik fluorescencija. Šie rezultatai charakterizuoja iminodibenzilfragmentą kaip perspektyvų donorą.

6.3.1. Sintezė

Tikslinių junginių sintezė atsispindi 4–6 schemose. Junginių struktūros įrodytos ^{1}H BMR, ^{13}C BMR ir masių spektrometrijos metodais.
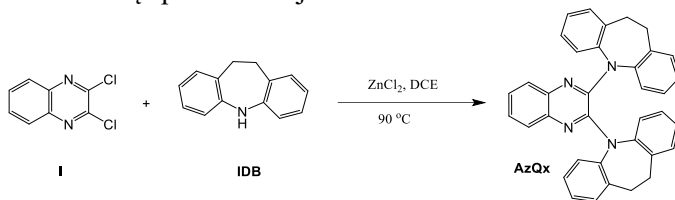
4 schema. AzQx sintezė
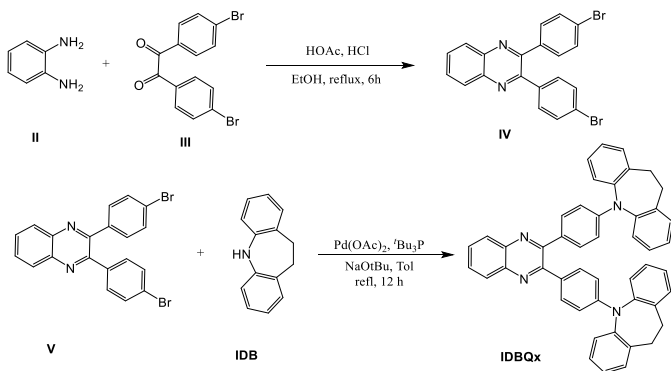
5 schema. IDBQx sintezė
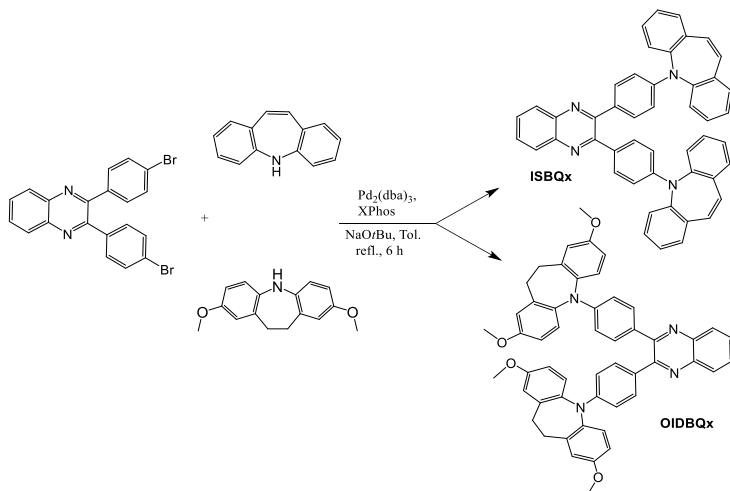
6 schema. ISBQx ir OIDBQx sintezė

6.3.2. Fotofizikinės savybės

Susintetinti junginiai, turintys donorinę-akceptorinę struktūrą, pasižymėjo ryškiu solvatochromizmu (3 pav.). Junginių, turinčių fenilentiltelį (IDBQx, ISBQx ir OIDBQx), CT pobūdis ne toks ryškus. AzQx, kuris neturi π-tiltelio.
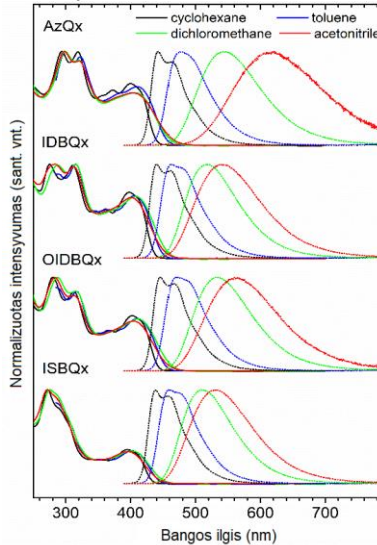
3 pav. Junginių tirpalų įvairiuose tirpikliuose absorbcijos ir PL spektrai

4 lentelė. Iminodibenzil ir iminostilbeno darinių fotofizikinės savybės

Junginys	Abs (nm)[a]	PL (nm)[b]	S_1 / T_1 (eV)[c]	ΔE_{ST} (eV)[d]	HOMO/ LUMO (eV)[e]
AzQx	299, 321, 406	545	2,92 / 2,41	0,51	-5,23/-2,77
IDBQx	288, 315, 408	518	2,93 / 2,41	0,52	-5,39/-2,79
OIDBQx	287, 315, 411	534	2,88 / 2,39	0,49	-5,41/-2,76
ISBQx	276, 402	511	2,91 / 2,40	0,51	-5,26/-2,75

[a]Dichloretano tirpalo absorbcijos spektro maksimumo bangos ilgis; [b] dichloretano tirpalo emisijos spektro maksimumo bangos ilgis; [c]kietųjų tirpalų Zeonex 1% (m/m) matricose singletinė ir tripletinė energija; [d]kietųjų tirpalų Zeonex 1% (m/m) matricose singletinės-tripletinės energijų skirtumas; [e]HOMO ir LUMO energijos nustatytos CV metodu

Dėl mažo Zeonex poliškumo iminodibenzil ir iminostilbeno darinių, kietųjų tirpalų šiame polimere ΔE_{ST} yra apie 0,5 eV (4 lentelė). Tai užkerta kelią efektyviai termiškai aktyvuotai atvirkštinei interkombinacinei konversijai (rISC). Dėl šios priežasties junginiai kambario temperatūroje nepažymėjo TADF.

Netikėtai molekulės, turinčios iminodibenzil fragmentus, charakterizuojamos stipria fosforescencija kambario temperatūroje (toliau – RTP). Tik junginiai, turintys iminodibenzilfragmentus, pasižymėjo šiokia tokia uždelstąja emisija kambario temperatūroje, o iminostilbeno darinys pasižymėjo tik fluorescencija. Tai gali būti paaiškinta nespindulinio gesimo slopinimu, kuris įgalina ilgos gyvavimo trukmės emisiją. Tačiau ΔE_{ST} dar yra pakankamas, kad šiluminė energija iš dalies konvertuotų

tripletinę būseną į singletinę, dėl ko iminodibenzil dariniuose tuo pačiu metu buvo pastebimi TADF ir RTP reiškiniai.
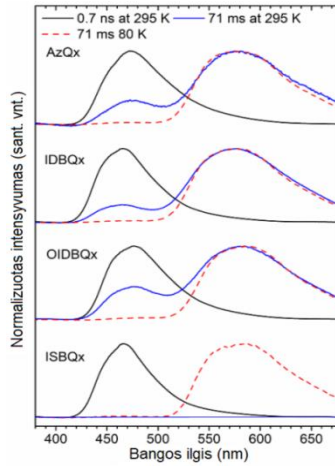
4 pav. Junginių kietųjų tirpalų Zeonex fluorescencijos (juodos linijos), fosforescencijos kambario temperatūroje ir TADF (mėlynos linijos) bei fosforescencijos žemoje temperatūroje (raudonos brūkšninės linijos) spektrai

Uždelstosios fluorescencijos intensyvumo linijinė priklausomybė nuo žadinimo dozės patvirtino TADF ir nepatvirtino tripletų anihiliacijos Paprastai santykis tarp TADF ir RTP koreliuoja su ΔE_{ST}, šiuo atžvilgiu OIDBQx labiausiai būdinga TADF.
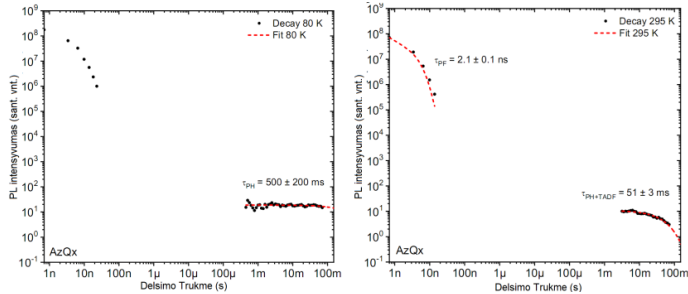
5 pav. AzQx kietojo tirpalo Zeonex fotoliuminescencijos gesimo kreivės 80 ir 295 K temperatūroje
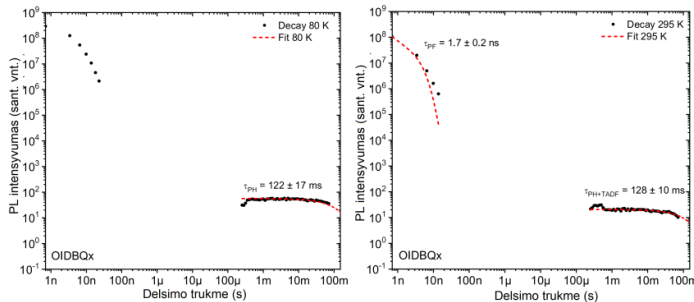
6 pav. OIDBQx kietojo tirpalo Zeonex fotoliuminescencijos gesimo kreivės 80 ir 295 K temperatūroje
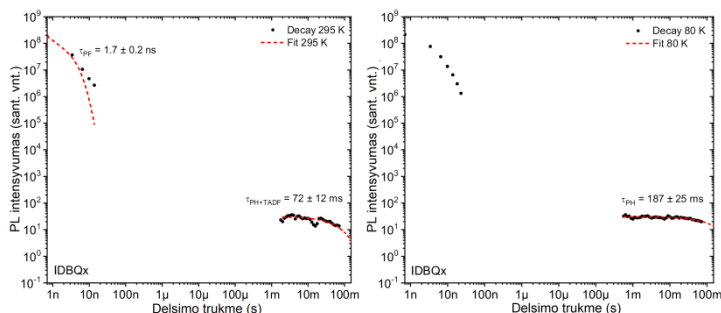
7 pav. IDBQx kietojo tirpalo Zeonex fotoliuminescencijos gesimo kreivės 80 ir 295 K temperatūroje

Junginio OIDBQx atveju RTP ir TADF intensyvumų santykis nesikeitė keičiant uždelsimo trukmes. Šio junginio kietajam tirpalui būdingas monoeksponentinis PL gesimas. Tai rodo, kad RTP ir TDF kyla iš tos pačios sužadintos būsenos (7 pav.). Junginių TADF ir RTP gyvavimo trukmės yra santykinai ilgos, nuo 51 ± 3 ms (AzQx) iki 128 ± 10 ms (OIDBQx) (žr. 5–7 pav.).

6.3.3. Mechanochrominės savybės

Paveikus išoriniais dirgikliais, užfiksuoti grįžtami OIDBQx liuminescencijos pokyčiai (8 pav.). Padinės būsenos junginio milteliai pasižymėjo žaliai mėlyna emisija, kurios maksimumas ties 494 nm. Miltelius sutrynus mentele, emisijos juosta praplatėjo, o jos maksimumas pasislinko ilgesnių bangų pusėn (522 nm). Pradinė būsena sugrąžinta bandinį 5 min. veikiant CH_2Cl_2 garais. Junginio sluoksnis pasižymėjo panašios energijos emisija, kaip ir sutrinti milteliai.
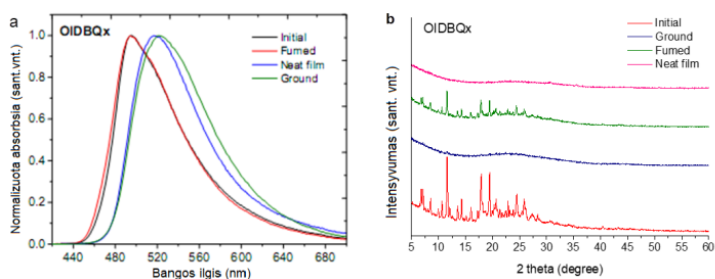
8 pav. OIDBQx įvairių formų, gautų veikiant įvairiems išoriniams dirgikliams, a) PL spektrai ir b) miltelių rentgeno spindulių difraktogramos. Sluoksniai gauti tirpalo liejimo būdu

OIDBQx miltelių XRD analizė parodė skirtingai apdorotų bandinių morfologijos skirtumus. 8 pav. matyti, kad pradinis ir tirpiklio garais paveiktas bandiniai yra kristaliniai, o trinti milteliai ir sluoksnis yra amorfiniai.

6.4. Akseptoriaus ir donoro įtaka mechanochrominėms savybėms ir uždelstajai fluorescencijai

Iki šiol publikuotos įvairios MCL medžiagos, bet vis dar nėra aiškios jų dizaino kryptys, kurios įgalintų gauti junginius, keičiančius emisijos spalvas, jiems reaguojant į išorinę stimuliaciją. Šioje darbo dalyje susintetinome ir ištyrėme naujas daugiafunkces medžiagas, kurios pasižymėjo MCL-TADF savybėmis. Sukurti ir susintetinti keturi nauji spinduoliai, ištirtos jų fotofizikinės, elektrocheminės ir MCL savybės. MCL pasireiškė dėl konformacinių kitimų ir / arba intramolekulinės sąveikos. Nors junginių struktūros panašios, MCL pasižymėjo tik trys junginiai.

6.4.1. Sintezė

Tikslinių junginių struktūros pateiktos 7 schemoje.
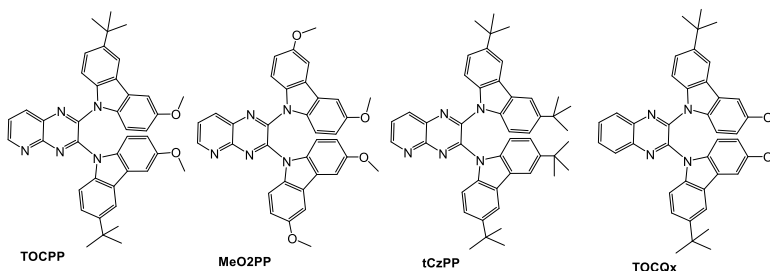
7 schema. Chinoksalino ir pirido[2,3-*b*]pirazino darinių struktūros

6.4.2. Fotofizikinės savybės

Junginių tolueno tirpalų UV-vis absorbcijos ir fluorescencijos spektrai pateikti 9 pav. Jų fotofizikinės charakteristikos pateiktos 5 lentelėje. Junginių absorbcijos maksimumai yra ties 290 nm ir 340 nm, juos galima atitinkamai priskirti π-π* ir n-π* elektronų virsmams. Absorbcijos juostos maždaug ties 450 nm bei jų solvatochrominis pobūdis gali būti priskirtas intramolekulinei krūvio pernašai. Junginių CzPP, TOCPP ir MeO2PP, turinčių piridopirazino fragmentą, THF tirpalų emisijos spektrai, be pagrindinių smailių, turi mažesnio intensyvumo smailes prieš 550 nm (10 pav.).
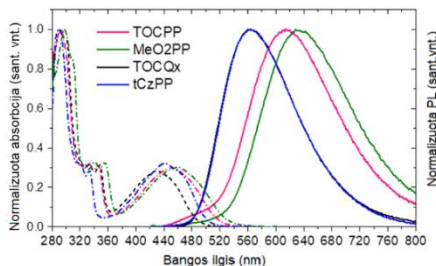
9 pav. Chinoksalino ir pirido[2,3-*b*]pirazino darinių tolueno tirpalų UV-vis absorbcijos bei fluorescencijos spektrai

Galima manyti, kad THF tirpaluose akseptorių lokalinių sužadintų būsenų emisija pasireiškia individualiai. Tokiais atvejais elektronų donoras daro įtaką akceptoriaus elektronų tankiui ir keičia jo PL spektrą.
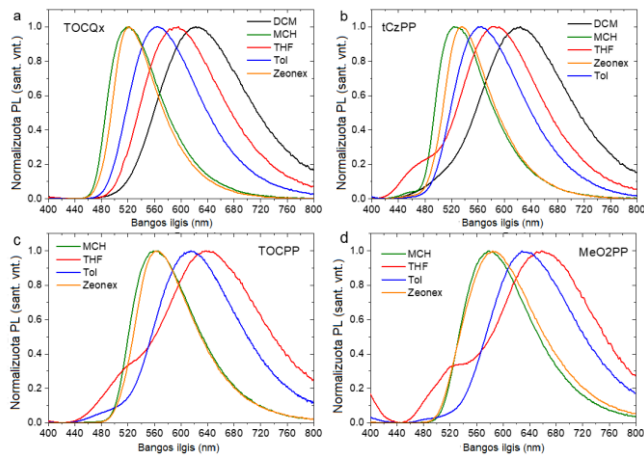
10 pav. Chinoksalino ir pirido[2,3-*b*]pirazino darinių tirpalų įvairiuose tirpikliuose PL spektrai (PL sužadinimo bangos ilgis λ_{ex}=350 nm)

5 lentelė. Chinoksalino ir pirido[2,3-*b*]pirazino darinių optinės charakteristikos

Junginys	Abs (nm)[a]	PL (nm)[b]	S_1 / T_1 (eV)[c]	ΔE_{ST} (eV)[d]	HOMO/ LUMO(eV)[e]	E_g (eV)[f]
TOCQx	430	564	2,64 / 2,46	0,18	-5,46/-3,12	2,53
tCzPP	441	565	2,56 / 2,46	0,10	-5,66/-3,38	2,47
TOCPP	451	614	2,49 / 2,36	0,13	-5,52/-3,37	2,38
MeO2PP	459	632	2,48 / 2,33	0,15	-5,45/-3,36	2,33

[a]Tolueno tirpalo absorbcijos CT juostos maksimumo bangos ilgis; [b]tirpalo toluene emisijos maksimumo bangos ilgis; [c]kietųjų tirpalų Zeonex 1% (m/m) matricose singletinė ir tripletinė energija; [d]kietųjų tirpalų Zeonex 1% (m/m) matricose singletinės ir tripletinės energijų skirtumas; [e]HOMO ir LUMO energijos, nustatytos CV)metodu dichlorometane; [f]energetinis tarpas

6.4.3. Mechanochrominės savybės

Kietieji junginių bandiniai, išskyrus TOCPP bandinį, veikiant išoriniais dirgikliais, pasižymėjo akivaizdžiomis mechanoliuminescencinėmis savybėmis. Visų atvejais, trinant bandinius, jų emisija pasislinko ilgesnių bangų pusėn dėl didėjančio molekulės susisukimo kampo arba augant tarpmolekulinei sąveikai. O, bandinius veikiant tirpiklių garais, emisijos pasislinko trumpesnių bangų kryptimi link pradinio PL spektro.

Pradiniai ir sutrinti TOCQx bandiniai TOCQx-i ir TOCQx-g pasižymėjo tokiu pačiu emisijos juostų pločiu ties puse intensyvumo maksimumo (FWHM) (80 nm). Tai leidžia daryti prielaidą, kad šiuo atveju MCL pasireiškia dėl molekulių susipakavimo ir orientacijos pokyčių. Junginių, veikiamų išorinių dirgiklių, PL spektrai pateikti 11 pav., o PL charakteristikos – 6 lentelėje.
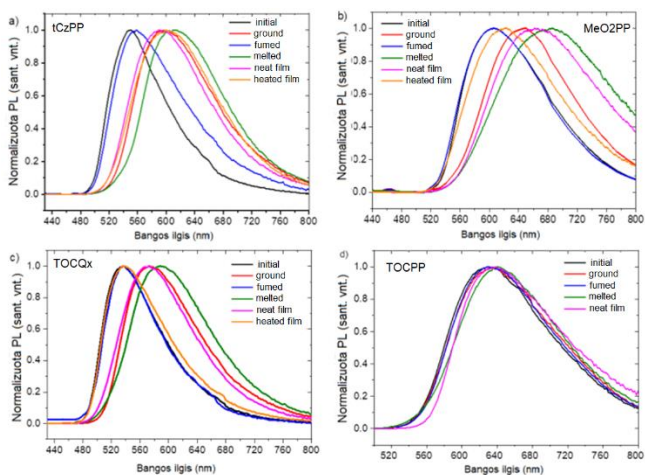
11 pav. Chinoksalino ir piridopirazino darinių, įvairiai apdorotų bandinių PL spektrai

MeO2PP, turintis stipriausią donorą tarp šios serijos junginių jiems esant pradinės būsenos, pasižymi rausva emisija, kurios intensyvumo maksimumas yra ties 608 nm. Lydytų TOCQx ir CzPP bandinių emisijos maksimumai pasislinkę 13 nm ir 12 nm, palyginti su atitinkamais sutrintų formų emisijos maksimumais. MeO2PP-g ir MeO2PP-m emisijos maksimumai skiriasi per 35 nm. Tai galima paaiškinti trumpesniais atstumais tarp gretimų molekulių ir dėl to besiformuojančių eksimerų. Šių skirtumų priežastis galėtų būti *tret*-butilgrupės, kurios padidina atstumus tarp gretimų liuminoforų.

6 lentelė. Chinoksalino ir piridopirazino darinių fotofizikinės charakteristikos

Junginys	Kieta būsena	Pradinis	Po trynimo	Paveiktas tirpiklių garais	Sluoksnis	Lydalas	Kaitintas sluoksnis
TOCQx	PL (nm)	536	577	537	572	588	537
	PLQY (%)	19	14	23	-	4	-
tCzPP	PL (nm)	550	600	557	590	612	601
	PLQY (%)	23	16	16	-	12	-
TOCPP	PL (nm)	630	636	632	637	642	-
	PLQY (%)	-	-	-	-	-	-
MeO2PP	PL (nm)	608	648	606	664	683	619
	PLQY (%)	3	1	2	-	0	-

6.5. IŠVADOS

1. Susintetinti nauji spinduoliai, turintys akceptorinius chinoksalino ar piridopirazino fragmentus bei donorinius karbazolo, iminodibenzil ar iminostilbeno fragmentus ir ištirti kaip daugiafunkcės medžiagos. Junginiai pasižymėjo spalvos pokyčiu veikiant išoriniams dirgikliams, uždelstąja fluorescencija bei fosforescencija kambario temperatūroje.

2. Tirpalų liejimo metodu pagaminti organiniai šviesos diodai, kuriuose kaip spinduoliai panaudoti karbazolo ir chinoksalino dariniai, pasižymėjo dideliu efektyvumu. Prietaisas su 2,3-bis(3,6-dimetoksi-9H-karbazol-9-il)chinoksaliną turinčiu emisiniu sluoksniu pasižymėjo 10,9% išoriniu kvantiniu efektyvumu ir 16760 cd m^{-2} skaisčiu.

3. Chinoksalino ar piridopirazino dariniai pasižymėjo efektyvia termiškai aktyvuota uždelstąja fluorescencija, jų singletinės-tripletinės energijų skirtumai išsidėstė nuo 0,10 eV iki 0,28 eV.

4. Nustatyta, kad chinoksalino / piridopirazino ir karbazolo dariniai pasižymi mechanochrominėmis savybėmis.

- Molekulėje esant stipresniam donorui, pastebimas didesnis emisijos spalvos pokytis veikiant išoriniams dirgikliams.
- Įvertinus skirtingų junginių būsenų, gautų veikiant išoriniams dirgikliams, termiškai aktyvintos uždelstosios fluorescencijos intensyvumą, įrodyta, kad mechanochrominis efektas pasireiškia dėl molekulių konformacinių kitimų.
- Junginio, turinčio *tret*-butilo grupes karbazolo fragmente, atveju, veikiant išoriniams dirgikliams, pasireiškia termiškai aktyvuotos uždelstosios fluorescencijos įsijungimas / išsijungimas.
- Pakeitus chinoksalino fragmentą stipresniu akceptoriumi – piridopirazinu, fluorescencijos spektro maksimumai pasislenka ilgesnių bangų pusėn.

5. Užfiksuota iminodibenzil ir chinoksalino darinio termiškai aktyvinta uždelstoji fluorescencija, nepaisant didelio energetinio tarpo tarp sužadintų singletinės ir tripletinės būsenų (apie 0,5 eV).

6. Iminodibenzil, neturinčio aromatinės struktūros bei susuktos konformacijos, ir chinoksalino darinių kietieji tirpalai polimere Zeonex pasižymėjo fosforescencija kambario temperatūroje. Junginio, neturinčio fenilentiltelio, emisija yra labiausiai pasislinkusi ilgesnių bangų pusėn, jis pasižymėjo trumpiausia tripletinės emisijos gyvavimo trukme (51 ms) kambario temperatūroje. Įterpus fenilentiltelį tarp donorinio ir akceptorinio fragmentų, pailgėjo emisijos gyvavimo trukmė. Chinoksalino darinys, turintis stipriausią donorinį fragmentą – dimetoksipakeistą iminodibenzilą, pasižymėjo didžiausia fosforescencijos gyvavimo trukme, kuri siekė 128 ms.

LITERATŪRA

1- XUE, P., et al. Recent progress in the mechanochromism of phosphorescent organic molecules and metal complexes. *Journal of Material Chemistry C*, 2016, 4, 6688-6706.
2- Bernanose, A., et al. A New method of light emission by certain organic compounds *Journal de Chimie Physique,* 1953, *50*, 64.
3- Tang, C. W.; Vanslyke, S. A. Organic electroluminescent diodes. *Applied Physics Letters.* 1987, *51*, 913.
4- Adachi, C. et al. Nearly 100% internal phosphorescence efficiency in an organic light-emitting device. *Journal of Applied Physics,* 2001, *90*, 5048.
5- Uoyama, H. et al. Highly Efficient Organic Light-Emitting Diodes from Delayed Fluorescence. *Nature* 2012, *492*, 234.
6- Derue, L. et al. All-Solution-Processed Organic Light-Emitting Diodes Based on Photostable Photo-cross-linkable Fluorescent Small Molecules. *ACS Applied Materials & Interfaces.* 2016, *8*, 16207–16217.
7- Lindh E. M. et al. Inkjet Printed Bilayer Light-Emitting Electrochemical Cells for Display and Lighting Applications. *Small* 2014, *10*, 4148-53.
8- Pashazadeh, R. et al. Multicolor Luminescence Switching and Controllable Thermally Activated Delayed Fluorescence Turn on/Turn off in Carbazole–Quinoxaline–Carbazole Triads. *The Journal of Physical Chemistry Letters*, 2018, 9, 1172-1177.
9- Pashazadeh, R. et al. An iminodibenzyl–quinoxaline–iminodibenzyl scaffold as a mechanochromic and dual emitter donor and bridge effects on optical properties *Chemical Communications,* 2018, *54*, 13857.

MOKSLINIŲ PUBLIKACIJŲ DISERTACIJOS TEMA SĄRAŠAS

Straipsniai *Web of Science* duomenų bazės leidiniuose

1. Pashazadeh, R.; Pander, P.; Lazauskas, A.; Dias, F.B.; Grazulevicius. J.V. Multicolor Luminescence Switching and Controllable Thermally Activated Delayed Fluorescence Turn on/Turn off in Carbazole–Quinoxaline–Carbazole Triads *The Journal of Physical Chemistry Letters*, 2018, 9, 1172-1177.
2. Pashazadeh, R.; Pander, P.; Bucinskas, A.; Skabara, P.J.; Dias, F.B.; Grazulevicius, J.V. An Iminodibenzyl-Quinoxaline-Iminodibenzyl Scaffold as Mechanochromic and Dual Emitter: Donor and Bridge Effects on Optical Properties *Chemical Communications,* 2018, *54*, 13857.

Pranešimai tarptautinėse konferencijose

1. 4th Workshop on Organic Electronics and Nanophotonics (WOREN 2016), France, ***Poster presentation***
2. 16th Baltic Polymer Symposium (BPS 2016), Lithuania, ***Poster presentation***
3. 22nd International Krutyn Summer School 2017: State of the Art in Organic-only TADF OLEDs – From Theory to Applications, Poland, ***Poster presentation***
4. 14th International Conference on Electrical and Related Properties of Organic Solids (ERPOS 2017), Scotland, ***Poster presentation***
5. 5th Workshop on Organic Electronics and Nanophotonics (WOREN 2018), Poland, ***Oral presentation***

6. 11th International Conference on Nanomaterials (ANM 2018), Portugal, *Oral presentation*
7. International Conference on Science and Technology of Synthetic Metals 2018 (ICSM 2018), Korea, *Oral presentation*

7. REFERENCES

1- Marin, L.; Kudrjasova, J.; Verstappen, P.; Penxten, H.; Robeyns, K.; Lutsen, L.; Vanderzande, D. J. M.; Maes, W.; Quinoxaline-Based Cyclo(oligophenylenes) *J. Org. Chem.* **2015**, *80*, 2425.

2- Thomas, K. R. J.; Lin, J. T.; Tao, Y.-T.; Chuen, C. H. Electroluminescent Bipolar Compounds Containing Quinoxaline or Pyridopyrazine and Triarylamine Segments *J. Mater. Chem.* **2002**, *12***, 3516-3522.

3- Kulkarni, A. P.; Zhu, Y.; Jenekhe, S. A. Quinoxaline-Containing Polyfluorenes: Synthesis, Photophysics, and Stable Blue Electroluminescence *Macromolecules* **2005**, *38*, 1553–1563.

4- Blanchard-Desce, M.; Wortmann, R.; Lebus, S.; Lehn, J.-M. Krämer, P. Intramolecular Charge Transfer in Elongated Donor-Acceptor Conjugated Polyenes *Chem. Phys. Lett.* **1995**, *243*, 526.

5- Nisha, S. K.; Asha, S. K. Donor–Acceptor Random Copolyesters Containing Perylenebisimide (PBI) and Oligo(p-phenylene vinylene) (OPV) by Melt Condensation Polymerization: Energy Transfer Studies *J. Phys. Chem. B* **2013**, *117*, 13710–13722.

6- Deng, Y.; Chen, Y.; Zhang, X.; Tian, H.; Bao, C.; Yan, D.; Geng, Y.; Wang, F. Donor–Acceptor Conjugated Polymers with Dithienocarbazoles as Donor Units: Effect of Structure on Semiconducting Properties *Macromolecules* **2012**, *45*, 8621– 8627.

7- Jadhav, T.; Choi, J. M.; Dhokale, B.; Mobin, S. M.; Lee, J. Y.; Misra, R. Effect of end groups on mechanochromism and electroluminescence in tetraphenylethylene substituted phenanthroimidazoles. *J. Phys. Chem. C* **2016**, *120*, 18487– 18495.

8- Park, Y.; Kim, B.; Lee, C.; Hyun, A.; Jang, S.; Lee, J.-H.; Gal, Y.-S.; Kim, T. H.; Kim, K.-S.; Park, J. Highly Efficient New Hole Injection Materials for OLEDs Based on Dimeric Phenothiazine and Phenoxazine Derivatives *J. Phys. Chem. C* **2011**, *115*, 4843– 4850

9- Xue, P.; Ding, J.; Wang, P.; Lu, R. Recent progress in the mechanochromism of phosphorescent organic molecules and metal complexes *J. Mater. Chem. C* **2016**, *4*, 6688.

10- Lee, Y.-A; Eisenberg, R. Luminescence Tribochromism and Bright Emission in Gold(I) Thiouracilate Complexes *J. Am. Chem. Soc.* **2003**, *125*, 7778–7779

11- Bernanose, A.; Comte, M.; Vouaux P. A New method of light emission by certain organic compounds *J. Chim. Phys.* **1953**, *50*, 64.

12- Tang, C. W.; Vanslyke, S. A. "Organic electroluminescent diodes". *Appl. Phys. Lett.* **1987**, *51*, 913.

13- Adachi, C.; Baldo, M. A.; Thompson, M. E.; Forrest, S. R. Nearly 100% internal phosphorescence efficiency in an organic light-emitting device. *J. Appl. Phys.* **2001**, *90*, 5048.

14- Uoyama, H.; Goushi, K.; Shizu, K.; Nomura, H.; Adachi, C. Highly Efficient Organic Light-Emitting Diodes from Delayed Fluorescence. *Nature* **2012**, *492*, 234.

15- Derue, L.; Olivier, S.; Tondelier, D.; Maindron, T.; Geffroy, B.; Ishow, E. All-Solution-Processed Organic Light-Emitting Diodes Based on Photostable Photo-cross-linkable Fluorescent Small Molecules. *ACS Appl. Mater. Interfaces* **2016**, *8*, 16207–16217.

16- Lindh E. M.; Sandstrom A.; Edman, L. Inkjet Printed Bilayer Light-Emitting Electrochemical Cells for Display and Lighting Applications. *Small* **2014**, *10*, 4148-53.

17- Sagara , Y.; Mutai, T.; Yoshikawa, I.; Araki, K. *J. Am. Chem. Soc.* **2007**, *129*, 1520.

18- Yang, K.; Li, S.-L.; Zhang, F.-Q.; and Zhang, X.-M. Simultaneous Luminescent Thermochromism, Vapochromism, Solvatochromism, and Mechanochromism in a C_3-Symmetric Cubane $[Cu_4I_4P_4]$ Cluster without Cu–Cu Interaction *Inorg. Chem.* **2016**, *55*, 7323–7325.

19- Sagara, Y.; Kato, T. Mechanically Induced Luminescence Changes in Molecular Assemblies. *Nature Chem.* **2009**, *1*, 605.

20- Luo, X. L.; Li, J. N.; Li, C. H.; Heng, L. P.; Dong, Y. Q.; Liu, Z. P.; Bo, Z. S.; Tang, B. Z. Reversible Switching of the Emission of Diphenyldibenzofulvenes by Thermal and Mechanical Stimuli *Adv. Mater.* **2011**, *23*, 3261– 3265

21- Takashima, Y.; Hatanaka, S.; Otsubo, M.; Nakahata, M,; Kakuta, T.; Hashidzume, A; Yamaguchi, H.; Harada, A. Expansion–contraction of photoresponsive artificial muscle regulated by host–guest interactions *Nat. Commun.* **2012**, 3, 1-8.

22- Ito, S.; Taguchi, T.; Yamada, T.; Ubukata, T.; Yamaguchi, Y.; Asami, M. Indolylbenzothiadiazoles with varying substituents on the indole ring: a systematic study on the self-recovering mechanochromic luminescence *RSC Adv*., **2017**, *7*, 16953-16962.

23- Butler, T.; Mathew, A. S.; Sabat, M.; Fraser, C. L. Camera Method for Monitoring a Mechanochromic Luminescent β-Diketone Dye with Rapid Recovery *ACS Appl. Mater. Interfaces* **2017**, *9*, 17603-17612.

24- Wang, C.; Li, Z.; Molecular conformation and packing: their critical roles in the emission performance of mechanochromic fluorescence materials *Mater. Chem. Front*., **2017**, *1*, 2174.

25- Chi, Z.; Zhang, X.; Xu, B.; Zhou, X.; Ma, C.; Zhang, Y.; Liu, S.; Xu, J. Recent Advances in Organic Mechanofluorochromic Materials *Chem. Soc. Rev*. **2012**, *41*, 3878– 3896.

26- Benito, Q.; Goff, X. F. L.; Maron, S.; Fargues, A.; Garcia, A.; Martineau, C.; Taulelle, F.; Kahlal, S.; Gacoin, T.; Boilot, J.-P.; Perruchas, S. Polymorphic Copper Iodide Clusters: Insights into the Mechanochromic Luminescence Properties *J. Am. Chem. Soc*. **2014**, *136*, 11311– 11320.

27- Yao, H.; Domoto, K.; Isohashi, T.; Kimura, K. In Situ Detection of Birefringent Mesoscopic H and J Aggregates of Thiacarbocyanine Dye in Solution *Langmuir* **2005**, *21*, 1067-1073.

28- Más-Montoya, M.; Janssen, R. A. J. The Effect of H- and J-Aggregation on the Photophysical and Photovoltaic Properties of Small Thiophene–Pyridine–

DPP Molecules for Bulk-Heterojunction Solar Cells Adv. *Funct. Mater*. **2017**, *27*, 1605779.

29- Deng, Y.; Yuan, W.; Jia, Z.; Liu, G. H- and J-Aggregation of Fluorene-Based Chromophores *J. Phys. Chem. B* **2014**, 118, 14536–14545.

30- Bricks, J.L.; Slominskii, Y.L.; Panas,I.D.; Demchenko, A.P. Fluorescent J-aggregates of cyanine dyes: basic research and applications review *Methods and Applications in Fluorescence* **2018**, *6*, 012001.

31- Davis, D. A.; Hamilton, A.; Yang, J.; Cremar, L. D.; Gough, D. V.; Potisek, S. L.; Ong, M. T.; Braun, P. V.; Martínez, T. J.; White, S. R.; Moore, J. S.; Sottos, N. R. Force-Induced Activation of Covalent Bonds in Mechanoresponsive Polymeric Materials. *Nature* **2009**, *459*, 68– 72.

32- Kim, J. W.; Jung, Y.; Coates, G. W.; Silberstein, M. N. Mechanoactivation of Spiropyran Covalently Linked PMMA: Effect of Temperature, Strain Rate, and Deformation Mode. *Macromolecules* **2015**, *48*, 1335– 1342,

33- Balch, A. L. Dynamic Crystals: Visually Detected Mechanochemical Changes in the Luminescence of Gold and Other Transition-Metal Complexes *Angew. Chem., Int. Ed.* **2009**, *48*, 2641– 2644

34- Wakabayashi, R.; Maeba, J.; Nozaki, K.; Iwamura, M. Considerable Enhancement of Emission Yields of [Au(CN)$_2$$^-$] Oligomers in Aqueous Solutions by Coexisting Cations *Inorg. Chem.* **2016**, *55*, 7739-7746.

35- Nagata, E.; Ara, T.; Nakano, H. Mechanochromic luminescence of 1-alkanoylaminopyrenes adsorbed onto cellulose papers *Dyes Pigm.* **2017**, *141*, 48-52.

36- Pengchong Xue, P.; Ding, J.; Wanga, P.; Lua, R. Recent progress in the mechanochromism of phosphorescent organic molecules and metal complexes *J. Mater. Chem. C* **2016**, *4*, 6688-6706.

37- Mauro, M. *et al.* Complex iridium (III) salts: luminescent porous crystalline materials *Angew. Chem. Int. Ed.* **2010**, *49*, 1222–1226.

38- Sun, H.; Liu, S.; Lin, W.; Zhang, K. Y.; Lv, W.; Huang, X.; Huo, F.; Yang, H.; Jenkins, G.; Zhao, Q.; Huang, W. Smart responsive phosphorescent materials for data recording and security protection *Nat*. *Commun*. **2014**, *5*, 3601.

39- Sagara, Y.; Mutai, T.; Yoshikawa, I.; Araki, K. Material Design for Piezochromic Luminescence: Hydrogen-Bond-Directed Assemblies of a Pyrene Derivative *J. Am. Chem. Soc*. **2007**, *129*, 1520–1521.

40- Loewe, C.; Weder, C. Oligo (p-phenylene vinylene) Excimers as Molecular Probes: Deformation-Induced Color Changes in Photoluminescent Polymer Blends *Adv. Mater.* **2002**, *14*, 1625-1629.

41- Jill Kunzelman, J.; Kinami, M.; R. Crenshaw, B.; Protasiewicz, J. D.; Weder, C. Oligo(p-phenylene vinylene)s as a "New" Class of Piezochromic Fluorophores *Adv. Mater.* **2008**, *20*, 119-122.

42- Yoon, S.-J.; Park, S. Y. Polymorphic and mechanochromic luminescence modulation in the highly emissive dicyanodistyrylbenzene crystal: secondary bonding interaction in molecular stacking assembly *J. Mater. Chem.* **2011**, *21*, 8338.

43- Sagara, Y.; Kubo, K.; Nakamura, T.; Tamaoki, N.; Weder, C. Temperature-dependent mechanochromic behavior of mechanoresponsive luminescent compounds *Chem. Mater*. **2017**, *29*, 1273–1278.

44- T Seki, T.; Tokodai, N.; Omagari, S.; Nakanishi, T.; Hasegawa, Y.; Iwasa, T.; Taketsugu, T.; Ito, H. Luminescent Mechanochromic 9-Anthryl Gold(I) Isocyanide Complex with an Emission Maximum at 900 nm after Mechanical Stimulation *J. Am. Chem. Soc*. **2017**, *139*, 6514–6517.

45- Ito, H.; Saito, T.; Oshima, N.; Kitamura, N.; Ishizaka, S.; Hinatsu, Y.; Wakeshima, M.; Kato, M.; Tsuge, K.; Sawamura, M. Reversible Mechanochromic Luminescence of [(C$_6$F$_5$Au)$_2$(μ-1,4-Diisocyanobenzene)] *J. Am. Chem. Soc*. **2008**, 130, 10044–10045.

46- Yagai, S.; Seki, T.; Aonuma, H.; Kawaguchi, K.; Karatsu, T.; Okura, T.; Sakon,A.; Uekusa, H.; Ito, H. Mechanochromic Luminescence Based on Crystal-to-Crystal Transformation Mediated by a Transient Amorphous State *Chem. Mater*. **2016**, *28*, 234–241

47- Jin, M.; Seki, T.; Ito, H. Luminescent mechanochromism of a chiral complex: distinct crystal structures and color changes of racemic and homochiral gold(I) isocyanide complexes with a binaphthyl moiety *Chem. Commun*. **2016**, *52*, 8083-8086.

48- Dong, Y.; Xu, B.; Zhang, J.; Tan, X.;, Wang, L.; Chen. J.; Lv, H.; Wen, S,; Li.; B.; Ye, L.;, Zou, B.; Tian, W. Piezochromic Luminescence Based on the Molecular Aggregation of 9,10-Bis((*E*)-2-(pyrid-2-yl)vinyl)anthracene *Angew. Chem. Int. Ed.* **2012**, *51*, 10782 –10785.

49- Zhang, Y. J.; Wang, K.; Zhuang, G. L.; Xie, Z. Q.; Zhang, C.; Cao, F.; Pan, G. X.; Chen, H. F.; Zou, B.; Ma, Y. G. Multicolored-Fluorescence Switching of ICT-Type Organic Solids with Clear Color Difference: Mechanically Controlled Excited State *Chem. – Eur. J*. **2015**, *21*, 2474–2479.

50- Ma, C.; Xu, B.; Xie, G.; He, J.; Zhou, X.; Peng, B.; Jiang, L.; Xu, B.; Tian, W.; Chi, Z.; Liu, S.; Zhang, Y.; Xu, J. An AIE-Active Luminophore with Tunable and Remarkable Fluorescence Switching Based on the Piezo and Protonation–Deprotonation Control *Chem. Commun*. **2014**, *50*, 7374– 7377.

51- Feng, C.; Wang, K.; Xu, Y.; Liu, L.; Zou, B.; Lu, P. Unique piezochromic fluorescence behavior of organic crystal of carbazole-substituted CNDSB *Chem. Commun.* **2016**, *52*, 3836-3839.

52- Nagura, K.; Saito, S.; Yusa. H.; Yamawaki, H.; Fujihisa, H.; Sato, H.; Shimoikeda, Y.; Yamaguchi, S. Distinct responses to mechanical grinding and hydrostatic pressure in luminescent chromism of tetrathiazolylthiophene *J. Am. Chem. Soc*. **2013**, *135*, 10322–10325.

53- Luo, X.; Zhao, W.; Shi, J.; Li, C.; Liu, Z.; Bo, Z.; Dong, Y. Q.; Tang, B. Z. Reversible Switching Emissions of Tetraphenylethene Derivatives among Multiple Colors with Solvent Vapor, Mechanical, and Thermal Stimuli *J. Phys. Chem. C* **2012**, *116*, 21967– 2197.

54- Sagara, Y.; Kato, T. Brightly Tricolored Mechanochromic Luminescence from a Single- Luminophore Liquid Crystal: Reversible Writing and Erasing of Images *Angew. Chem. Int. Ed.* **2011**, *50*, 9128 –9132.

55- Lavrenova ,A.; Balkenende ,D.W.; Sagara, Y.; Schrettl, S.; Simon Y.C.; Weder, C. Mechano- and Thermoresponsive Photoluminescent Supramolecular Polymer *J. Am. Chem. Soc.* **2017**, *139*, 4302–4305.

56- Seki, T.; Ozaki, T.; Okura, T.; Asakura, K.; Sakon, A.; Uekusa, H.; Ito, H. Interconvertible multiple photoluminescence color of a gold(I) isocyanide complex in the solid state: solvent-induced blue-shifted and mechano-responsive red-shifted photoluminescence *Chem. Sci.* **2015**, *6*, 2187-2195.

57- Rajamalli, P.; Senthilkumar, N.; Gandeepan, P.; Ren-Wu, C.Z.; Lin H.W.; Chemg, C.-H.; A thermally activated delayed blue fluorescent emitter with reversible externally tunable emission *J. Mater. Chem. C* **2016**, *4*, 900.

58- Okazaki, M.; Takeda, Y.; Data, P.; Pander, P.; Higginbotham, H.; Monkman, A. P.; Minakata, S. Thermally Activated Delayed Fluorescent Phenothiazine–dibenzo[*a,j*]phenazine–phenothiazine Triads Exhibiting Tricolor-Changing Mechanochromic Luminescence *Chem. Sci.* **2017**, *8*, 2677– 2686.

59- Tsujimoto, H.; Ha, D. G.; Markopoulos, G.; Chae, H. S.; Baldo, M. A.; Swager, T. M. Thermally Activated Delayed Fluorescence and Aggregation Induced Emission with Through-Space Charge Transfer *J. Am. Chem. Soc.* **2017**, *139*, 4894– 4900.

60- Xu, B.; Mu, Y.; Mao, Z.; Xie ,Z.; Wu, H.; Zhang, Y.; Jin, C.; Chi, Z.; Liu, S.; Xu, J.; Wu, Y.C.; Lu PY.; Lien, A.; Bryce, MR.; Achieving remarkable mechanochromism and white-light emission with thermally activated delayed fluorescence through the molecular heredity principle *Chem. Sci.* **2016**, *7*, 2201-2206.

61- Suter, D.; van Summeren, L.T.C.G.; Blacque, O.; Venkatesan, K. Highly Stable and Strongly Emitting N-Heterocyclic Carbene Platinum(II) Biaryl Complexes *Inorg. Chem.* **2018**, *57*, 8160–8168.

62- Yam, V. W.-W.; Wong, K. M.-C. Luminescent metal complexes of d^6, d^8 and d^{10} transition metal centres. *Chem. Commun.* **2011**, *47*, 11579– 11592.

63- Chi, Y.; Chou, P.-T. Transition-metal phosphors with cyclometalating ligands: fundamentals and applications. *Chem. Soc. Rev.* **2010**, *39*, 638– 655.

64- Chou, P-T.; Chi, Y. Osmium- and Ruthenium-Based Phosphorescent Materials: Design, Photophysics, and Utilization in OLED Fabrication *Eur. J. Inorg. Chem.* **2006**, 3319–3332

65- Burroughes, J. H.; Bradley, D. D. C.; Brown, A. R.; Marks, R. N.; MacKay, K.; Friend, R. H.; Burns, P. L.; Holmes, A. B. Light-emitting diodes based on conjugated polymers *Nature* **1990**, *347*, 539–541.

66- Baldo, M. A.; O'Brien, D. F.; You, Y.; Shoustikov, A.; Sibley, S.; Thompson, M. E.; Forrest, S.R. Highly Efficient phosphorescent emission from organic electroluminescent devices. *Nature* **1998**, *395*, 151–154.

67- Miwa, T.; Kubo, S.; Shizu, K.; Komino, T.; Adachi, C. Kaji, H. Blue organic light-emitting diodes realizing external quantum efficiency over 25% using thermally activated delayed fluorescence emitters *Sci. Rep.* **2017**, *7*, 284.

68- Li, T.-Y.; Liang, X.; Zhou, L.; Wu, C.; Zhang, S.; Liu, X.; Lu, G.-Z.; Xue, L.-S.; Zheng, Y.-X.; Zuo, J.-L. N-heterocyclic carbenes: versatile second

cyclometalated ligands for neutral iridium(III) heteroleptic complexes. *Inorg. Chem.* **2015**, *54*, 161–173.

69- Jacquemin, D.; Escudero, D. The short device lifetimes of blue PhOLEDs: insights into the photostability of blue Ir(III) complexes *Chem. Sci*. **2017**, *8*, 7844-7850

70- Endo, A.; Ogasawara, M.; Takahashi, A.; Yokoyama, D.; Kato, Y.; Adachi, C. Thermally Activated Delayed Fluorescence from Sn^{4+}–Porphyrin Complexes and Their Application to Organic Light Emitting Diodes - A Novel Mechanism for Electroluminescence *Adv. Mater.* **2009**, *21*, 4802.

71- Uoyama, H.; Goushi, K.; Shizu, K.; Nomura, H.; Adachi, C. Highly Efficient Organic Light-Emitting Diodes from Delayed Fluorescence *Nature* **2012**, *492*, 234.

72- Liu, Y.; Li, C.; Ren, Z.; Yan, S.; Bryce M.R. All-organic thermally activated delayed fluorescence materials for organic light-emitting diodes *Nat. Rev. Mater.* **2018**, *3*, 18020.

73- Zhang, Q.; Kuwabara, H.; Potscavage, W.J.Jr.; Huang, S.; Hatae, Y.; Shibata, T.; Adachi, C. Anthraquinone-Based Intramolecular Charge-Transfer Compounds: Computational Molecular Design, Thermally Activated Delayed Fluorescence, and Highly Efficient Red Electroluminescence *J. Am. Chem. Soc.* **2014**, *136*, 18070– 18081.

74- Wong, M.Y.; Zysman-Colman, E. Purely Organic Thermally Activated Delayed Fluorescence Materials for Organic Light-Emitting Diodes *Adv. Mater.* **2017**, 1605444.

75- Yang, Z.; Mao, Z.; Xie, Z.; Zhang, Y.; Liu, S.; Zhao, J.; Xu, J.; Chi, Z.; Aldred, M. P. Recent Advances in Organic Thermally Activated Delayed Fluorescence Materials. *Chem. Soc. Rev.* **2017**, *46*, 915– 1016.

76- Sarma, M.; Wong, K.-T.; Exciplex: An Intermolecular Charge-Transfer Approach for TADF *ACS Appl. Mater. Interfaces* **2018**, *10,* 19279–19304.

77- Grybauskaite-Kaminskiene, G.; Ivaniuk, K.; Bagdziunas, G.; Turyk, P.; Stakhira, P.; Baryshnikov, G.; Volyniuk, D.; Cherpak, V.; Minaev, B.; Hotra, Z.; Agren, H.; Grazulevicius, J.V. Contribution of TADF and exciplex emission for efficient "warm-white" OLEDs *J. Mater. Chem. C* **2018**, *6*, 1543-1550.

78- Tsujimoto, H.T.; Ha, D.G.; Markopoulos, G.; Chae, H.S.; Baldo, M.A.; Swager, T.M. Thermally Activated Delayed Fluorescence and Aggregation Induced Emission with Through-Space Charge Transfer *J. Am. Chem. Soc*. **2017**, *139*, 4894–4900

79- Spuling, E.; Sharma, N.; Samuel, I. D. W.; Zysman-Colman, E.; Braese, S. (Deep) blue through-space conjugated TADF emitters based on [2.2]paracyclophanes *Chem. Commun*. **2018**, *54*, 9278-9281.

80- Kawasumi, K.; Wu, T.; Zhu, T.; Chae, H.S.; Van Voorhis, T.; Baldo, M.A.; Swager, T.M. Thermally Activated Delayed Fluorescence Materials Based on Homoconjugation Effect of Donor–Acceptor Triptycenes *J. Am. Chem. Soc*. **2015**, *137*, 11908–11911.

81- Shao, S.; Hu, J.; Wang, X.; L.;, Xiabin W.; J.; Wang, F. Blue Thermally Activated Delayed Fluorescence Polymers with Nonconjugated Backbone and Through-Space Charge Transfer Effect *J. Am. Chem. Soc.* **2017**, *139*, 17739–17742.

82- Shizu, K.; Tanaka, H.; Uejima, M.; Sato, T.; Tanaka, K.; Kaji, H.; Adachi, C. Strategy for Designing Electron Donors for Thermally Activated Delayed Fluorescence Emitters *J. Phys. Chem. C* **2015**, *119*, 1291– 1297.

83- Hirata, S.; Sakai, Y.; Masui, K.; Tanaka, H.; Lee, S.Y.; Nomura, H.; Nakamura, N.; Yasumatsu, M.; Nakanotani, H.; Zhang.; Q.; Shizu, K.; Miyazaki. H.; Adachi, C. Highly efficient blue electroluminescence based on thermally activated delayed fluorescence *Nat. Mater.* **2015**, *14*, 330–336.

84- Yokoyama, D.; Sakaguchi, A. ; Suzuki, M.; Adachi, C. Horizontal orientation of linear-shaped organic molecules having bulky substituents in neat and doped vacuum-deposited amorphous films *Org. Electron.* **2009**, *10*, 127–137

85- Yokoyama, D. Molecular orientation in small-molecule organic light-emitting diodes *J. Mater. Chem.* **2011**, *21*, 19187–19202.

86- Sun, J. W.; Baek, J. Y.; Kim, K. H.; Moon, C. K.; Lee, J. H.; Kwon, S. K.; Kim, Y. H.; Kim, J. J. Thermally Activated Delayed Fluorescence from Azasiline Based Intramolecular Charge-Transfer Emitter (DTPDDA) and a Highly Efficient Blue Light Emitting Diode *Chem. Mater.* **2015**, *27*, 6675–6681.

87- Liu, H.; Bai, Q.; Yao, L.; Zhang, H.; Xu, H.; Zhang, S.; Li, W.; Gao, Y.; Li, J.; Lu, P.; Wang, H.; Yang, B.; Ma, Y. Highly efficient near ultraviolet organic light-emitting diode based on a meta-linked donor–acceptor molecule *Chem. Sci.* **2015**, *6*, 3797-3804.

88- Wang, Z.; Li, Wanyu X.; Shitong Z.; Z.; Li, H.; Yu, Z.; Chen, Y.; Lu, P.; Chen, P. The effect of meta coupling on colour purity, quantum yield, and exciton utilizing efficiency in deep-blue emitters from phenanthroimidazole isomers *Phys. Chem. Chem. Phys*. **2015**, *17*, 31894.

89- Nakagawa, T.; Ku, S.Y.; Wong, K. T.; Adachi, C. Electroluminescence based on thermally activated delayed fluorescence generated by a spirobifluorene donor–acceptor structure *Chem. Commun*. **2012**, *48*, 9580–9582.

90- Fu, H.; Cheng, Y.-M.; Chou, P.-T.; Chi, Y. Feeling blue? Blue phosphors for OLEDs *Mater. Today* **2011**, *14*, 472–479.

91- Chen, W.-C.; Lee, C.-S.; Tong, Q.-X. Blue-emitting organic electrofluorescence materials: progress and prospective *J. Mater. Chem. C* **2015**, *3*, 10957–10963.

92- Bui, T.T.; Goubard, F.; Ibrahim-Ouali, M.; Gigmes, D.; Dumur, F. Recent advances on organic blue thermally activated delayed fluorescence (TADF) emitters for organic light-emitting diodes (OLEDs) *Beilstein J Org Chem*. **2018**, *14*, 282–308.

93- Sun, J. W.; Baek, J. Y.; Kim, K.-H.; Moon, C.-K.; Lee, J.-H.; Kwon, S.-K.; Kim, Y.-H.; Kim, J.-J. Thermally Activated Delayed Fluorescence from Azasiline Based Intramolecular Charge-Transfer Emitter (DTPDDA) and a

Highly Efficient Blue Light Emitting Diode *Chem. Mater*. **2015**, *27*, 6675–6681.

94- Sun, J. W.; Baek, J. Y.; Kim, K.-H.; Huh, J.-S.; Kwon, S.-K.; Kim, Y.-H.; Kim, J.-J. Azasiline-Based Thermally Activated Delayed Fluorescence Emitters for Blue Organic Light Emitting Diodes *J. Mater. Chem. C* **2017**, *5*, 1027–1032.

95- Tsai, W.-L.; Huang, M. – H.; Lee, W.-K.; Hsu, Y.-J.; Pan, K. – C.; Huang, Y. – H.; Ting, H. – C.; Sarma, M.; Ho, Y.-Y.; Hu, H. – C.; Chen, C. – C.; Lee, M. – T.; Wong, K. – T.; Wu, C. – C. A Versatile Thermally Activated Delayed Fluorescence Emitter for Both Highly Efficient Doped and Non-Doped Organic Light Emitting Devices *Chem. Commun*. **2015**, 51, 13662– 13665.

96- Tanaka, H.; Shizu,, K.; Miyazaki, H.; Adachi, C. Efficient Green Thermally Activated Delayed Fuorescence (TADF) from a Phenoxazine–Triphenyltriazine (PXZ–TRZ) Derivative *Chem. Commun.* **2012**, *48*, 11392–11394.

97- Bucinskas, A.; Bagdziunas, G.; Tomkeviciene, A.; Volynyuk, D.; Kostiv, N.; Gudeika, D.; Jankauskas, V.; Rutkis, M.; Grazulevicius, J. V. Structure–Property Relationship of Isomeric Diphenylethenyl-disubstituted dimethoxycarbazoles. *RSC Adv*. **2015**, *5*, 49577-49589.

98- Gudeika, D.; Grazulevicius, J. V.; Volyniuk, D.; Butkute, R.; Juska, G.; Miasojedovas, A.; Gruodis, A.; Jursenas, S. Structure-Properties Relationship of the Derivatives of Carbazole and 1,8-naphthalimide: Effects of the Substitution and the Linking Topology. *Dyes Pigm*. **2015**, *114*, 239-252.

99- Sato, K.; Shizu, K.; Yoshimura, K.; Kawada, A.; Miyazaki, H.; Adachi, C. Organic Luminescent Molecule with Energetically Equivalent Singlet and Triplet Excited States for Organic Light-Emitting Diodes *Phys. Rev. Lett*. **2013**, *110*, 247401.

100- Lee, S.Y.; Yasuda, T.; Nomura, H.; Adachi, C. High-Efficiency Organic Light-Emitting Diodes Utilizing Thermally Activated Delayed Fluorescence from Triazine-Based Donor–Acceptor Hybrid Molecules *Appl. Phys. Lett*. **2012**, *101*, 093306.

101- Mayr, C.; Lee, S.Y.; Schmidt, T.D.; Yasuda, T.; Adachi,C.; Brütting, W. Efficiency Enhancement of Organic Light-Emitting Diodes Incorporating a Highly Oriented Thermally Activated Delayed Fluorescence Emitter *Funct.Mater*. **2014**, *24*, 5232–5239.

102- Hirata, S.; Sakai, Y.; Masui, K.; Tanaka, H.; Lee, S.Y.; Nomura, H.; Nakamura, N.; Yasumatsu, M.; Nakanotani, H.; Zhang, Q.; et al. Highly Efficient Blue Electroluminescence Based on Thermally Activated Delayed Fluorescence. *Nat. Mater*. **2015**, *14*, 330–336.

103- Cui, L.-S.; Deng, Y.-L.; Tsang, D. P.-K.; Jiang, Z.-Q.; Zhang, Q.; Liao, L.-S.; Adachi, C. Controlling Synergistic Oxidation Processes for Efficient and Stable Blue Thermally Activated Delayed Fluorescence Devices *Adv. Mater*. **2016**, *28*, 7620–7625.

104- Lee, S.Y.; Yasuda, T.; Yang, Y.S.; Zhang, Q.; Adachi, C. Luminous Butterflies: Efficient Exciton Harvesting by Benzophenone Derivatives for

Full-Color Delayed Fluorescence OLEDs *Angew. Chem. Int. Ed.* **2014**, *125*, 6502.

105- Zhang, Q.; Li, J.; Shizu, K.; Huang, S.; Hirata, S.; Miyazaki, H.; Adachi, C. Design of Efficient Thermally Activated Delayed Fluorescence Materials for Pure Blue Organic Light Emitting Diodes *J. Am. Chem. Soc*. **2012**, *134*, 14706–14709.

106- Wu, S.; Aonuma, M.; Zhang, Q.; Huang, S.; Nakagawa, T.; Kuwabara, K. Adachi, C. High-Efficiency Deep-Blue Organic Light-Emitting Diodes Based on a Thermally Activated Delayed Fluorescence Emitter *J. Mater. Chem. C* **2014**, *2*, 421–424.

107- Zhang, Q. S.; Li, B.; Huang, S. P.; Nomura, H.; Tanaka, H.; Adachi, C. Efficient Blue Organic Light-Emitting Diodes Employing Thermally Activated Delayed Fluorescence *Nat. Photonics* **2014**, *8*, 326–332.

108- Zhang, Q.; Tsang, D.; Kuwabara, H.; Hatae, Y;. Li, B.; Takahashi, T.; Lee, S. Y.; Yasuda, T. Adachi, C. Nearly 100% internal quantum efficiency in undoped electroluminescent devices employing pure organic emitters *Adv. Mater*. **2015**, *27*, 2096–2100.

109- Dias, F. B.; Bourdakos, K. N.; Jankus, V.; Moss, K. C.; Kamtekar, K. T.; Bhalla, V.; Santos, J.; Bryce, M. R.; Monkman, A. P. Triplet Harvesting with 100% Efficiency by Way of Thermally Activated Delayed Fluorescence in Carge Transfer OLED Emitters *Adv. Mater.* **2013**, *25*, 3707–3714.

110- Kim, J. H.; Hwang, S. H.; Kim, O. Y.; Lee, J. Y. P-131: Synthesis and Device Application of a Dibenzothiophene Derivative as Thermally Activated Delayed Fluorescence Material for Green Fluorescence OLED *SID Symposium Digest of Technical Papers* **2015**, *46*, 1658–1660.

111- Yu, L.; Wu, Z.; Xie, G.; Zeng, W.; Ma, D.; Yang, C. Molecular Design to Regulate the Photophysical Properties of Multifunctional TADF Emitters Towards High-Performance TADF-Based OLEDs with EQEs up to 22.4% and Small Efficiency Roll-Offs. *Chem. Sci.* **2018**, *9*, 1385– 1391

112- Cai, X.; Li, X.; Xie, G.; He, Z.; Gao, K.; Liu, K.; Chen, D.; Cao Y.; Su, S. J. Rate-Limited Effect of Reverse Intersystem Crossing Process: the Key For Tuning Thermally Activated Delayed Fluorescence Lifetime and Efficiency Roll-off of Organic Light Emitting Diodes *Chem. Sci*. **2016**, *7*, 4264–4275.

113- Zhang, Q.; Kuwabara, H.; Potscavage, W. J.; Huang, S.; Hatae, Y.; Shibata, T.; Adachi, C. Anthraquinone-Based Intramolecular Charge-Transfer Compounds: Computational Molecular Design, Thermally Activated Delayed Fluorescence, and Highly Efficient Red Electroluminescence. *J. Am. Chem. Soc.* **2014**, *136*, 18070−18081.

114- Obafemi, C. A.; Pfleiderer, W. Permanganate Oxidation of Quinoxaline and Its Derivatives. *Helv. Chim. Acta* **1994**, *77*, 1549.

115- Liu, Y. Nishiura, M.; Wang,Y.; Hou, Z. Rapid Freeze-Quench ENDOR Study of Chloroperoxidase Compound I: The Site of the Radical. *J. Am. Chem. Soc*. **2006**, *128*, 5592–5593.

116- Baryshnikov, G. V.; Gawrys, P.; Ivaniuk, K.; Witulski, B.; Whitby, R. J.; Al-Muhammad, A.; Minaev, B.; Cherpak, V.; Stakhira, P.; Volyniuk, D.; Wiosna-Salyga, G.; Luszczynska, B.; Lazauskas, A.; Tamulevicius, S.; Grazulevicius, J. V. Nine-Ring Angular Fused Biscarbazoloanthracene Displaying a Solid State Based Excimer Emission Suitable for OLED Application. *J. Mater. Chem. C* **2016**, *4*, 5795-5805.

117- Pashazadeh, R.; Pander, P.; Lazauskas, A.; Dias, F. B.; Grazulevicius, J. V. Multicolor Luminescence Switching and Controllable Thermally Activated Delayed Fluorescence Turn on/Turn off in Carbazole–Quinoxaline–Carbazole Triads. *J. Phys. Chem. Lett.* **2018**, *9*, 1172– 1177.

118- Pashazadeh, R.; Pander, P.; Bucinskas, A.; Dias, F. B.; Grazulevicius, J. V. An Iminodibenzyl–Quinoxaline–Iminodibenzyl Scaffold as a Mechanochromic and Dual Emitter Donor and Bridge Effects on Optical Properties *Chem. Commun.* **2018**, *54*, 13857.

8. Curriculum vitae

Name and surname	Ramin Pashazadeh
E-mail	razichem@gmail.com

Education

2005 – 2009	Pure chemistry, University of Tehran, Tehran, Iran
2009 – 2012	Organic chemistry, Tarbiat Modares University, Tehran, Iran

Work experience

2015 – 2018	Horizon 2020, project Excilight: "Donor-Acceptor light emitting EXCIplexes as materials for easily to tailor ultra-efficient OLED LIGHTing". Junior researcher at the department of polymer chemistry and technology, Kaunas University of Technology
2018 – 2019	Projekto " Synthesis, studies and applications of organic bipolar semiconductors exhibiting high luminescence quantum yields in the solid state". Junior researcher at the department of polymer chemistry and technology, Kaunas University of Technology

9. LIST OF PUBLICATIONS

1. Pashazadeh, R.; Pander, P.; Lazauskas, A.; Dias, F.B.; Grazulevicius. J.V. Multicolor Luminescence Switching and Controllable Thermally Activated Delayed Fluorescence Turn on/Turn off in Carbazole–Quinoxaline–Carbazole Triads *J. Phys. Chem. Lett.* **2018**, *9*, 1172–1177.

2. Pashazadeh, R.; Pander, P.; Bucinskas, A.; Skabara, P.J.; Dias, F.B.; Grazulevicius, J.V. An Iminodibenzyl-Quinoxaline-Iminodibenzyl Scaffold as Mechanochromic and Dual Emitter: Donor and Bridge Effects on Optical Properties *Chem. Commun*. **2018**, *54*, 13854.

List of international scientific attendances

1. 14th International Symposium on Functional π-Electron Systems (*Fpi14 2019*), Germany*, **Poster Presentation***

2. 5th Workshop on Organic Electronics and Nanophotonics (WOREN 2018), Poland, ***Oral presentation***

3. 11th International Conference on Nanomaterials (ANM 2018), Portugal, ***Oral presentation***

4. International Conference on Science and Technology of Synthetic Metals 2018 (ICSM 2018), Korea, ***Oral presentation***

5. 14th International Conference on Electrical and Related Properties of Organic Solids (ERPOS 2017), Scotland, ***Poster presentation***

6. 22nd International Krutyn Summer School 2017: State of the Art in Organic-only TADF OLEDs – From Theory to Applications, Poland, ***Poster presentation***

7. 4th Workshop on Organic Electronics and Nanophotonics (WOREN 2016), France, ***Poster presentation***

8. 16th Baltic Polymer Symposium (BPS 2016), Lithuania, ***Poster presentation***

10. ACKNOWLEDGEMENTS

My short stay in Lithuania is also ended, please accept my apologies
if I may hurt anyone.

I render my acknowledgements to everyone who has ever had
any impact on my life, whatever it was.

My sincere gratitude to the sincere friend,
who was like a sister, God bless you,
it was a great honor to meet you.

Teşekkürler Ya Rabbim!